Medium and Reaction Engineering of Light-driven Biotransformations

PhD THESIS

to achieve the university degree of

PhD in Engineering at Aarhus University

and

Doktor der Naturwissenschaften at Graz University of Technology

Only one of the degrees may be held at a time

submitted to

Aarhus University &

Graz University of Technology

Supervisor

Prof. Selin Kara

Department of Biological and Chemical Engineering, Aarhus University

Prof. Robert Kourist

Institute of Molecular Biotechnology, Graz University of Technology

Aarhus, July 2021

AFFIDAVIT

I declare that I have authored this thesis independently, that I have not used other than the declared sources/resources, and that I have explicitly indicated all material which has been quoted either literally or by content from the sources used. The text document submitted to GSTS and uploaded to TUGRAZonline is identical to the present doctoral thesis.

31.07.2021 

Date, Signature

ACKNOWLEDGEMENTS

After three years of hard work, this is my PhD thesis. However, it is not only my work that led to its completion, it was also the advice, help and support from numerous other people that I want to acknowledge here.

First of all, I am grateful to Prof. Selin Kara for taking me onboard her newly formed BioBio group at Aarhus University and her continuous supervision and advice. Furthermore, I would like to thank my co-supervisor Prof. Robert Kourist (Graz University of Technology, Austria) for hosting my stay in Graz and for his advice and input that helped advance my work. Thanks to the whole Kourist Group for welcoming me and special thanks to Hanna Grimm for the introducing to cyanobacteria. Along the same lines I express my gratitude to Prof. Frank Hollmann (Delft University of technology, Netherlands) and his group for warmly welcoming and hosting me in Delft and for his academic input on my research. Additionally, I want to thank the European Union for funding this project.

However, to get through three years of the PhD life halfway intact, you need more than solid academic advice and funding. Therefore I would like to thank all my dear past, current and visiting BioBio friends in Aarhus, for either giving scientific advice or just chatting about a random obscure topic during our coffee breaks. Thank you for being not only good colleagues, but also genuinely great people who helped me get my mind off work when necessary with disc golf, dinners and whisky tastings. I am also thankful to my colleagues at TU Graz, who made my stay there so enjoyable. Along similar lines, I want to thank everyone involved in the PhotoBioCat ITN for the collaboration and good times during the pre-COVID-19 meetings all over Europe. Additionally I want to thank all my friends back in Austria, who reliably made my infrequent visits there feel way too short. Beyond that I want to thank my mother, father and sister for supporting me along my long academic path.

Most of all however, I am grateful to Katie for being the great person she is, having my back throughout this thesis and always being close to me, regardless of the physical distance between us.

ABBREVIATIONS

2LPS	2-liquid-phase system
2-MeTHF	2-methyltetrahydrofuran
2-MM	2-methylmaleimide
2-MS	2-methylsuccinimide
ABTS	2,2'-azino-bis(3-ethylbenzothiazoline-6-sulfonic acid)
***Aae*UPO**	Unspecific peroxygenase from *Agrocybe aegerita*
a_w	water activity
BCR	bubble column reactor
Chla	chlorophyll a
CND	carbon nanodots
CPME	cyclopentyl methyl ether
CYP	cytochrome P450 monooxygenases
DCW	dry cell weight
DES	deep eutectic solvent
DIPE	diisopropyl ether
ee	enantiomeric excess
EtOAc	ethyl acetate
FAP	fatty acid photodecarboxylase
FDH	formate dehydrogenase
FMN	flavin mononucleotide
FOx	Formate oxidase
GC	gas chromatography
KPi	potassium phosphate buffer
LED	Light emitting diode
MTBE	Methyl tert-butyl ether
NAD(P)$^+$	nicotinamide adenine dinucleotide (phosphate) oxidized form
NAD(P)H	nicotinamide adenine dinucleotide (phosphate) reduced form
NanoDSF	Nano differential scanning fluorometry
NBD	3,4-(methylenedioxy) nitrobenzene
N-CNDs	nitrogen-doped carbon nanodots
PBR	photobioreactor
ROS	reactive oxygen species
SVR	surface-volume-ratio
^{tert}BuOOH	tert-butyl hydroperoxide
T_i	Infliction temperature
TON	turnover number
UPO	unspecific peroxygenase
WLE	wireless light emitter

SUMMARY

The hydroxylation of unactivated C-H bonds is an important step in synthetic chemistry and the starting point for numerous further modifications. The relatively recently discovered enzyme unspecific peroxygenase (UPO) hydroxylates such bonds with just H_2O_2 as cosubstrate. However, the application of this enzyme faces two major challenges: its inactivation by excess H_2O_2 and the low water solubility of its hydrophobic substrates. While the first challenge has already been solved with in situ H_2O_2 synthesis systems like photocatalysis, the latter remained mostly untouched. Therefore, one of the main aims of this PhD project was to use UPO with a photocatalyst in organic medium maximizing the substrate's accessibility for the enzyme in the hydroxylation of the model substrate cyclohexane. Furthermore, the upscaling of a photobiocatalytic reaction was investigated, as most light driven systems suffer the same problem: self-shading due to high optical density.

Firstly, the UPO PaDa-I was immobilized via entrapment in calcium alginate to facilitate its use in organic solvents. In a solvent screening, neat cyclohexane was selected as the best reaction medium being both solvent and substrate simultaneously. For the in situ H_2O_2 provision nitrogen-doped carbon nanodots (N-CNDs) were chosen as photocatalyst. When combining N-CNDs with alginate entrapped PaDa-I in cyclohexane, the photocatalyst was confined to the beads, producing a 2-in-1 heterogeneous photobiocatalyst. It was active under process conditions for up to seven days, producing cyclohexane in a millimolar range.

Secondly, the upscaling of a photobiotransformation the N-CND/PaDa-I system was not productive enough, therefore another model system was chosen. The biotransformation with cyanobacterium *Synechocystis* sp. PCC 6803 expressing YqjM for the reduction of 2-methylmaleimide was selected for its high reaction rates and low substrate volatility. A bubble column reactor with internal illumination using wireless light emitters (WLEs) was used. After optimizing the reaction conditions, 650 mg pure (*R*)-2-methylsuccinimide was produced in 22 h (>99% *ee*, 73% isolated yield). Internal illumination provided more than two-fold higher reaction rates than external illumination and proved the applicability of the WLE system for scalable light driven biotransformations.

RESUMÉ

Hydroxyleringen af ikke-aktiverede CH-bindinger er et vigtigt trin i syntetisk kemi og udgangspunktet for adskillige yderligere ændringer. Det relativt nyligt opdagede enzym uspecifik peroxygenase (UPO) er i stand til at hydroxylere sådanne bindinger med kun H_2O_2 som cosubstrat. Imidlertid står enzymet over for to store udfordringer: dets inaktivering ved overskydende H_2O_2 og den lave vandopløselighed i dets typisk hydrofobe substrater. Første udfordring er allerede blevet løst med in situ H_2O_2-syntesesystemer som fotokatalyse, men sidstnævnte er stort set uberørt. Derfor er et af hovedformålene med dette ph.d.-projekt at bruge UPO med en fotokatalysator i organisk medium for at maksimere substratets tilgængelighed for enzymet i hydroxyleringen af modelsubstratet cyclohexan. Derudover bliver opskalering af en fotobiokatalytisk reaktion undersøgt, da de fleste lysdrevne systemer lider under det samme problem: selvskygge på grund af høj optisk densitet.

Først blev UPO PaDa-I fanget i calciumalginat for at facilitere dets anvendelse i organiske opløsningsmidler. I en opløsningsmiddelscreening blev ren cyclohexan valgt som det bedste reaktionsmedium, hvilket betyder at det fungerer som både opløsningsmiddel og substrat. Til in situ H_2O_2-bestemmelse blev nitrogen-dopede carbon nanodots (N-CNDs) valgt som fotokatalysator. Ved kombination af N-CND'er med indesluttet alginat PaDa-I i cyclohexan blev fotokatalysatoren begrænset til alginatperlerne, der producerede en 2-i-1 heterogen fotobiokatalysator. Det var aktivt under procesbetingelserne i op til syv dage og producerede cyclohexan i et millimolært interval.

Til opskalering af en fotobiotransformation var N-CND/PaDa-I-systemet ikke produktivt nok, derfor blev der valgt et andet modelsystem. Biotransformationen med cyanobacterium Synechocystis sp. PCC 6803, der udtrykker YqjM til reduktion af 2-methylmaleimid, blev valgt for dets høje reaktionshastigheder og lave substratvolatilitet. Opskalering fandt sted i en boblesøjlereaktor med intern belysning ved hjælp af trådløse lysemittere. Efter optimering af reaktionsbetingelser blev 650 mg rent (*R*)-2-methylsuccinimid produceret i 22 timer (> 99% ee, 73% isoleret udbytte). Intern belysning gav mere end to gange højere reaktionshastigheder end ekstern belysning og derved beviste fordelene ved brugen af de trådløse lysemittere til skalerbare lysdrevne biotransformationer.

ZUSAMMENFASSUNG

Die Hydroxylierung von nicht aktivierten C-H-Bindungen ist ein wichtiger Schritt in der synthetischen Chemie. Das erst kürzlich entdeckte Enzym unspezifische Peroxygenase (UPO) ist in der Lage, solche Bindungen lediglich mit H_2O_2 als Cosubstrat zu hydroxylieren. Allerdings steht das Enzym vor zwei großen Herausforderungen: seine Inaktivierung durch überschüssiges H_2O_2 und die geringe Wasserlöslichkeit seiner typischerweise hydrophoben Substrate. Während die erste Herausforderung bereits mit In-situ-H_2O_2-Synthesesystemen wie Photokatalyse gelöst wurde, blieb die zweite weitgehend unberührt. Daher war eines der Hauptziele dieses Promotionsprojekts die Verwendung von UPO mit einem Photokatalysator in organischem Medium, Konzentration des Modellsubstrats Cyclohexan zu maximieren. Darüber hinaus wurde das Upscaling einer photobiokatalytischen Reaktion untersucht, da die meisten lichtgetriebenen Systeme unter dem gleichen Problem leiden: Selbstbeschattung aufgrund der hohen optischen Dichte.

Zunächst wurde die UPO PaDa-I fuer mehr Stabilität in organischen Lösungsmitteln in Calciumalginat eingeschlossen. In einem Lösungsmittel-Screening wurde reines Cyclohexan als bestes Reaktionsmedium ausgewählt. Für die in situ H_2O_2-Produktion wurden stickstoffdotierte Kohlenstoffnanodots (N-CNDs) als Photokatalysator gewählt. Der Photokatalysator bleibt mit PaDa-I in den Alginatkügelchen und mischt sich nicht mit dem organischen Medium. So entsteht eine heterogener 2-in-1-Photobiokatalysator. Er war im Prozess bis zu sieben Tage lang aktiv und produzierte Cyclohexanol im millimolaren Bereich.

Für das Upscaling einer Photobiotransformation war das N-CND/PaDa-I-System nicht produktiv genug, daher wurde ein anderes Modellsystem gewählt: das Cyanobakterium *Synechocystis* sp. PCC 6803, das YqjM für die Reduktion von 2-Methylmaleimid exprimiert. Das Upscaling erfolgte in einem Blasensäulenreaktor mit interner Beleuchtung durch drahtlose Lichtemittenten (WLEs). Nach Optimierung der Reaktionsbedingungen wurden 650 mg reines (*R*)-2-Methylsuccinimid in 22 Stunden produziert (>99% ee, 73% isolierte Ausbeute). Die interne Beleuchtung lieferte mehr als zweifach höhere Reaktionsraten als die externe und bewies die Anwendbarkeit des WLE-Systems für skalierbare, lichtgetriebene Biotransformationen.

LIST OF PUBLICATIONS

Review:

Hobisch, M.; Holtmann, D.; Gomez de Santos, P.; Alcalde, M.; Hollmann, F.; Kara, S. Recent developments in the use of peroxygenases - Exploring their high potential in selective oxyfunctionalisations, *Biotechnology Advances* 2020, 107615, DOI: 10.1016/j.biotechadv.2020.107615

Article I:

Hobisch, M.; van Schie, M. M. C. H.; Kim, J.; Andersen, K. R., Alcalde, M.; Kourist, R.; Park, C.B.; Hollmann, F.; Kara, S. Solvent-Free Photobiocatalytic Hydroxylation of Cyclohexane, *ChemCatChem* 2020, 12, 4009 – 4013. DOI: 10.1002/cctc.202000512 (Editors' choice for Front Cover) (Selected for Hot Topic: Carbon, Graphite, and Graphene)

Article II:

Hobisch, M;* Spasic, J.;* Barone, G.; Malihan-Yap, L.; Castiglione, K.; Tamagnini, P.; Kara, S.; Kourist, R. Internal Illumination to Overcome the Cell Density Limitation in the Scale-up of Whole-cell Photobiocatalysis, *ChemSusChem* 2021, in press, DOI: 10.1002/cssc.202100832 (* authors contributed equally)

Technical Report:

Hobisch, M.; Kara, S., Automated Feeding and Fermentation Phase Transitions for the Production of Unspecific Peroxygenase by *Pichia pastoris*, Biorxiv 2021, preprint, DOI: 10.1101/2021.07.29.454275

Section 2.4 and subsections contain relevant parts of the review researched and written by me. The full article can be found in the appendix.

Section 3 and subsections are identical to article I, with some additional results (indicated in the text) not contained in the original publication.

Section 4 and subsections are identical to article II.

The Technical Report can be found in the appendix.

CONTRIBUTION TO PUBLICATIONS

Review: I was involved in the conceptualization of the article, did the research and writing for chapter 4 and was responsible for polishing and formatting of the whole manuscript.

Article I: I was involved in the conceptualization of the research, did all experiments on enzyme stability, immobilization and all reactions on cycloalkanes. Furthermore, I was involved in the construction of the two UV photoreactors and was the main responsible for writing, polishing and formatting of the manuscript.

Article II: I made a major contribution to the conceptualization of the research, established the experimental setting and did the BCR experiments on cell density and WLE number. Furthermore, I was involved in the writing and the formatting of the manuscript.

Technical report: I established the *Pichia pastoris* fermentation in our DASGIP system, monitored the fermentation, did the measurements and wrote the manuscript.

TABLE OF CONTENTS

1. Aims and Objectives 1
2. Theoretical Background 2
   2.1. Hydroxylation by Chemical Catalysis 2
   2.2. Cytochrome P450 Monooxygenases 3
   2.3. Unspecific Peroxygenases 5
   2.4. Reaction Engineering for UPOs 8
   2.5. Photobioreactors 15
3. Solvent-free Photobiocatalytic Hydroxylation of Cyclohexane 19
   3.1. Abstract 19
   3.2. Introduction 19
   3.3. Results and Discussion 21
   3.4. Conclusion 28
   3.5. Material and Methods 29
4. Internal Illumination to Overcome the Cell Density Limitation in the Scale-up of Whole-cell Photobiocatalysis 35
   4.1. Abstract 35
   4.2. Introduction 35
   4.3. Results and Discussion 37
   4.4. Conclusion 45
   4.5. Material and Methods 45
5. Conclusion 48
6. Outlook 50
7. References 52

8. Supplementary Information 59
8.1. SI Article I 59
8.2. SI Article II 68
9. Appendix ..... A
9.1. Review ..... A
9.2. Technical Report ..... B

1. Aims and Objectives

The first part of the here presented PhD thesis aims at identifying the key process parameters for the use of unspecific peroxygenase (UPO) in the light driven hydroxylation of cyclohexane in organic medium. For this goal four key objectives are set:

- Evaluation of the effect of organic solvents on UPO,
- Finding an immobilization technique to stabilize UPO in organic solvents,
- Implementing the light-driven hydroxylation reaction in organic medium, and
- Identifying key reaction parameters.

The second part of the PhD thesis aims at upscaling light-driven photobiotransformations and overcoming the challenge of self-shading in optically dense reaction media. As a possible solution for this limitation, a bubble column reactor with internal illumination equipped with wireless light emitters (WLEs) is investigated. The system was introduced by Buchholz *et al*.[1] and previously only used for the cultivation of photoautotrophic microorganisms. The model system is *Synechocystis* P_{cpcB}::*yqjM,* a cyanobacterium expressing the ene reductase YqjM applied for the reduction of 2-methylmaleimide. Three objectives are defined:

- Investigation of the system's potential in optically dense photobiotransformations,
- Optimization of the process efficiency by varying number of WLEs as well as cell density, and,
- Application of the photobiotransformation in a preparative scale.

2. Theoretical Background

2.1. Hydroxylation by Chemical Catalysis

The oxyfunctionalization of unreactive C–H bonds is an important starting point in organic synthesis as many of the target compounds are common platform chemicals or desired products themselves, working as bioactive compounds like agrochemicals and pharmaceuticals.[2] Traditional chemistry provides a wide range of metal catalysts for this job, but they mostly work under harsh conditions like high temperature and pressure.[3] Looking at the model substrate cyclohexane a variety of methods for its hydroxylation is available, the industrially prevalent one being liquid-phase air oxidation.[4] The reaction can be performed in a series of reactors at temperatures ranging from 140 °C to 180 °C at a pressure between 8 bar and 20 bar with or without a metal catalyst. The intermediate cyclohexyl hydroperoxide is formed and subsequently converted to cyclohexanol, cyclohexanone and some by-products (mono- and dicarboxylic acids, aldehydes, esters, **Scheme 1**). The reaction mainly yields a mix of cyclohexanol and cyclohexanone in a ratio which is influenced by the choice of catalyst. Using a cobalt catalyst, a ratio of 3.5 (cyclohexanol : cyclohexanone) is obtained. This reaction mixture is often referred to as KA (ketone alcohol) oil. The cyclohexanol content can be increased to a ratio of 5 – 10 by using palladium as catalyst. Byproducts of this reaction include cyclohexyl hydroperoxide and esters, aldehydes and a wide range of dicarboxylic acids.

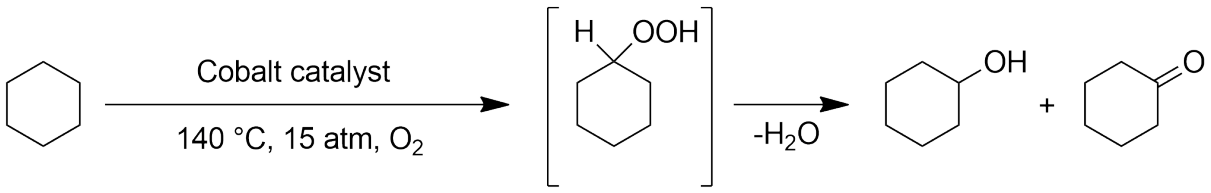

Scheme 1. Cobalt catalyzed liquid phase air oxidation of cyclohexane to a mix of cyclohexanol and cyclohexanone.

Another approach to produce cyclohexanol from cyclohexane is boric acid modified oxidation. In this approach anhydrous metaboric acid is added to the process and binds the formed cyclohexyl hydroperoxide, producing cyclohexyl perborate ester. This ester reacts with cyclohexane, forming cyclohexanol and a borate ester. Hydrolysis then releases

cyclohexanol and boric acid. While the yield for cyclohexanol is increased in this method, the additional process steps for recovery and recycling highly increase the investment and operating costs for the plant.[4]

Besides those established and industrially applied methods, there is also more current research. A novel method revolves around a "quasi metal-free catalyst", titled partially graphitic carbon. It is produced in hydrothermal synthesis from glucose, resorcinol and cobalt nitrate hydrate. After washing and drying the product was calcined at 1100 °C for 4 h under nitrogen atmosphere. The reaction was conducted in a mix of cyclohexane and acetonitrile in an autoclave under 15 bar O_2 and 125 °C for eight hours. 55% conversion were reached and the product consisted of 11% cyclohexanol, 34% cyclohexanone and other byproducts, such as 33% adipic acid.[5] Overall, in the chemical hydroxylation of alkanes low specificity, and rather harsh reaction conditions are prevalent, which still fuels research in the topic, as well as a search for more specific and environmentally friendly alternatives.

2.2. Cytochrome P450 Monooxygenases

Metal catalysis is not the only way to hydroxylate unactivated carbon substrates and the heme containing cytochrome P450 monooxygenases (CYPs) present the previously most used enzymatic approach for regio- and steroselective hydroxylations.[6] For terminal hydroxylation of fatty acids and *n*-alkanes CYP from *Candida tropicalis* can be applied. However, this enzyme is membrane bound, which poses disadvantages in its expression and applicability.[7] Soluble cytosolic CYPs have been the focus of protein engineering efforts. Naturally, CYP101A1 from *Pseudomonas putida* stereo- and regioselectively hydroxylates (+)-camphor, but was engineered stepwise towards smaller alkane substrates, producing hexanol,[8] butanol and propanol[9] and finally ethanol[10]. Similar results were reported for CYP102A1 from *Bacillus megaterium*. A combination of site-specific mutagenesis and directed evolution led to a redefinition of the enzymes substrate scope from hydroxylation of dodecane to ethane.[11] A different approach was taken using CYP102A1 wild-type enzyme in combination with perfluorocarboxylic acids. Those acids served as a filler molecules in the enzyme's long substrate channel, facilitating conversion of small substrates like gaseous *n*-alkanes or cyclohexane.[12] For the conversion of cycloalkanes there were also protein

engineering efforts undertaken and a double mutant catalyzing the hydroxylation of several substrates was designed.[13] Cyclohexane, octane and myristic acid were successfully hydroxylated in a two-liquid phase system (2LPS), containing an aqueous and a hydrophobic organic phase. Another advance in cycloalkane hydroxylation was made in 2018, when the CYP450chx was discovered in *Acidovorax* sp. CHX100, which has the ability to utilize alkanes as sole carbon source.[14] The enzyme was heterologously expressed in *E. coli*, which was used as a whole-cell biocatalyst to hydroxylate C5-C8 cycloalkanes.

While CYPs definitely perform useful reactions, their application is limited to fine chemical and pharmaceutical production. A major cost factor in the preparative application of CYPs is the need to for nicotinamide cofactors, nicotinamide adenine dinucleotide phosphate (NADPH) for most (Scheme 1). As NADPH is rather cost-intensive and needed in molar quantities, cofactor regeneration is crucial for any industrially relevant process.[15] With NADPH-specific alcohol dehydrogenase[16] or formate dehydrogenase,[17] enzymatic regeneration systems are available, they add further complexity to the system. This is because their inherent reaction mechanism causes some severe issues. They rely on reducing equivalents delivered by molar amounts of nicotinamide cofactors, which unfortunately not always reach their destined target, the substrate. Some of the reducing power is spent in futile reactions reducing molecular oxygen to hydrogen peroxide, the so called *uncoupling* (Scheme 2).[18] Not only does this mean a loss of valuable reducing equivalents, but also the formation of reactive oxygen species (ROS) that impair enzyme stability. While this can be countered with the addition of enzymatic ROS scavengers like catalase or superoxide dismutase, it adds to the cost of the system.[18]

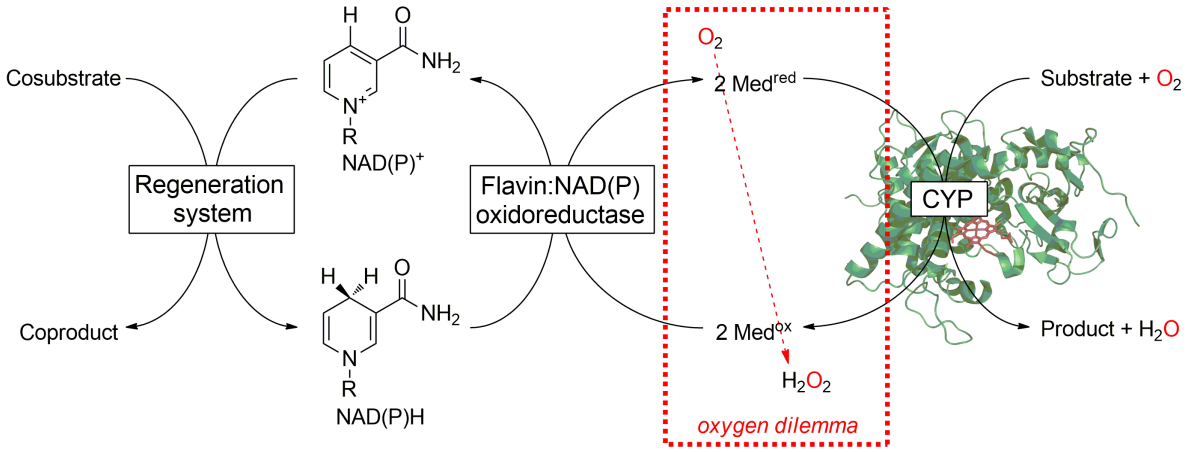

Scheme 2. The oxygen dilemma of cytochrome P450 monooxygenases (CYPs). The necessary mediators for hydride transfer to the enzyme's active site react in an uncoupling reaction with O_2 yielding H_2O_2.[18] Scheme Adapted from Hobisch *et al.*[19]

2.3. Unspecific Peroxygenases

An alternative to cytochrome P450 monooxygenases was found in unspecific peroxygenases (UPOs, EC 1.11.2.1), also known as heme-thiolate peroxidases.[20] As in CYPs, the active site of UPOs features a Cys bound heme group. Therefore, UPOs catalyze similar oxyfunctionalization reactions as CYPs, however with the advantage of being cofactor independent, as their only requirement is hydrogen peroxide (H_2O_2) as cosubstrate. [21] This also means that they are not subject to the aforementioned *oxygen dilemma*, which is another advantage for biocatalytic applications. The proposed dual mechanism contains two possible pathways (**Scheme 3**). One being the peroxidase cycle as seen in horseradish peroxidase[22] and the other being similar to CYPs.[23] As shown with 4-methylphenol as substrate, the latter yields the hydroxylated product, while the peroxidase cycle produces a phenoxy radical (**Scheme 3**). In the ground state, water acts as a distal ligand to the heme. After H_2O_2 replaces the water and gets deprotonated by a conserved Glutamate residue, compound 0 is formed. By heterolytical decay and electron rearrangement the metastable key intermediate compound I is formed. This is where the pathways diverge. Either a protonated compound II is formed, leading to the hydroxylated peroxygenase product through a benzyl radical, or a deprotonated compound II leads to the formation of two phenoxy radicals.[24] The peroxidase route yielding those radicals is generally undesired when working with phenolics but can be reduced by addition of ascorbic acid as radical scavenger.[25]

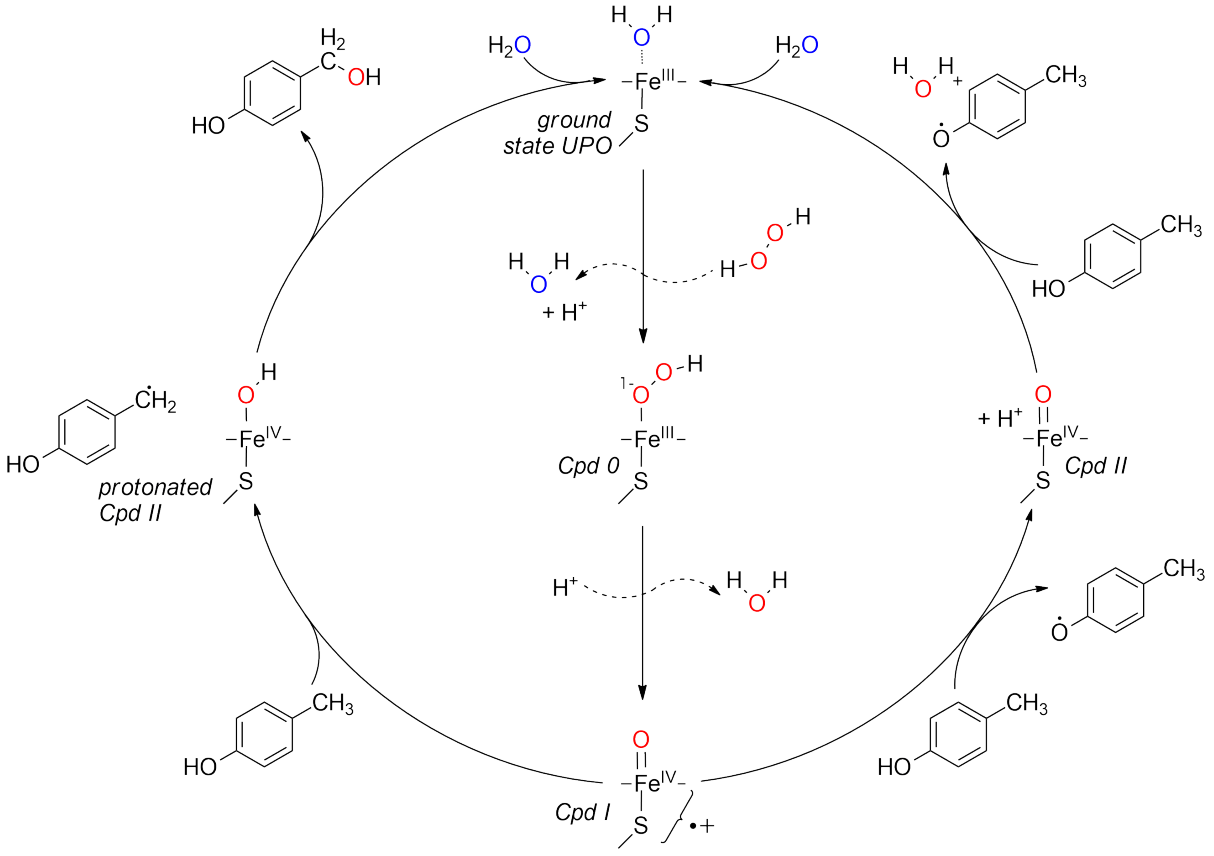

Scheme 3. Proposed mechanism of unspecific peroxygenase, showing its peroxygenase (left) and peroxidase activity (right). Adapted from Hofrichter *et al.*[24]

The first reported enzyme in this sub-subclass was found to be secreted by the edible mushroom *Agrocybe aegerita* in 2004 and at first classified as a haloperoxidase, until it was approved in 2011 as an unspecific peroxygenase (UPO) and subsequently named *Aae*UPO.[24] In the first publication *Aae*UPO was described to oxidize aryl alcohols to aldehydes and then into benzoic acids.[21d] Numerous publications followed describing a broad substrate scope of *Aae*UPO. Hydroxylation of sp^3-hybridized C–H bonds was performed on alkanes,[26] cycloalkanes,[27] fatty acids,[28] alkylbenzenes[29] and 5-hydroxymethyl furfural[30] by *Aae*UPO. Furthermore, hydroxylation of aromatic C–H bonds,[31] epoxidation of C–C double bonds[32] and even sulfoxidation of aryl alkyl sulfides[33] were reported.

Besides *Aae*UPO, several other UPOs have been isolated from different fungal cultures: *Apa*UPO from *Agrocybe parasitica*,[23b] *Cra*UPO from *Coprinellus radians*, *Cve*UPO from *Coprinopsis verticillata*,[34] *Mro*UPO from *Marasmius rotula*,[35] *Cgl*UPO from *Chaetomium globosum*,[36] *Mwe*UPO from *Marasmius wettsteinii*[37] and *Pab*UPO from *Psathyrella*

aberdarensis.[24] Beyond that, Blast searches in NCBI genome database and JGI Mycocosm yielded over 4,300 unique UPO sequences.[24] However, with this abundance of potential candidates for UPO biocatalysis, the efficient heterologous production of functional enzymes is still the bottleneck. Only a handful of examples have been described in the literature. Novozymes has established the expression of r*Cci*UPO from Coprinopsis cinerea[38] and rNOVO from an undetermined mold[39] in Aspergillus oryzae. Furthermore, *Mro*UPO[40] and *Cvir*UPO from *Collariella virescens* [41] have recently been expressed in *Escherichia coli*. The widely used r*Aae*UPO, an evolved variant called PaDa-I (**Figure 1**), is produced in *Pichia pastoris.*[42] The mutant is the product of several rounds of directed evolution and carries 9 amino acid substitutions, with four of them located in the signal peptide for secretion. Due to its efficient expression in *Pichia pastoris*, PaDa-I was selected as the UPO for this project.

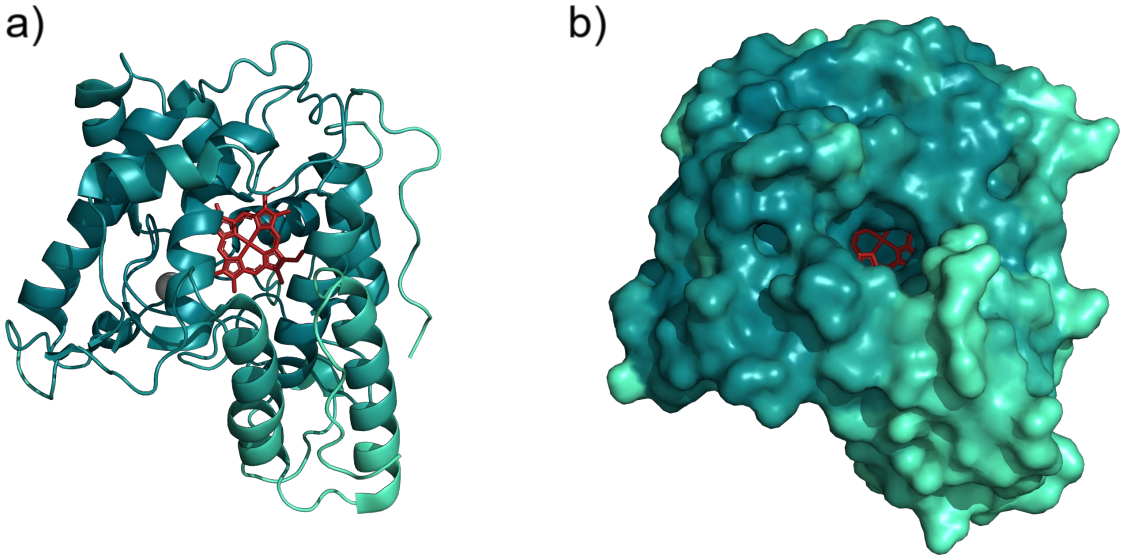

Figure 1. Crystal structure of PaDa-I with red heme residue and grey structural magnesium in ribbon (a) and surface view (b). PDB code 5oxu

2.4. Reaction Engineering for UPOs

Chapter 2.4 and its sub-chapters are taken from the *review on peroxygenases*[19] *and passages on chloroperoxidase were removed to only include information on unspecific peroxygenase. The page layout was changed and small stylistic alterations were done without changing the main content.*

The following parts will focus on the specific applications of peroxygenases. Firstly, H_2O_2 as an essential but also destructive reaction component and photobiocatalysis as a possible solution for this challenge will be discussed. Secondly, enzyme immobilization approaches followed for peroxygenases will be introduced, as it is an integral part of many biocatalytic industrial applications to increase enzyme stability and facilitate reuse of the biocatalyst. At last, a second important aspect of economic feasibility will be discussed: the increase of substrate loading for hydrophobic peroxygenase substrates by using non-conventional media, which may in turn necessitate the use of immobilized enzymes for increased stability.

2.4.1. H_2O_2 Challenge and Photobiocatalysis

The use of hydrogen peroxide (H_2O_2) needed at stoichiometric amounts for enzymatic oxidation reactions (e.g. peroxidase-, peroxygenase catalysed) faces the challenge of heme oxidation leading to enzyme inactivation. To alleviate this limitation, several strategies have been developed for *in situ* supply of H_2O_2. Those include enzymatic production using glucose oxidase[43] or formate oxidase[44], electrochemistry[45], chemical catalysis[46] and photocatalysis.

This part will mainly focus on the latter strategy, provision of peroxygenases with H_2O_2 by photocatalysis. Those light-driven methods generally rely on a photocatalyst that when excited by light, can oxidize an electron donor and can transfer the reducing equivalents to oxygen, generating H_2O_2 (**Scheme 4**).

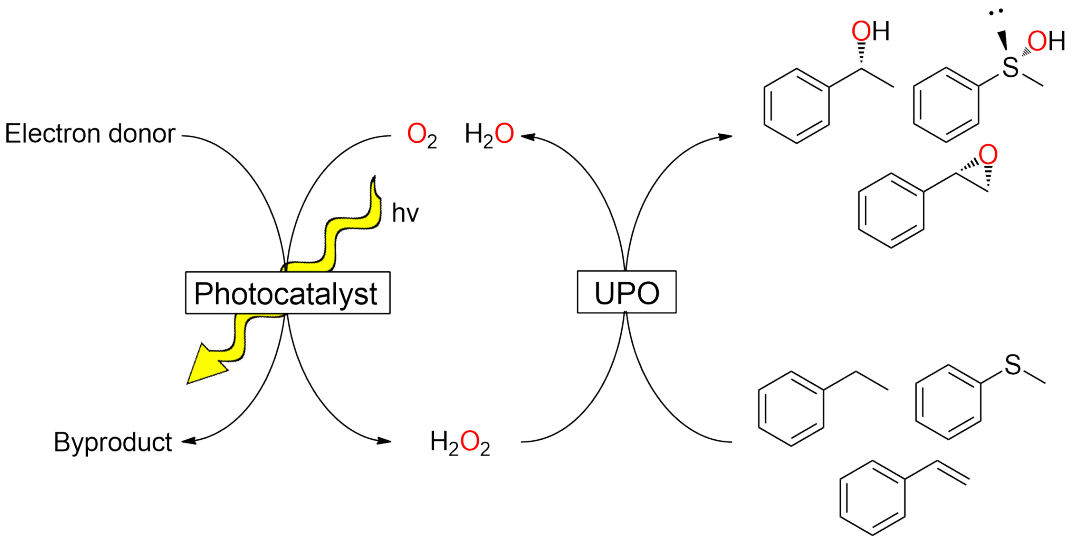

Scheme 4. Photocatalytic *in situ* synthesis of H_2O_2 for UPO catalysis. Adapted from Hobisch *et al.*[19]

One of the first published examples of this light-driven approach was the use of *Aae*UPO in combination with flavin adenine mononucleotide (FMN) as photocatalyst and ethylenediaminetetraacetic acid (EDTA) as co-substrate. This system was able to hydroxylate a range of alkylic and aromatic substrates and to catalyse the epoxidation reaction of styrene and some of its derivatives.[27]

Later on, an approach with higher atom efficiency was reported by Zhang *et al.* using gold loaded rutile titanium dioxide (Au-TiO_2) as photocatalyst and methanol as sacrificial electron donor, in combination with the engineered *Aae*UPO PaDa-I. Upon illumination with visible light, full conversion of the model substrate ethylbenzene (15 mM) was reached within 72 hours and (*R*)-1-phenylethanol was produced with high selectivity (98.2% *ee*). In line with the previously discussed substrate scope of *Aae*UPO, they were also able to hydroxylate other alkanes producing only minor amounts of the corresponding ketone as side product. In ^{1}H-NMR analysis, they found methanol was photocatalytically oxidized not only to formaldehyde, but also subsequently to formate. When using formaldehyde and formate as electron donors and comparing it to methanol, the authors reported H_2O_2 formation rates to be 75% higher and reaction rates to be 32% and 18% higher, respectively.[47] One interesting prospective of using Au-TiO_2 is that due to its water oxidation activity, also water as sacrificial electron donor for the *in situ* generation of H_2O_2 comes into reach. While the hydroxylation of ethylbenzene achieved lower yields than with co-substrate, a linear

correlation between concentration of photocatalyst and concentration of acetophenone, the over-oxidized side product was observed. This prompted the researchers to extend the photocatalytic reaction with a second enzyme. Phenylethanol was oxidized to acetophenone by PaDa-I and rutile Au-TiO_2, which was then converted to (*R*)- *and* (*S*)-phenyl ethylamine by addition of ω-transaminases from *Aspergillus terreus* and *Bacillus megaterium*, respectively. Similarly, they oxidized toluene to benzaldehyde and then added benzaldehyde lyase from *Pseudomonas fluorescence* to perform a benzoin condensation, yielding (*R*)-benzoin. Overall, artificial cascade pathways could be successfully demonstrated initiated with photobiocatalytic oxyfunctionalization step. Promising results were also achieved with carbon nanodots (CNDs) as non-metal photocatalysts. The combination of PaDa-I, CNDs and FMN yielded a higher initial rate (0.81 $mM \cdot h^{-1}$ vs 0.16 $mM \cdot h^{-1}$) and higher enzyme turnover numbers (TONs, 100,000 vs 21,000) when compared with Au-TiO_2. Furthermore, Au-$BiVO_4$ and g-C_3N_4 were investigated for their applicability with PaDa-I. While Au-$BiVO_4$ yielded comparably low product formation, g-C_3N_4 produced more overoxidation products. [48]

While the system using Au-TiO_2 worked well, the reaction proceeded quite slowly, reaching full conversion of 15 mM after 72 h.[48] This was partially due to the fact that the photocatalyst can only be excited by light below 413 nm, which makes up only 0.7% of the light emitted by the lamp used. [47] An effort to accelerate this PaDa-I reaction by expanding the usable spectrum of visible light was made by Willot *et al.,* using a combination of three photosensitizers covering a wide range of wavelengths. They were applied in combination with a formate dehydrogenase (*Cb*FDH from *Candida boidinii*) reducing NAD^+ to NADH and oxidising formate to carbon dioxide. The produced NADH was used by the excited photocatalysts (FMN, phenosafranine and methylene blue) to produce H_2O_2, which was then utilized by PaDa-I to hydroxylate ethylbenzene (10 mM). After only 4 h, full conversion to 10 mM (*R*)-1-phenylethanol was achieved. While the reaction proceeded remarkably fast, its robustness was lacking. Especially the photocatalyst FMN and *Cb*FDH were rather unstable, exhibiting turnover numbers of only 649 and 135, respectively.[49]

Another photobiocatalytic application of *Aae*UPO added electrochemistry to the system. Choi *et al.* demonstrated the hydroxylation of ethylbenzene using single walled carbon

nanotube (SWNT) electrodes. To reduce the overpotential required to reduce O_2 and produce H_2O_2 the SWNTs were hybridized with lumichrome, a flavin derivative. When exposed to visible light this treatment facilitated the transfer of electrons to O_2, reducing the required overpotential substantially, which resulted in a more energy efficient H_2O_2 synthesis. [50]

2.4.2. Strategies for UPO Immobilization

While photocatalytic provision of H_2O_2 has been explored using alternative photocatalyst and cosubstrates, it remains as a challenge to develop peroxygenase-catalyzed biotransformations with high productivity and low cost contribution of the enzyme. Robust heterogeneous biocatalysts, that are resistance at process conditions and that can be recovered and reused, may result in process simplification and reduced processing time combined with a higher product quality and a smaller environmental footprint. Enzyme immobilization in turn enables the use of non-conventional media for biocatalysis as it restricts conformational mobility and avoids consequent unfolding allowing highly productive biocatalysis in non-aqueous media.

However, the need for enzyme immobilization has to be assessed carefully, as described below, before making the decision. Based on the turnover number (TON, $mol_{product} \cdot mol_{enzyme}^{-1}$) achievable, a judgement can be made if there is a need for enzyme immobilization or not. It was proposed that if the TON is too low, immobilization is not economically viable due to the cost of most of the solid supports, unless they come from a waste stream.[51] On the other hand, if the TON is very high with a free enzyme or if the product is highly expensive, making a cost contribution of the enzyme <0.05% compared to overall operational costs, then there is no need to immobilize the enzyme. Hence, if the TON value lies in between these borders, then enzyme immobilization is recommended. The following parts summarizes the studies on immobilization of UPOs with the aim to have quantitative comparisons mainly on TON values.

Since UPOs are a relatively new addition to the biocatalytic toolbox, there is not a whole lot of publications on their immobilization available (**Table 1**). Covalent immobilization of *Aae*UPO on methacrylate polymer was used to increase enzyme stability in the

photobiocatalytic oxidation of ethylbenzene. The removal of the enzyme from the oxidative influence of the used TiO_2 photocatalyst proved beneficial for the reaction's robustness as the enzyme's TON was increased by a factor of eight.[48] A particularly sophisticated approach, published by Molina et al., was the directed unique-point covalent immobilization (DUCI) of *Aae*UPO. For this the previously produced mutant PaDa-I[42d] was further modified to carry one Cys residue on the enzyme surface opposite to the entrance of the active site. This Cys was then used for the covalent attachment of the enzyme to two different carriers (epoxy polymethylacrylate and agarose). While for both carriers the recovered activity was around 15%, further experiments with the agarose preparation showed increased robustness against acetonitrile and pH greater than 5 and improved temperature stability.[52] The only carrier-free immobilization approach previously published for UPOs was the encapsulation of *Mro*UPO and *Aae*UPO in PVA/PEG gel.[53] While the kinetic parameters K_M and k_{cat} for the substrates diclofenac, dimethylene-5-nitrobenzene and 1,4-dimethoxybenzene were hardly influenced by the entrapment an interesting effect was reported for the storage of the immobilized enzyme. While the activity towards 3,4-(methylenedioxy) nitrobenzene (NBD) decreased already after 6 days of storage in potassium phosphate buffer at pH 7, the storage in non-polar solvents (hexane, cyclohexane) increased the activity by up to 190% after 1 day and still showed 30% higher activity than the fresh preparation after 160 days. A possible explanation for this increase in activity is that the unipolar solvent makes the rather polar immobilization matrix more accessible for relatively non-polar substrates like NBD. Furthermore, the entrapped *Aae*UPO was used for diclofenac hydroxylation in a stirred tank reactor with a continuous H_2O_2 feed, where it showed a 60-fold improved turnover number (TON) of 61,041, compared to <1,000 for the free enzyme.

Table 1. Overview for immobilization of unspecific peroxygenases (UPOs). Adapted from Hobisch *et al*.[19]

Enzyme	Carrier (Interaction)	Immobilisation yield	Recovered activity	Reaction catalyzed	Remarks	Ref.
Carrier-bound approaches						
*Aae*UPO	Methacrylate polymers (covalent)	n.d.	4%	Ethylbenzene hydroxylation	Used in neat substrate	[54]
*Aae*UPO	Methacrylate polymers (covalent)	n.d.	n.d.	Photo-biocatalytic ethylbenzene hydroxylation	8x increase of TON compared to free enzyme	[48]
*Aae*UPO	Agarose (covalent)	n.d.	15%	Styrene epoxidation	Increased stability against acetonitrile, high temperature, high pH	[52]
*Aae*UPO	Polyacryl (covalent)	72.8%	3%	Styrene epoxidation	Up to 360 mM product	[55]
Carrier-free approaches						
*Mro*UPO/ *Aae*UPO	PVA/PEG Gel (entrapment)	n.d.	86%	Diclofenac oxidation	60 fold increase in TON, storage in cyclohexane increased activity	[53]
n.d. = not determined						

Due to the inconsistent nature of the published data on the various techniques, it is not possible to point out any general recommendations for peroxygenase immobilization, but the wide variety of the reported methods, can still give valuable input for new immobilization approaches.

2.4.3. Use of Peroxygenases in Non-Conventional Media

In biocatalysis, many interesting substrates are rather hydrophobic and exhibit low water solubility, which is especially true for UPOs. Therefore, use of non-conventional media like organic solvents or neat substrate (solvent-free) conditions are a possibility to increase substrate loadings and therefore productivity.[56] One example for such an approach is the use of *Aae*UPO for ethylbenzene hydroxylation. At first free *Aae*UPO in combination with an alcohol oxidase from *Pseudomonas putida* (*Pp*AOx) for continuous H_2O_2 production from methanol was used in a two-liquid phase system (2LPS), where the aqueous phase holds the enzymes and the organic phase serves as a product sink and substrate reservoir. This approach suffered from poor enzyme stability and ethylbenzene hydroxylation ceased after 24 h. In an effort to increase stability, the enzymes were covalently immobilized on Relizyme™ HA 403/M resin to use them in neat substrate conditions. However, this combination only yielded trace amounts of the hydroxylated product.[29] The use of immobilized *Aae*UPO with a portion wise addition of *tert*-butyl hydroperoxide in neat ethylbenzene was the next approach. In a reaction volume of 250 mL 40 mM enantiopure (*R*)-1-phenylethanol was produced in three hours, which corresponded to a turnover number (TON) of 67,500 for *Aae*UPO. [54] In another article, an immobilized preparation of *Aae*UPO was employed in the epoxidation of neat styrene derivatives using a continuous feed of *tert*-butyl hydroperoxide (^{tert}BuOOH). Besides several successful epoxidations performed this way in 1.5 ml vials, the epoxidation of *cis*-β-methylstyrene was realized on a 10 mL scale using an exponential ^{tert}BuOOH feed. The peroxide still caused major enzyme inactivation, but with resupplying fresh enzyme three times, a (1*R*,2*S*)-*β*-methylstyrene oxide concentration of 360 mM was obtained. This reaction was also extended to a chemoenzymatic cascade by adding methylamine to the mix to produce (pseudo)ephedrine.[55] Furthermore, PaDa-I was used in hydroxylation and epoxidation reactions containing natural deep eutectic solvents (NADES). While utilising several different electron bond donors, these NADES were all based on choline chloride as electron bond acceptor. That was essential, since a choline chloride oxidase was used for continuous H_2O_2 supply. Applying this system, 22.43 mM (*R*)-1-phenylethanol and 8.68 mM *cis*-β-methylstyrene oxide were produced equalling 224,300 and 86,800 TONs for UPO

respectively. Among others, the researchers found that using 50% (v/v) NADES in the reaction mixture increased process stability. [57]

As of yet there are not many published applications of peroxygenases in non-conventional media. The ever-rising interest in reactions catalyzed by this enzyme group will certainly be a driving force behind application-oriented research towards alternative reaction media. Since many UPO substrates are rather hydrophobic, especially neat substrate applications are a promising approach that should be further pursued. A neat system could dramatically increase substrate and subsequently product titres.

2.5. Photobioreactors

As described above, light can be a useful tool to produce H_2O_2 when working with UPOs, but its usefulness far exceeds the niche of selective hydroxylation reactions. Especially in light of the ongoing climate crisis, the use of photoautotrophic microorganisms fixing CO_2 has been a focus in research towards a more sustainable economy.[58] Those organisms include eukaryotic micro algae and prokaryotic cyanobacteria. The range of products obtainable from these microorganisms is wide, including biofuels,[59] bioactive compounds,[60] pigments[61] and biomass for the food and feed industry.[62]

The cultivation of photoautotrophic organisms can be achieved harnessing the power of sunlight in a variety of systems that are either open or closed. While open systems such as raceway ponds are cheap in construction, upkeep and operation, they are prone to contaminations and therefore only useable for products with low value and purity standards.[63] For high value products, closed photobioreactors (PBRs) are necessary. They are more cost-intensive, but offer control over culture conditions and minimize contamination risks. Reactors for production of algae and cyanobacteria can be as simple as a stirred tank reactor with external or internal illumination.[64] While this design has its drawbacks, like a low surface-to-volume ratio and mechanical stress on cells caused by stirring, it is widely used in laboratory and industry settings.[65] More specialized designs are flat panel[66] or tubular PBRs,[65a] striving for high surface-to-volume ratios. Especially tubular PBRs are widespread in largescale outdoor production facilities, being used in horizontal, vertical or helical settings.[65a, 67]

Looking into these reactor designs, it is obvious that the cultivation of photoautotrophic microorganisms chases a goal that is of high importance across the whole field of photo(bio)catalysis: a high surface-to-volume ratio which allows the efficient use of light by the system. This is especially true when you think about the upscaling of light-driven reactions, as with identical light penetration, the efficiency loss is much higher in larger volumes than in smaller ones. Therefore, the inclined photobiotechnologist can get plenty of inspiration from this field of research.

An especially interesting concept was published for the cultivation of single-cell green algae *Chlamydomonas reinhardtii*, featuring dynamic internal illumination by wireless light emitters (WLEs).[1] Those WLEs consist of a polycarbonate shell containing a single light emitting diode (LED), and a receiving coil. Transmitting coils on the outside of the reactor power the freely floating lights by resonant inductive coupling. This principle lends itself perfectly to the use with a bubble column and one such reactor was kindly provided to us by Prof. Kathrin Castiglione (Friedrich-Alexander-University of Erlangen, Nuremberg). Previously only used for cultivation purposes, this reactor should be assessed regarding its suitability for photobiocatalytic applications.

Not only does the research field of microalgal biotechnology provide interesting reactor concepts, it also offers a range of photobiocatalytic model systems to choose from. Especially cyanobacteria can be used for more specialized purposes than the bulk applications mentioned above. Besides the fact that they use the greenhouse gas CO_2 as carbon source, they also have an advantage regarding biocatalytic oxidoreductase reactions. The often tedious and expensive cofactor recycling necessary for many EC 1 enzymes can be coupled to the cell's photosystem, providing light driven NADPH regeneration.[68]

Compared to firmly established hosts for heterologous enzyme expression like *E. coli* and *P. pastoris* the tools and protocols for genetic engineering of cyanobacteria are still in their infancy.[68-69] Nevertheless, researchers were able to express a variety of oxidoreductases in the photoautotrophic hosts, converting a variety of substrates (**Scheme 5**). Non-filamentous, unicellular strains like *Synechococcus elongatus* PCC 7942 and *Synechocystis* sp. PCC 6803 are most used for engineering endeavors. The first proof of principle for the use of the

photosystem for cofactor regeneration of recombinant enzymes was the ene-reductase YqjM in *Synechocystis* sp. PCC 6803.[70] It was successfully used to reduce C=C bonds with high optical purity, efficiently powered by water splitting at the cell's photosystem. Furthermore, *Synechocystis* sp. PCC 6803 was manipulated to express a Baeyer–Villiger monooxygenase from *Acinetobacter* sp. and used to convert methyl substituated ketones.[71] Furthermore, *Synechocystis* sp. PCC 6803 was the host for the expression of three different imine reductases (IREDs).[72] Initial low reaction rates were overcome by promotor engineering and optimized reaction conditions, yielding respectable initial rates of up to 6.3 mM h^{-1}. An NADPH dependent alcohol dehydrogenase from *Lactobacillus kefir* was expressed in *Synechococcus elongatus* PCC 7942.[73] That way, 20 mM acetophenone was reduced to (*R*)-1-phenylethanol with 99% *ee*, rivalling *Aae*UPO's most widely used model reaction, the hydroxylation of ethylbenzene yielding the same product. Also the UPO model substrate for this PhD thesis, cyclohexane, was successfully converted to cyclohexanol in a cyanobacterial whole cell biotransformation.[74] For that purpose, the aforementioned CYP from *Acidovorax* sp. CHX100 was expressed in *Synechocystis* sp. PCC 6803. Cyclohexane was provided in three different ways: In solution, through the gas phase, and as a 2LPS. The latter provided the best performance with a productivity of 0.04 g L^{-1} h^{-1}.

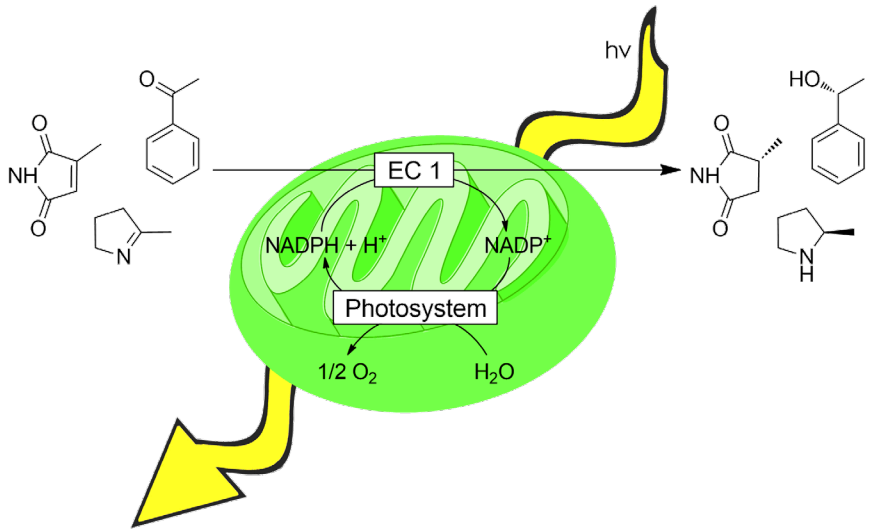

Scheme 5. A selection of substrates converted in reductive reactions performed by genetically engineered cyanobacteria expressing different EC 1 enzymes: Ene reductase,[70] alcohol dehydrogenase[73] and imine reductase[72].

Since the photobiocatalytic upscaling was to take place in the bubble column reactor mentioned above, a model reaction with a low volatility substrate was necessary. Therefore, the classic ene reductase YqjM expressed in *Synechocystis* sp. PCC 6803 was selected to assess the usability of WLEs for photobiocatalytic reactions.

3. Solvent-free Photobiocatalytic Hydroxylation of Cyclohexane

Chapter 3 and its sub-chapters are taken from Article I[75] with changes only regarding the page layout and small stylistic alterations without changing the main content.

3.1. Abstract

The use of neat reaction media, that is the avoidance of additional solvents, is the simplest and the most efficient approach to follow in biocatalysis. Here, we show that unspecific peroxygenase from Agrocybe aegerita (*Aae*UPO) can hydroxylate the neat model substrate cyclohexane. H_2O_2 was photocatalytically generated in situ by nitrogen-doped carbon nanodots (N-CNDs) and UV LED illumination. *Aae*UPO entrapment in alginate beads increased enzyme stability and facilitated the reaction in neat cyclohexane. N-CNDs absorption in beads containing *Aae*UPO created a 2-in-1 heterogeneous photobiocatalyst that was active for up to seven days under reaction conditions and produced cyclohexanol, 2.5 mM. To increase productivity, the bead size and the photocatalyst-to-enzyme ratio have been identified as promising targets for optimisation.

3.2. Introduction

Selective oxyfunctionalization still represents a major challenge for preparative organic synthesis.[3] A biocatalytic alternative to usually metal based chemocatalysts[76] was found in P450 monooxygenases, which have been reported to catalyse a broad range of selective oxidation and oxyfunctionalization reactions.[21a, 21b] Their use however, has not yet exceeded the synthesis of pharmaceutical ingredients. This may be due to their dependency on nicotinamide cofactors (NAD(P)H). These cofactors are exclusively water-soluble thereby confining P450 monooxygenase catalysis to aqueous reaction media. The majority of reagents of interest, however, is rather hydrophobic and therefore incompatible with the requirements of P450 monooxygenases for mostly aqueous media. One major drawback of aqueous reaction media is the low solubility of hydrophobic substrates and products.[77]

More recently, peroxygenases have gained increased attention as alternatives to P450 monooxygenases.[78] As heme-thiolate enzymes, their reaction scope is comparable to that

of P450 monooxygenases, but unlike P450s, peroxygenases utilize simple H_2O_2 or organic hydroperoxides as oxidants, which makes them independent from NAD(P)H and principally enables their application in non-aqueous media.

As early as the 1980s, Klibanov and coworkers[79] reported the application of peroxidases in non-aqueous media. However, it has not yet received much attention. Recently, some examples of the use of an immobilized peroxygenase under non-aqueous conditions for selective hydroxylation and epoxidation reactions have been reported.[52, 54-55] To drive the reaction stoichiometric amounts of ^{tert}BuOOH may be used, leaving equimolar amounts of ^{tert}BuOOH waste behind. More elegantly, the stoichiometric oxidant would be generated *in situ* from O_2 (**Scheme 6**).[80]

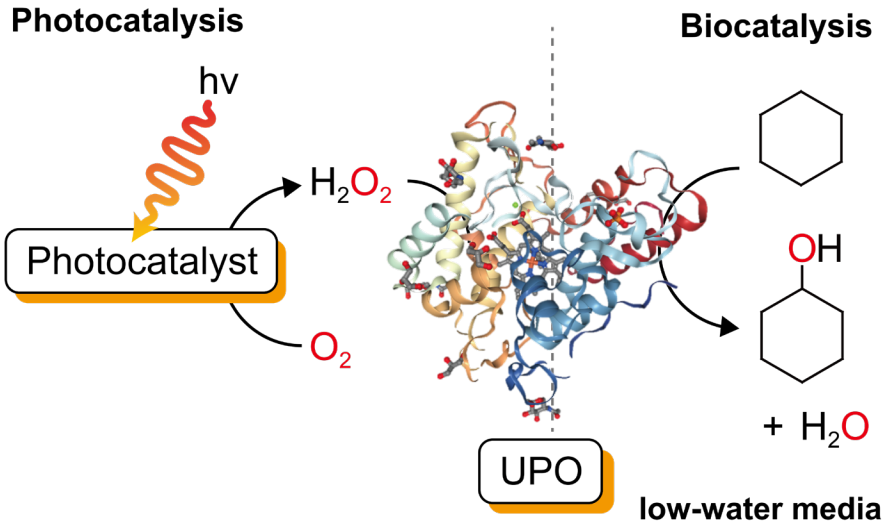

Scheme 6. UPO-mediated photobiocatalytic hydroxylation of cyclohexane in low-water media.

The photocatalytic synthesis of H_2O_2 was achieved using flavin[27, 81], different water oxidation catalysts[48] and carbon nanodots (CNDs), which were reported to be most efficient. Use of CNDs gave five-times higher reaction rates compared to gold nanoparticles deposited on titanium dioxide (Au-TiO_2).[48] Those results drew our attention to CNDs for *in situ* H_2O_2 generation.

In this study, we focused on medium engineering to explore photobiocatalytic UPO-catalysed reactions in non-aqueous media to alleviate aforementioned water-related limitations. Cyclohexane was chosen as poorly water-soluble (0.06 g L^{-1}, 0.7 mM at 20 °C)

model substrate, whereas the work dedicated to the evaluation of the photocatalyst was based on ethylbenzene (water solubility of 0.2 g L^{-1}, 1.4 mM at 20 °C), a standard substrate for UPO. PaDa-I is a laboratory-evolved variant of UPO from *Agrocybe aegerita*[42d] with strong heterologous expression, high activity and stability. Hence, *Aae*UPO PaDa-I became the enzyme of choice for the here presented study.

3.3. Results and Discussion

For the first experiment we examined the hydroxylation of cyclohexane using free enzyme in six organic solvents: Ethyl acetate (EtOAc), 2-methyl tetrahydrofuran (2-MeTHF), di*iso*propyl ether (DIPE), cyclopentyl methyl ether (CPME), heptane, and octane. In addition to those, a neat substrate system using only cyclohexane was evaluated. They were all brought to a uniform water activity (a_W) of 0.53 by incubation with a saturated solution of $Mg(NO_3)_2$ in a desiccator. The water activity was chosen based on a literature survey by Adlercreutz, suggesting that oxidoreductases require an optimal a_W value of 0.1 – 0.7.[82] Reactions (1 mL, 0.15 µM PaDa-I either in organic solvents with 50 mM cyclohexane or in neat substrate cyclohexane) were incubated at 30 °C at 1200 rpm for 5 h and started with the addition of 1 µL 3.5% H_2O_2, which was repeated every hour, resulting in a final H_2O_2 concentration of 5.8 mM. After 5 h, no cyclohexanol could be detected, which was most probably due to the deactivation of the enzyme exposed to high amounts of organic media.

In an attempt to stabilize PaDa-I in organic media, enzyme immobilisation was employed. Gel entrapment was the method of choice owing to its simplicity in preparation and the promising results documented in the literature by the research groups of Hofrichter[53] and of Plou, independently.[83] In the here presented study *Aae*UPO PaDa-I was entrapped in calcium alginate beads. During the immobilisation process, a 19.2% loss of enzyme amount was observed and the beads were highly uniform regarding size (2.77 ± 0.09 mm) and weight (11.6 ± 0.8 mg). For a first assessment whether the entrapment provided stability in organic media, 1 g of alginate beads (37.9 U) was incubated in a stirred tank reactor (30 °C, 500 rpm) with 5 mL cyclohexane and hourly addition of H_2O_2 over 7 h, resulting in a H_2O_2 concentration of 5.6 mM. The reaction was then left to run overnight and a sample was taken after 24 h, dried and used for GC analysis. A distinct cyclohexanol peak in the chromatogram

indicated that the enzyme entrapment had a positive effect on enzyme stability (**SI Figure 11**). The manual addition of aqueous H_2O_2 to the organic media however, was less than ideal.

An alternative strategy for H_2O_2 supply was found using nitrogen-doped carbon nanodots (N-CNDs).[84] Their ability for light-driven H_2O_2 production was first evaluated in the hydroxylation of ethylbenzene (50 mM) with PaDa-I (100 nM) and N-CNDs (5 mg ml^{-1}) in potassium phosphate buffer (KPi, 100 mM, pH 7) under white light illumination at 30 °C and magnetic stirring (600 rpm). After 47 h 9.0 mM (18% theoretical yield) (*R*)-1-phenyl ethanol in excellent enantiomeric excess (*ee*) (**SI Figure 19**) and 0.5 mM overoxidation product acetophenone were produced (**Figure 2**). This corresponds to a productivity of 1.91 $mM_{product}$ mM_{enzyme}^{-1} h^{-1}. A previously reported application of CNDs and FMN to run the UPO driven hydroxylation of ethylbenzene in the same light reactor gave 1.39 $mM_{product}$ mM_{enzyme}^{-1} h^{-1}.[48] The light intensity of the light reactor setup used for this experiment is shown in **SI Figure 12**.

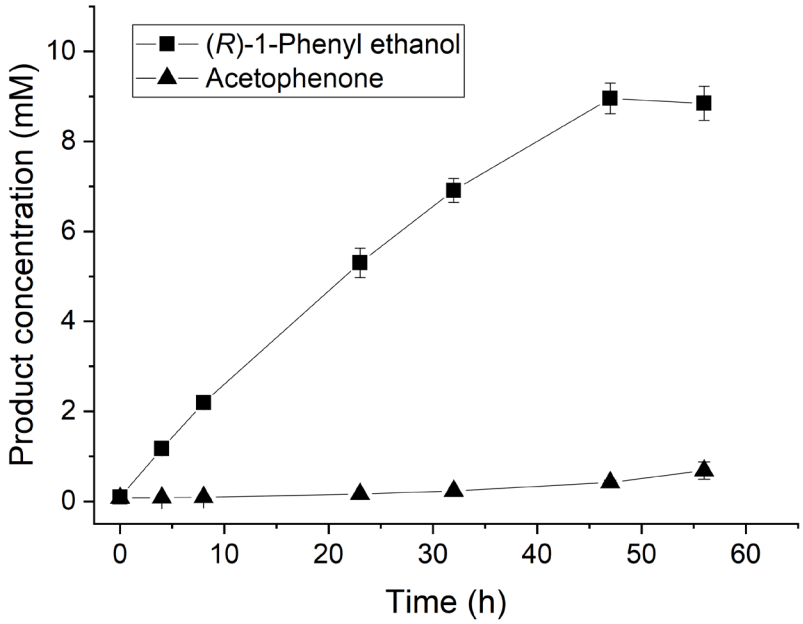

Figure 2. Light driven conversion of ethylbenzene (50 mM) to (*R*)-1-phenyl ethanol (squares) and acetophenone (triangles, overoxidation product) in potassium phosphate buffer (100 mM, pH 7) with N-CNDs (5 mg mL^{-1}) and UPO (100 nm) at 30 °C, magnetic stirring (600 rpm) and white light. Results are average values of duplicates. The data points are connected by a solid line to guide the eye.

The reaction rate and low overoxidation looked promising, but the mechanism of the light-driven H_2O_2 formation was still unclear at this stage. Experiments conducted to understand

the mechanism showed: (i) no product formation without O_2 (**SI Figure 13),** (ii) no O^{18}-labelled product detected when O^{18}-labelled water was used as the reaction medium (**SI Figure 14**), (iii) when illuminating N-CNDs, hydroxyl radicals ($HO^{\bullet}$) were formed (**SI Figure 15**) and (iv) N-CNDs were degraded under illumination (**SI Figure 16**). Even though radicals were produced, the addition of formate or methanol as radical scavengers did not further improve the product formation rates. The experiments (i) and (ii) show that O_2 is incorporated into the product and therefore essential for the reaction, and the presence of hydroxyl radicals (iii) is to be expected in a light-driven reaction involving H_2O_2. However, the degradation of N-CNDs under illumination (iv) suggests some kind of light-induced self-oxidation. Those results did not lead us to a clear conclusion. Therefore, we must conclude that the complete elucidation of the light induced H_2O_2 formation mechanism is beyond the scope of this communication.

With the right tools to stabilize the enzyme and to continuously provide H_2O_2 *in situ*, the next step was to select a solvent for the organic reaction medium to increase cyclohexane availability to the enzyme. Octane, heptane, cyclopentylmethylether (CPME), di*iso*propyl ether (DIPE), methyl *tert*-butylether (MTBE), 2-methyl tetrahydrofuran (2-MeTHF) and neat substrate were the possible candidates. First, enzyme stability was evaluated. Solutions of *Aae*UPO PaDa-I (0.5 mg mL^{-1}) in KPi buffer (100 mM, pH 7) saturated with organic solvents were prepared and subjected to NanoDSF measurements to assess the solvents effect on enzyme stability by determination of the infliction temperature (T_i). While the enzyme showed a T_i of 72.0 °C in untreated KPi buffer, and barely any stability loss with the hydrocarbon solvents, its stability and therefore T_i steadily decreased with increasing water solubility of the solvents, reaching 54.6 °C for 2-MeTHF (**Table 2**). The analysis of T_i values showed a clear trend where the T_i value decreases with decreasing *log*P values and therefore increasing hydrophilicity (**Table 2**). This can be explained by the enzyme's stability loss due to the molecular toxicity of the applied organic solvents dissolved in the aqueous medium. For example, the water solubility of 2-MeTHF is >2,000-fold higher than that of cyclohexane. However, the decrease in the T_i value from buffer to cyclohexane was only 0.6 °C, which makes it difficult to explain why no product formation was observed with free enzyme in

neat cyclohexane. Regardless, it showed that the use of cyclohexane as a neat substrate system is favoured compared to the other solvents screened.

Table 2. The list of solvents used to saturate KPi (50 mM, pH 7) buffer and the infliction temperature (T_i) of *Aae*UPO PaDa-I measured in solvent-treated aqueous media.

Organic solvent	*log*P	Solubility of the solvent in water at 20 °C (g L^{-1})	Infliction Temperature (T_i, °C)[a]
None	–	–	72.0
Octane	5.15	0.007	71.2
Heptane	4.66	0.02	71.7
Cyclohexane	3.4	0.06	71.4
DIPE	1.5	12	69.8
CPME	1.6	11	66.8
MTBE	0.9	42	66.5
2-MeTHF	1.1	140	54.6

[a] T_i values measured with Tycho NT.6 (NanoTemper Technologies, Germany) over T increase from 35 °C to 95 °C.

To conclude the solvent screening, the previously investigated solvents were used in combination with the PaDa-I alginate beads and N-CNDs in a small-scale photoreactor. As the N-CNDs (**SI Figure 17**), mainly absorb light in the UV range, with only a slight tailing into the visible wavelengths, UV LEDs with an emission peak at 391 nm were chosen. For the photocatalytic reactions, the reaction media were the organic solvents from **Table 2**, supplemented with 10 mM cyclohexane or the neat substrate cyclohexane. All organic solvents were saturated with water (a_w = 1). While heptane and octane were part of the NanoDSF analysis and gave valuable information about the relation of water solubility and enzyme stability, they are also potential substrates for UPOs[21c] and were therefore excluded from the following experiments. *Aae*UPO PaDa-I alginate beads (0.8 g, 13.5 U) and N-CNDs (4 mg) were mixed in the 4 mL glass vials by brief shaking, so the hydrophilic N-CNDs could spread throughout the water-rich beads. After addition of organic solvents and substrate the brown N-CNDs were clearly confined to the beads and did not mix with the organic phase surrounding them (**SI Figure 18 a**). The samples were then incubated in the photoreactor (**Figure 5**) at 30 °C and 200 rpm for 44 h. The GC analysis of the samples showed that cyclohexanol was only produced in the neat cyclohexane samples. Based on these results, neat cyclohexane was selected as the reaction medium of choice for further experiments.

After this proof-of-principle, an experiment to investigate the time course of the reaction and the effect of varying N-CND amounts was conducted. Three ratios of N-CNDs to enzyme (mg:nmol) were applied in the light-driven hydroxylation of neat cyclohexane: 4:1, 8:1 and 24:1. PaDa-I alginate beads (1 g, 28 U, 0.696 nmol enzyme) were mixed with the appropriate amount of N-CNDs and incubated with 1 mL cyclohexane for seven days under UV illumination at 200 rpm and 30 °C. 50 µL samples were taken every 24 h. While reactions with 4:1 and 8:1 ratio showed similar productivity up to day three, the one with 4:1 ratio stopped thereafter, whereas the 8:1 reaction continued until day five at the same rate (**Figure 3**).

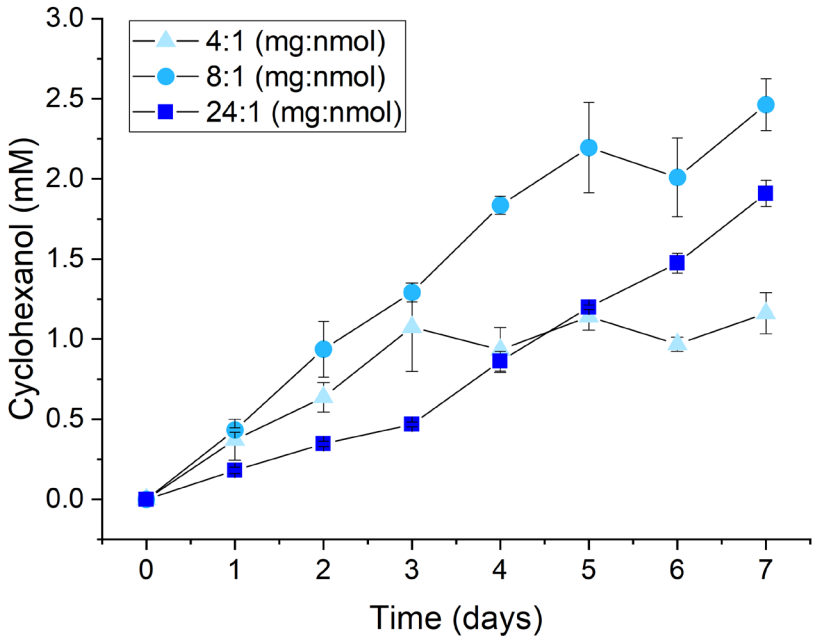

Figure 3. Hydroxylation of neat cyclohexane with PaDa-I alginate beads and varying ratios of N-CNDs to enzyme (mg:nmol): 4:1 (light blue triangles), 8:1 (blue circles), 24:1 (dark blue squares). Reactions run at 30 °C, shaking at 200 rpm, UV-LED illumination. The data points are connected by a solid line to guide the eye.

The 24:1 reaction however, showed a much lower product formation rate, only reaching 0.5 mM after three days (half the rate as compared to 4:1 and 8:1 reactions). It steadily continued at this rate and even after seven days showed no sign of slowing down (**Figure 3**). The low reaction rate of the 24:1 samples might be due to the excess amounts of N-CNDs having a shading effect thereby hindering the efficient use of light. Overoxidation in form of

cyclohexanone production was not detected. Negative controls with alginate beads without *Aae*UPO PaDa-I, but otherwise under identical conditions did not yield any product, ruling out hydroxylation of cyclohexane by N-CNDs. This also confirms the excellent *ee* value of (*R*)-1-phenyl ethanol by UPO catalysis. A regular sample incubated in the dark showed only trace amounts of product formation, demonstrating the reaction's dependence on light.

We also set up two reactions with a photocatalyst-to-enzyme ratio of 4:1 under the same conditions applied in **Figure 3**, where one reaction was resupplied with N-CNDs after three and five days. No increase in productivity upon fed-batch photocatalyst addition was detected (data not shown). Hence, enzyme stability rather than photocatalyst stability is a limiting factor in this reaction.

In order to show the applicability for another substrate, the small alginate beads were used for the hydroxylation of cyclopentane (**SI Figure 22**). Applying the same conditions as in **Figure 3** with an 8:1 N-CND-to-enzyme ratio, the reaction only produced 1 mM cyclopentanol after three days, exhibiting a much lower performance than for cyclohexane.

To investigate whether mass transfer limitations were also involved, smaller alginate beads ($ø_{bead}$ of 0.9 mm instead of 2.7 mm) were prepared and used for light driven cyclohexane hydroxylation with N-CNDs. The beads were only one third in diameter compared to the previously used ones and therefore had three times the specific surface area. However, this also increased enzyme loss during immobilisation. When used in the reaction with a 8:1 (mg:nmol) N-CND:enzyme ratio under UV illumination as described above, the smaller beads yielded similar reaction rates as the big ones, with only a third of the enzyme amount (**SI Figure 21**). Producing 2.25 mM cyclohexanol in four days they showed a productivity of 0.08 $mM_{product}\ \mu M_{UPO}^{-1} \times h^{-1}$ with 7,806 turnovers per enzyme.

The following results on the 365 nm light reactor and product absorption were not part of the original publication, but are still included in the thesis as they deliver some more insight:

A major factor in all light driven reactions is light intensity. With the current setup however, adjustment of light intensity was not possible. Therefore a new light reactor featuring high power adjustable 365 nm LEDs was constructed (**Figure 6**). A parameter to consider when using high power lights is the heat that is released. To look into this, a solution of N-CNDs (2 mg/mL) was incubated in the reactor and the temperature measured with a Pt100 probe. The heating above ambient temperature (23 °C) was quite drastic for higher power settings, increasing the temperature by 25 °C and 15 °C for 100% and 50% power respectively. For the lower setting of 27%, temperature increased by a moderate 9 °C. The old reactor using 391 nm LED strips increased the temperature by 8 °C, therefore the 27% setting of the new reactor was nicely comparable to the old reactor. Both reactors were used for the hydroxylation of 1 mL neat cyclohexane using 1 g PaDa-I alginate beads (1 mm diameter) and 8:1 N-CNDs to enzyme (mg:nmol) at 30 °C and 200 rpm. The new photoreactor delivered a higher initial reaction rate, but the reaction stopped earlier, producing 1.7 mM cyclohexanol while the old reactor reached 2.25 mM after four days. Furthermore, the 365 nm reactor produced more of the overoxidation product cyclohexanone (**Figure 4**). This indicates that the light intensity is definitely a factor to optimize in future experiments.

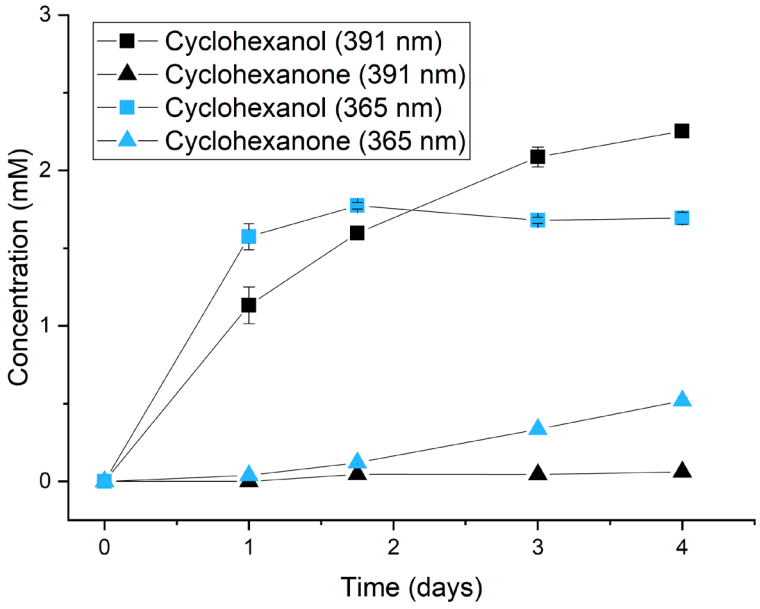

Figure 4. Formation of cyclohexanol and cyclohexanone with PaDa-I alginate beads and N-CNDs under illumination of 365 nm and 391 nm.

Another factor is the relatively large amount of alginate beads, 1 $g_{beads}/mL_{cyclohexane}$. In an effort to understand how much product is adsorbed to the beads, 0.5 g alginate beads were incubated with 0.5 mL cyclohexane containing 20 mM cyclohexanol and cyclohexanone. GC analysis of the liquid phase showed that 54% of cyclohexanol and 27% of cyclohexanone were removed from the solution and stuck to the biocatalyst preparation (**SI Figure 24**).

3.4. Conclusion

In conclusion, we demonstrated the application of UPO-catalysed hydroxylation of neat alkane model substrate coupled with a photocatalyst. While the productivity of this system is still lacking, it demonstrates a proof-of-principle for the application of photobiocatalysis in organic media. Finally, the fact that the 2-in-1 heterogeneous photobiocatalyst works for several days and the possibility to optimize the enzyme-to-photocatalyst ratio, are promising starting points for further developments towards higher volumetric productivities. These principles demonstrated here can be used for future hydroxylations of hydrophobic value added compounds in neat conditions.

3.5. Material and Methods

Chemicals: Chemicals were purchased from Carl Roth (Germany), Acros (USA), Merck (Germany), Sigma-Aldrich (USA) and VWR (USA) in synthesis quality and used without further treatment.

Enzyme production: A crude concentrate of *Aae*UPO PaDa-I (30.3 µM), expressed in *Pichia pastoris*[42g] was supplied by Dr. Florian Tieves (TU Delft).[44]

Standard ABTS activity assay: The assay was done in 100 mM sodium phosphate/citrate buffer pH 4.4, with 0.3 mM 2,2'-azino-bis(3-ethylbenzothiazoline-6-sulphonic acid) (ABTS) and 2 mM H_2O_2 in semi-micro cuvettes. The measurements were done at 25 °C and 405 nm in a Cary 60 UV-Vis spectrophotometer (Agilent Technologies Inc., USA), and the activity was calculated with the millimolar extinction coefficient of oxidized ABTS at 405 nm (36.8 mM^{-1} cm^{-1}).

Enzyme immobilization in alginate beads: 5 mL solution of 2.5% sodium alginate (Sigma-Aldrich) was prepared and slowly mixed with 150 µL enzyme solution (30.3 µM). The solution was filled into a syringe and dripped into a stirred 100 mM $CaCl_2$ solution through a syringe needle (0.6 x 30 mm). After stirring for five more minutes, the alginate beads were recovered by filtration. To determine the enzyme loss during immobilization the enzyme activity in the left over $CaCl_2$ solution was determined by ABTS assay, alongside with the enzyme solution used for immobilization. By relating the known enzyme concentration in the initial enzyme solution to the measured activities, the loss and enzyme concentration in the beads could be calculated. To decrease the bead size, air with a pressure of 2 bar was streamed through a tube (Saint-Gobain 0.125 x 0.250) over the needle.

Water activity (a_w) adjustments: In initial experiments solvents were adjusted to an a_W value of 0.53 by incubating them in a desiccator containing a saturated $Mg(NO_3)_2$ solution for three days at room temperature. Correct a_w values were confirmed by using the humidity sensor HMT337 (Vaisala, Finland). The a_w value of 1.0 was achieved by combining the solvent 1:1 with water, vigorous shaking and phase separation by centrifugation. The organic phase saturated with water was then used for the experiments.

Emission spectrum of LEDs: A MSC15 spectrometer (Gigahertz-Optik, Germany) was used to measure the emission spectra of blue (YourLED Stripe basic set 1.5m RGB, Paulmann, Germany, 40 LEDs/m) and UV LEDs (UV Black Light Strip, DeepDream Inc., China, 60 LEDs/m) by holding one LED directly on the sensor under a black cloth cover.

Synthesis of N-CNDs: Nitrogen doped carbon nanodots (N-CNDs) were prepared according to Kim et al. 2018.[84] Briefly, citric acid (105 mg ml^{-1}) and ethylene diamine (33.5 µL ml^{-1}) were dissolved in deionized water. The solution was transferred to a stainless steel autoclave reactor and heated at 200 °C for five hours. After the hydrothermal process, the autoclave was cooled down to acquire a dark brown solution of N-CNDs. For purification, the solution was centrifuged at 15,000 rpm for 30 min to eliminate insoluble large particles; the supernatant was dialyzed (molecular weight cut-off: 1,000 Da) against deionized water for three days. The purified solution was lyophilized to obtain the powder of N-CNDs. Carbon nanodots were already used for light driven UPO reactions before.[48] However, they were made solely from citric acid. In the production of the carbon nanodots used in this study, ethylene diamine was added, providing the nitrogen doping.

Absorption measurement of N-CNDs: Absorption spectrum of a 0.02 mg mL^{-1} N-CND solution in deionized water was determined with a Cary 60 UV-Vis spectrophotometer (Agilent Technologies Inc., USA).

Stability measurements with NanoDSF: For the assessment of the influence of organic solvents enzyme stability potassium phosphate (KPi) buffer pH 7 (50 mM) was mixed 1:1 (v:v) with the solvent, vortexed and the phases were separated by centrifugation. The solvent-saturated buffer was then used to prepare a dilution of the 30.3 µM PaDa-I solution (14 µL enzyme + 86 µL buffer) of 0.5 mg enzyme per mL. This solution was used to fill Tycho™ Nt.6 capillaries and for fluorescence measurement during a temperature increase from 35 °C to 95 °C. *Aae*UPO PaDa-I contains one tryptophan (Trp) and nine tyrosine (Tyr) residues, which can be detected in the fluorescence measurements by the Tycho NT.6 (Nano

Temper Technologies GmbH, Germany). As the protein unfolds, the fluorescence ratios of 350 nm / 330 nm change and the infliction temperature (T_i) is determined. Higher T_i value states higher stability since unfolding occurs first at higher temperatures.

Photoreactions: The reactions in aqueous media using ethylbenzene as a model substrate, were conducted in a photoreactor previously described by Zhang et al. at TU Delft.[85] It is illuminated by a light bulb (Philips 7748XHP 150 W, white light bulb) positioned 3.6 cm from the reaction vials. Whereas, the photoreactor used for cyclohexane hydroxylation consists of a crystalizing dish (14 cm x 7.5 cm) wrapped with 1.5 m UV LED strip (DeepDream Black Light Strip) and contains a custom-built holder for twelve 4 mL glass vials (**Figure 5**). There is a distance of 8 mm between the vials and the light source. The reactor is mounted on the adhesive pad of a New Brunswick™ Innova® 44R incubator for shaking and temperature control. Since the vial holder is not fixed to the reactor, it rotates slowly (~1 rpm at 200 rpm shaking) inside the crystalizing dish, providing uniform illumination for all vials.

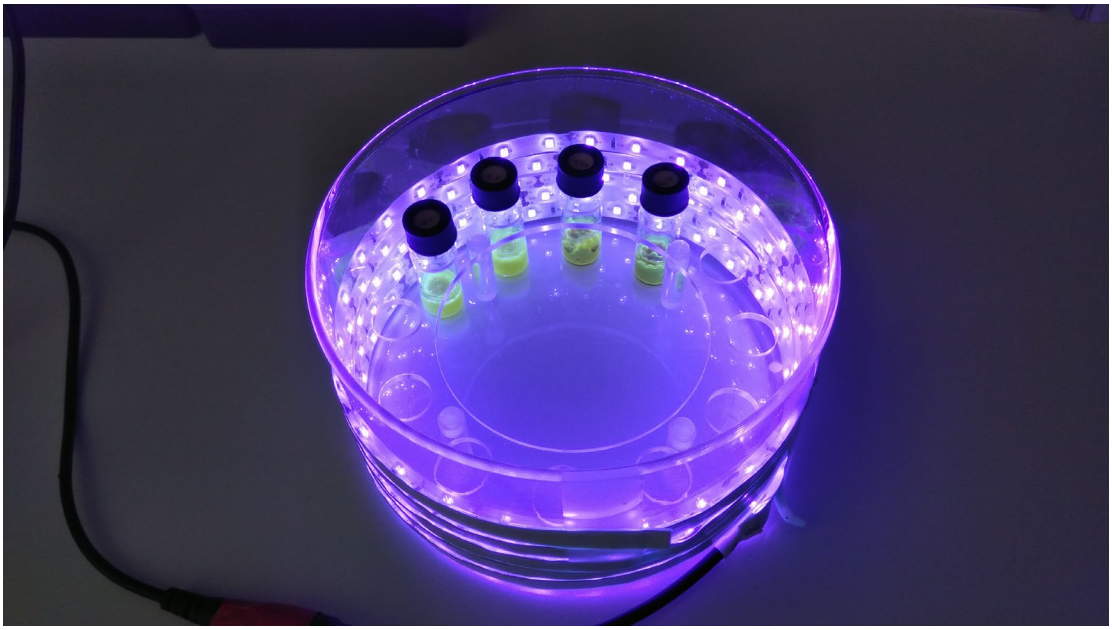

Figure 5. 391 nm UV photoreactor holding four out of 12 possible vials.

GC Analysis: For qualitative analysis of cyclohexane hydroxylation the samples were dried with $MgSO_4$ and injected into the GC, while for quantitative analysis a multipoint

calibration with dodecane as an internal standard was used (both method 1). 50 µL of sample were mixed with 50 µL of MTBE containing 5 mM dodecane. Both were measured with a Bruker SCION 436-GC and CP-8400 Autosampler with helium as the mobile phase on a ß-DEX 120 column (30 m × 0.2 mm ID × 0.25 µm, Supelco® Analytical, USA). (**Figure 3, S2 & S12**) Method 1: 50 °C hold for 3 min, 20 °C/min to 100 °C, 5 °C/min to 130 °C, 40 °C/min to 220 °C. Retention times: cyclohexanone 9.66 min, cyclohexanol 10.75 min, dodecane (internal standard) 11.6 min.

For evaluation of ethylbenzene hydroxylation with Method 2 (**Figure 2 & S4**), sample analyses were performed on Shimadzu GC-2010 Plus GC with an AOC-20i Auto injector with FID (Shimadzu, Japan), using N_2 as the carrier gas on a CP wax 52 CB column (25 m × 0.2 mm ID × 1.20 µm). Samples were extracted 1:1 with ethyl acetate. Method 2: 150 °C, hold for 2.2 min, 25 °C/min to 210 °C, hold for 3.8 min, 30 °C/min to 250 °C, hold for 1.0 min. Retention times: ethylbenzene (2.9 min), 1-octanol (5.2 min), acetophenone (6.7 min), and phenylethanol (8.0) min.

The enantiomeric excess (ee) value of *(R)*-(1)-phenyl ethanol was determined on a Chirasil Dex CB column (25m, 0.32 mm x 0.25 µm) with a linear velocity of 29.8 cm per second. Method: 120 °C, hold for 2.6 min, 15 °C/min to 135 °C, hold for 3.3 min, 25 °C /min to 225 °C, hold for 1.0 min.

The light driven hydroxylation of cyclohexane and cyclopentane with N-CNDs and smaller PaDa-I alginate beads (**SI Figure 21** & **Figure 22**) was analyzed in a Shimadzu Nexis GC-2030 with AOC-20 Autosampler on a ß-DEX 120 column (30 m × 0.2 mm ID × 0.25 µm, Supelco® Analytical, USA) and FID detector with method 3: 70 °C hold for 5 min, 10 °C/min to 120 °C, hold for 5 min, 20 °C/min to 210, hold for 1 min.

GC-MS: A GC-MS (GC-2010) system from Shimadzu (Japan) with auto-injector (AOC-20i) was used to determine ^{18}O insertion. Column: Agilent CP SIL-5, length: 25 m, ID: 0.25 mm, film thickness: 0.40 µm. Helium was used as the mobile phase.

Method: 70 °C hold for 3 min., 25 °C/min to 120 °C, hold for 0.5 min, 30 °C/min to 325 °C, hold for 1 min.

N-CND degradation by light: The potential degradation of N-CNDs by light was monitored by incubating an N-CND solution (0.04 mg ml^{-1}) in the UV light reactor in a shaking incubator at 30 °C and 200 rpm. The samples were prepared in H_2O, pH was adjusted to pH 7.0 with NaOH. As a reference, two samples (one with 2 mM H_2O_2 added) were incubated in the dark under otherwise identical conditions. After 24 h the sample was diluted 1:2 and the absorption spectrum was measured as described above.

EPR Spectroscopy: Electron paramagnetic resonance (EPR) spectroscopy was performed with 2.5 mg ml^{-1} of N-CND and 50 mM of DMPO (5,5-dimethyl-1-pyrroline N-oxide)(to get stable spin adducts) in a 100 mM KPi buffer at pH 7.0 and at room temperature. The EPR tube was illuminated by a Kaiser Fiber Optic Lighting system 15 V, 150 W (visible light).

Light reactions at 365 nm: The more powerful photoreactor was constructed featuring dimmable 365 nm LED bars (PowerBar V3 LED Module 365 nm) mounted on a heat sink (both LUMITRONIX® LED-Technik GmbH, Germany) powered by a general purpose power supply (Blanko PS-3005, Sintron Vertirebs GmbH, Germany), holding up to six 4 mL vials**.** Reactor was mounted on adhesive pads in a New Brunswick™ Innova® 44R incubator for shaking and temperature control.

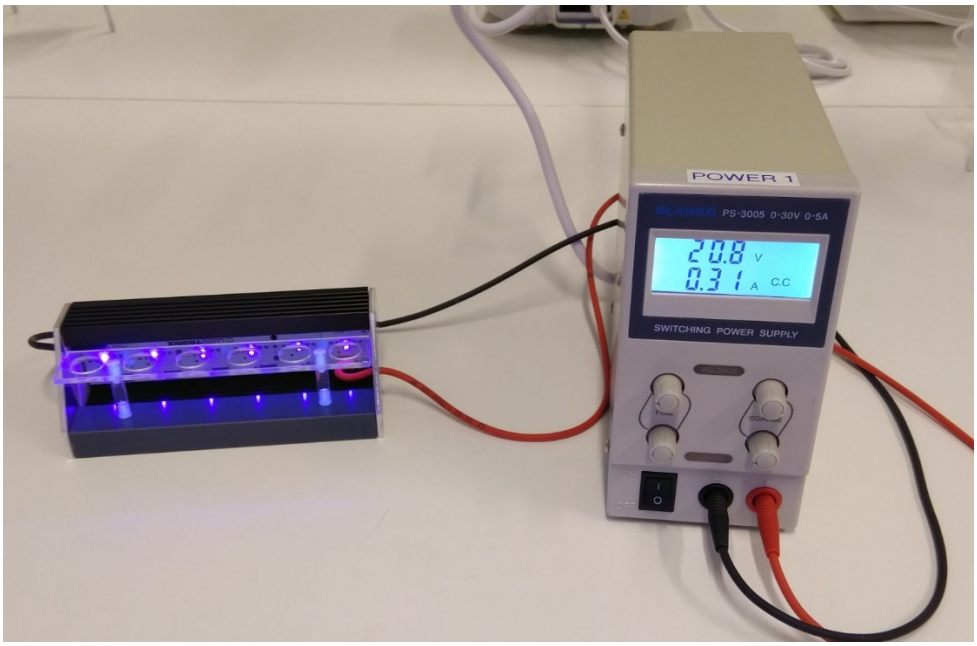

Figure 6. 365 nm photoreactor with adjustable powersource.

Product absorption on Alginate beads: To determine product absorption on alginate beads, 0.5 mL cyclohexane containing 20 mL cyclohexanol and cyclohexanone was incubated with 0.5 g alginate beads in glass GC vials at 30 °C and 800 rpm. The decrease of cyclohexanol and cyclohexanone was measured over time.

4. Internal Illumination to Overcome the Cell Density Limitation in the Scale-up of Whole-cell Photobiocatalysis

Chapter 4 and its sub-chapters are taken from Article II[86] with changes only regarding the page layout and small stylistic alterations without changing the main content.

4.1. Abstract

Cyanobacteria have the capacity to use photosynthesis to fuel their metabolism, which makes them highly promising production systems for the sustainable production of chemicals. Yet, their dependency on visible light limits the cell-density, which is a challenge for the scale-up. Here, we show with the example of a light-dependent biotransformation that internal illumination in a bubble column reactor equipped with wireless light emitters (WLEs) can overcome this limitation. Cells of the cyanobacterium *Synechocystis* sp. PCC 6803 expressing the gene of the ene-reductase YqjM were used for the reduction of 2-methylmaleimide to (*R*)-2-methylsuccinimide with high optical purity (>99% *ee*). Compared to external source of light, illumination by floating wireless light emitters allowed a more than two-fold rate increase. Under optimized conditions, product formation rates up to 3.7 mM h^{-1} and specific activities of up to 65.5 U g_{DCW}^{-1} were obtained, allowing the reduction of 40 mM 2-methylmaleimide with 650 mg isolated enantiopure product (73% yield). The results demonstrate the principle of internal illumination as a means to overcome the intrinsic cell density limitation of cyanobacterial biotransformations, obtaining high reaction rates in a scalable photobioreactor.

4.2. Introduction

Photobiocatalysis has emerged as a new, exciting research area that combines photocatalysis and biocatalysis, two of the most research-intensive fields of catalysis.[68] In particular, whole-cell biotransformations in cyanobacteria allows to produce highly selective biocatalysts from carbon dioxide and water, and to exploit photosynthesis for the regeneration of ATP and redox cofactors.[70] This allows the saving of stoichiometric addition of auxiliary cosubstrates such as isopropanol and glucose for redox biotransformations. As

only a minor part of the electrons donor molecules is used for the redox reaction, the use of catalytic water splitting leads to a more favorable atom economy, one of the 12 principles of green chemistry.[87] Furthermore, the formation of coupled by-products often complicates downstream processing. Using water as a sacrificial electron donor is a radical approach that has the potential to solve this critical limitation of the sustainability of enzymatic redox processes. Coupling of oxidoreductases to the photosynthetic electron transport chain of cyanobacteria has been demonstrated for a wide range of biocatalytic reactions,[68, 88] including ene-reductases,[70] alcohol dehydrogenases,[73] Baeyer-Villiger monooxygenases,[71] heme-independent monooxygenases,[89] P450 monooxygenases,[74, 90] and imine reductases[91] with reaction rates as high as 150 units per gram cells.[92] A major environmental advantage of cyanobacterial biotransformation is the sustainable production of the biocatalyst, with light as an energy source and CO_2 as a carbon source.[93] From a physiological viewpoint it is important to note that light-driven biotransformations consume electrons from the photosynthetic electron transport chain, but do not require fixation of carbon dioxide. This could be an explanation why cyanobacterial photobiotransformations are much faster than the production of various C-metabolites.[94] For the metabolic engineering of cyanobacterial whole-cell biocatalysts, both the variation of the intracellular enzyme concentration[91] and the deletion of other electron-consuming processes[90, 92] have been proven as successful strategies. While photobiotransformations have been established with high reaction rates, the scale-up of the reaction requires a photobioreactor geometry with very short light penetration pathways. On the one hand, this regards the overall light availability in a reactor, taking into account that the light penetration in water is limited and cells strongly absorb visible light. On the other hand, the reactor should have a continuous light distribution to avoid fluctuation, which has physiological consequences for the cells.[95] Typical photobioreactors are based on flat-panels or tube reactors with low to moderate surface-to-volume ratios. Internal illumination shortens light pathways.[96] Among them is a new reactor concept developed by Buchholz *et al*., which utilizes freely suspended wireless light emitters (WLEs).[97] These WLEs consist of a single light emitting diode (LED) with a receiving coil encapsulated in a polycarbonate shell powered via induction by emitting coils from outside of the reactor. Among the various concepts mentioned above, this approach shows the highest surface-to-volume ratio (SVR)[64b] and provides evenly distributed light

within the photobioreactors;[97] this was exploited recently by Duong and coworkers for the intensification of a photoenzymatic reaction.[98] This concept is especially intriguing as it allows to work with column reactors of a larger diameter than externally illuminated photobioreactors.

As a model system, we chose the light-driven ene-reduction of 2-methylmaleimide (2-MM) catalyzed by an ene-reductase YqjM from *Bacillus subtilis* heterologously expressed in a model cyanobacterium *Synechocystis* sp. PCC 6803 (*Synechocystis* from here). This reaction proceeds with high stereoselectivity and represents a typical stereoselective redox reaction for the synthesis of fine chemicals. The specific activity of 180 µmol per hour and per mg chlorophyll a (µmol $mg_{chl\,a}^{-1}$ h^{-1})[92] consumes a considerable part of the total photo-production of NADPH that has been estimated to be in the range of 530 to 1070 µmol $mg_{chl\,a}^{-1}$ h^{-1}.[99] In this article, we investigate the effect of internal illumination on the initial reaction rate and volumetric yield in the scale-up of a photobiocatalytic asymmetric enzymatic ene-reduction in recombinant cells of *Synechocystis*.

4.3. Results and Discussion

Synechocystis P_{cpcB}::*yqjM* was cultivated in 200 mL gas washing bottles under continuous light illumination reaching an OD_{750} 1-3 (**SI Figure 27 a**), harvested and utilized in whole cell light-driven reduction of 2-methylmaleimide (2-MM) to (*R*)-2-methylsuccinimide (2-MS) (**Figure 7 a**) with external illumination using LED lamps (200 µE m^{-2} s^{-1}). As reported previously[70, 92], the specific activity and the product formation rates showed a strong dependency on the cell density applied (**Figure 7**). Within the analyzed cell density range (0.48 – 2.4 g L^{-1}) at 1 mL scale, the specific activity of the cells dropped notably at cell densities higher than 1.2 g L^{-1}. Notably, the specific activity at 2.4 g L^{-1} was only about half of that at 0.48 g L^{-1} (**Figure 7 b**). The correlation between the initial reaction rate with cell density was observed up to a cell density of 1.8 g L^{-1}, where a further increase to 2.4 g L^{-1} did not improve the rate anymore.

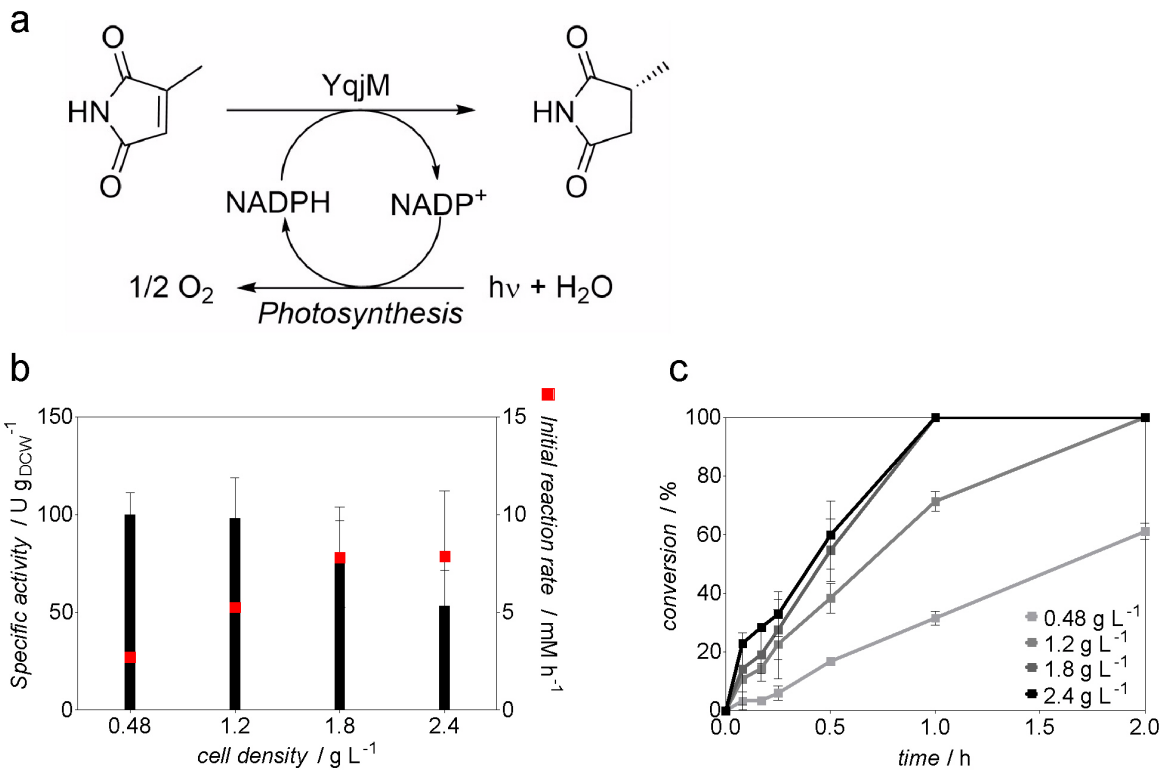

Figure 7. a): Whole cell light-driven biotransformations catalyzed by *Synechocystis* P_{cpcB}::*yqjM*. b) Specific activity and initial product formation rates achieved at 1 mL-scale using various cell densities, independent biological triplicates; c) Conversion of 2-MM during photobiotransformations (1 mL, 10 mM 2-methylmaleimide, 160 rpm, 30 °C, 200 µE m^{-2} s^{-1}), independent biological triplicates.

The results in 1 mL scale show a clear decrease of productivity per cell at higher cell density. A larger reaction volume with longer light pathways is expected to increase this effect. Yet, achieving high reaction rates requires higher cell densities. Additionally, it should also be noted that a steady light intensity is important because fluctuating light affects the physiology of the cyanobacteria.[100] On basis of these considerations, we reasoned that it would be difficult to achieve a high productivity at cell densities exceeding 1.8 g L^{-1} with external illumination. Internal illumination, however, provides much shorter light pathways and the beneficial effect for photo-biocatalytic reactions has been demonstrated recently.[70] Therefore, a bubble column reactor (BCR) with internal illumination provided by WLEs appeared to be the ideal solution for the intensification and scale-up of cyanobacterial biotransformations (**Figure 8**).

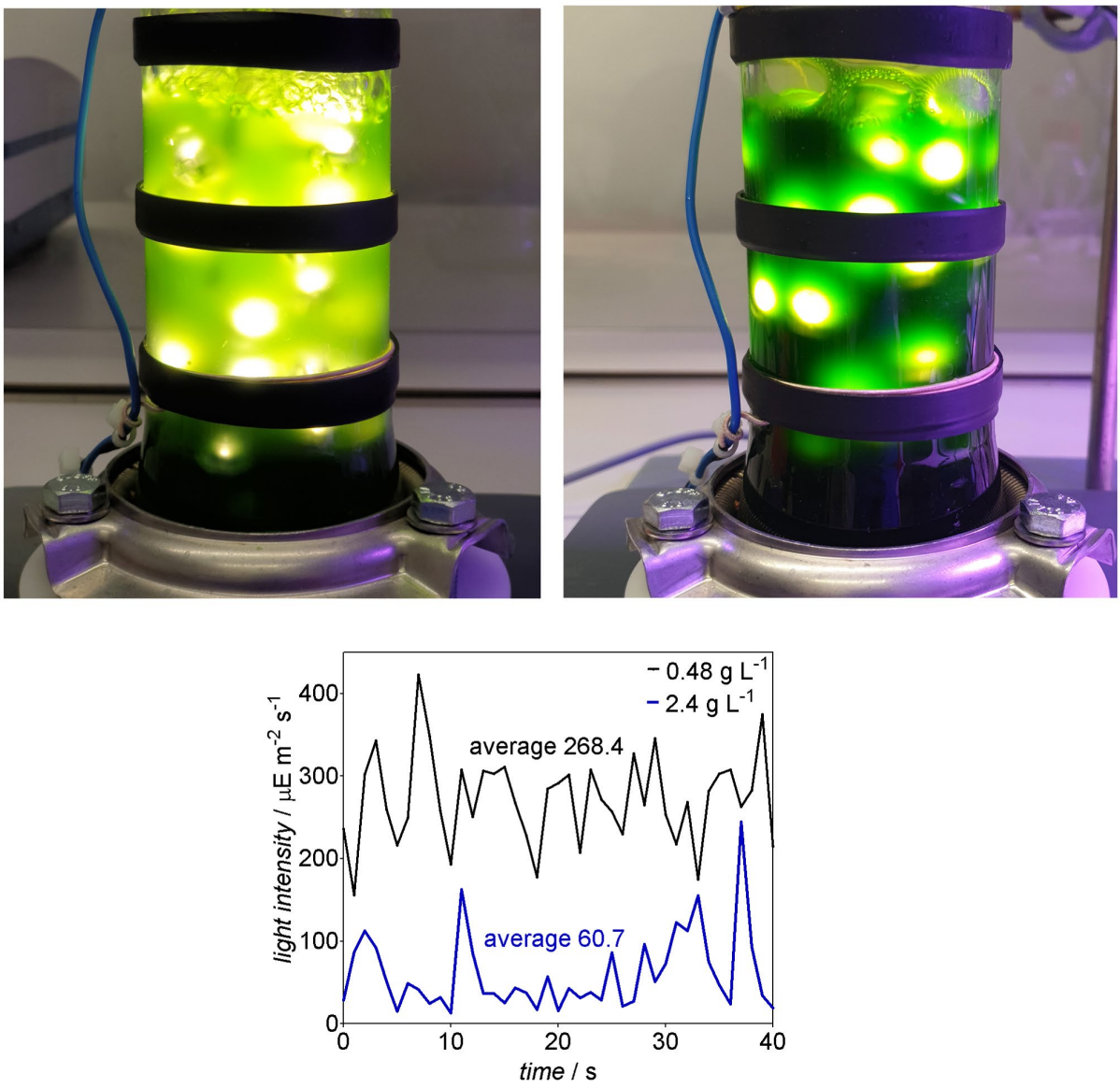

Figure 8. Above: Photo-biotransformations performed in the BCR with internal illumination provided by 40 floating wireless light emitters at a cell density of 0.48 g L^{-1} (left side) and 2.4 g L^{-1} (right side). Below: determination of the light intensity inside BCR with internal illumination by 40 WLEs at a cell density of 0.48 g L^{-1}or 2.4 g L^{-1}, respectively.

The effect of the number of WLEs on the photo-biotransformations was initially evaluated. Therefore, 20, 30 or 40 WLEs were used in a 200 mL reaction volume with *Synechocystis* P_{cpcB}::*yqjM* at a cell density of 0.48 g L^{-1} and 30 °C and 10 mM 2-methylmaleimide as a substrate. Among the investigated numbers of WLEs, the use of 40 yielded the highest specific activity of 83 U g_{DCW}^{-1}, which is well within the range of the rates observed in 1 mL scale experiments (**Figure 9 a**, **Figure 7 b**). At a cell density of 1.2 g L^{-1}, 20 WLEs led to an

activity of 35.8 U g_{DCW}^{-1}, whereas 40 WLEs allowed to reach an activity of 65.5 U g_{DCW}^{-1} (corresponding to 5.31 U mg_{Chla}^{-1}) (**Figure 9 a**). The initial product formation rate for the latter reaction was 3.6 mM h^{-1}. Besides the overall availability of the light, its distribution should be as even as possible in the photobioreactor because the cells adapt to fluctuating light with the activation of protection systems such as flavodiiron proteins that constitute an additional electron sink.[95] **Figure 8** shows that at a cell density of 0.48 g L^{-1}, the light distribution in the bubble column reactor is quite even. At a cell density of 2.4 g L^{-1}, however, a considerable light fluctuation is apparent, both visually and by measuring at a specific site at different time points.

Further increasing the cell density to a value of 2.4 g L^{-1} resulted in shortening the reaction time, which allowed to achieve a full conversion after 3.5 h with an initial activity of 32.5 U g_{DCW}^{-1} (2.74 U mg_{Chla}^{-1}) and an initial reaction rate of 3.7 mM h^{-1} (**Figure 9 a**). At a cell density of 2.4 g L^{-1}, the strong effect of the light absorption of the cells could be clearly seen as light intensity inside the BCR dropped by 53% (**Figure 8**). Increasing the cell density from 0.48 to 2.4 g L^{-1} resulted in a 61% decrease of the specific activity. This activity drop is stronger than the one observed in the externally illuminated 1-mL scale. Nevertheless, using internal illumination allowed to retain 80% of activity at a cell density of 0.48 g L^{-1}, 64% at 1.2 g L^{-1} and 58% at 2.4 g L^{-1} compared to the 1 mL-scale reactions. Using cells at a density of 2.4 g L^{-1} resulted in the highest initial reaction rate of 3.7 mM h^{-1}, corresponding to 47% of the initial product formation rate from 1-mL scale. Keeping the reaction time short is not only important for cost-effectiveness, but also needed for selectivity towards the target product as the cells can also unproductively consume the substrate 2-MM (**SI Figure 30**). Doubling the cell concentration and the number of WLEs increased the reaction rate almost two-fold, as 1.2 g L^{-1} of cells with 20 WLEs resulted in 1.2 mM h^{-1} while for 2.4 g L^{-1} and 40 WLEs resulted in 2.3 mM h^{-1}.

Comparison of internal illumination using WLEs with external illumination and biotransformations without illumination underlined clearly the beneficial effect of the WLEs on the productivity of the whole-cell biocatalyst. It is known that *Synechocystis* cells have the capacity to achieve some conversion in darkness or in presence of inhibitors of photosynthesis[70, 88g, 101], which has been attributed to the utilization of storage compounds

that were accumulated during the cultivation phase. During the light cycle, cyanobacteria produce NADPH via photosynthesis. In absence of light, the pentose phosphate pathway is assumed to be the main source of reducing equivalents.[102] It should be noted, however, that the contribution of glycolytic routes in cyanobacteria is far from being understood.[103] For these reasons, we expected some conversion for reactions in darkness or with external illumination. Indeed, external illumination with an intensity of 300 µE m^{-2} s^{-1} provided by LED strips (**SI Figure 31**), resulted in a 75% drop of specific activity for cell density of 1.2 g L^{-1} and 81% for 2.4 g L^{-1}.

At 1.2 g L^{-1} and 2.4 g L^{-1} of cell density, the specific activity was 2.7 and 3-fold higher respectively when using internal illumination with 40 WLEs, clearly showing the advantage of the WLE technology. The specific activities of *Synechocystis* P_{cpcB}::*yqjM* at a cell density of 2.4 g L^{-1} externally illuminated were surprisingly similar to the reaction in darkness, although the dark reaction slows down over time (**Figure 9 d**). Light measurements inside the BCR using external illumination (2 µE m^{-2} s^{-1}, **SI Figure 26 c**) show that cells might be facing darkness occurring locally or temporarily, which is a typical problem of large-scale photobioreactors.[64b] Nevertheless, the comparison of the internal and external illumination clearly shows the advantage of the former for photobiotransformations at higher cell densities.

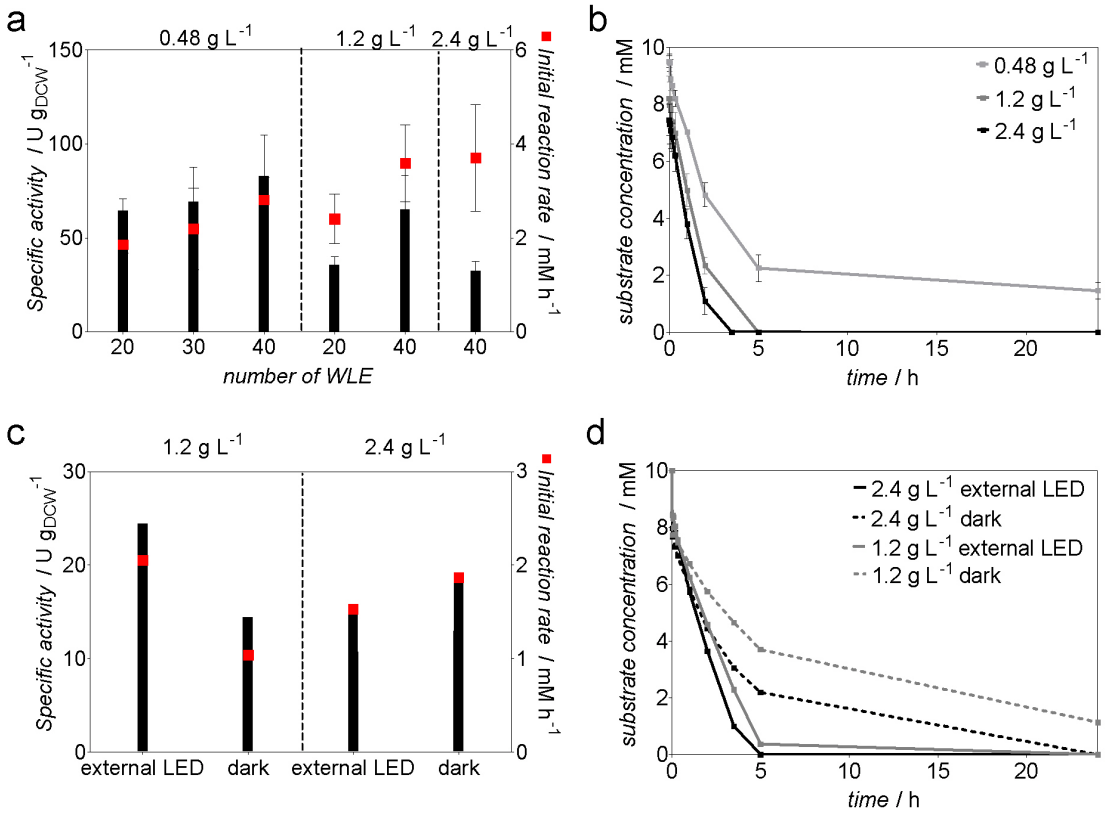

Figure 9. Whole cell biotransformation catalyzed by *Synechocystis* P_{cpcB}::*yqjM* in a BCR. a) Specific activity and initial product formation rate of *Synechocystis* P_{cpcB}::*yqjM* in a BCR with internal illumination provided by WLEs (200 mL, 10 mM 2--methylmaleimide, 0.6 L min^{-1} airflow), independent biological triplicates; b) Time course of the reactions using different cell densities with 40 WLEs, independent biological triplicates; c) Specific activity and initial product formation rate of *Synechocystis* P_{cpcB}::*yqjM* in a BCR externally illuminated with LED strips (300 µE m^{-2} s^{-1}) or in dark (200 mL, 10 mM 2-methylmaleimide, 0.6 L min^{-1} airflow), single measurements; d) Time course of the reactions with external illumination or in dark, single measurements.

We have shown previously that a higher cellular enzyme concentration leads to improved reaction rates.[72, 101] Therefore, we use the light-inducible promoter P_{psbA2} for the expression of the enzyme. For induction, we cultivated the cells at a light intensity of 230 µE m^{-2} s^{-1}, which is sufficient for an induction of this promoter. The results of the biotransformation with *Synechocystis* P_{psbA2}::*yqjM* indicated a slight improvement in the initial specific activity of 38 U g_{DCW}^{-1} compared to 32.5 U g_{DCW}^{-1} obtained with *Synechocystis* P_{cpcB}::*yqjM*, with 4.1 mM h^{-1} product formation rate (**Figure 10 b**). In order to achieve fast full conversion, a reaction was run with *Synechocystis* P_{cpcB}::*yqjM* at a cell density of 2.4 g L^{-1} and 40 WLEs using 10 mM 2-MM as substrate (**Figure 10 c**). The product was isolated after 5h of the reaction.

After cell removal and extraction with ethyl acetate, NMR analysis showed an isolated yield of 157.4 mg pure product (71% yield) (*R*)-2-methylsuccinimide (2-MS) in outstanding optical purity (99% *ee*).

It should be noted that the product could be obtained in very high purity without the need for purification by flash chromatography, which simplifies the downstream processing and cuts the costs (**SI Figure 28** & **Figure 29**). Further intensifying the process by the addition of 40 mM 2-MM by substrate feeding approach resulted in full conversion in 22h (**Figure 10 d**), producing 650 mg pure (*R*)-2-methylsuccinimide (73% yield) with >99% *ee*.

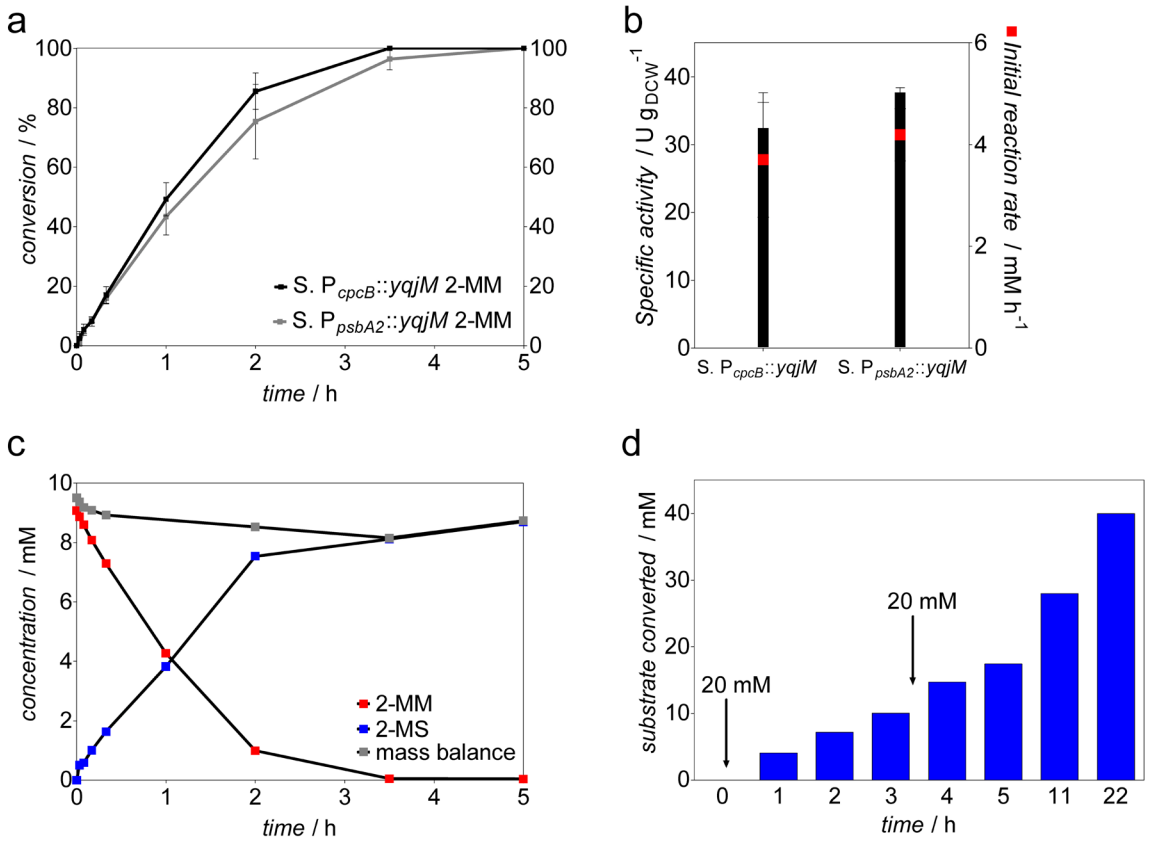

Figure 10. a) Conversion of 10 mM 2-MM into corresponding 2-MS during photobiotransformations catalyzed by *Synechocystis* P_{cpcB}::*yqjM* and *Synechocystis* P_{psbA2}::*yqjM* both at a cell density of 2.4 g L^{-1}; b) Specific activity and initial product formation rate of *Synechocystis* P_{cpcB}::*yqjM* and *Synechocystis* P_{psbA2}::*yqjM*; c) Time course of the preparative 10 mM 2-MM photobiotransformation catalyzed by *Synechocystis* P_{cpcB}::*yqjM,* single measurements; d) 2-MM substrate converted by *Synechocystis* P_{cpcB}::*yqjM* cells (2.4 g L^{-1}) using a substrate feeding approach, with initial substrate concentration introduced 20mM and a subsequent feeding of 20 mM at 3 h, single measurements.

Previous light-driven biotransformations scale-up systems using stirred-tank photobioreactors at the cell density of 0.5-0.8 g L^{-1}[74] or 1.6 g L^{-1}[104] point to the problem of high cell densities to be applied. Photobiotransformations could benefit from the developed technologies for the high cell density cultivation that reached up to 50 g L^{-1}, such as thin-layer cascade photobioreactors[105] and CellDeg system cultivations.[106] However, the application of these set-ups in the scale-up of light-driven biocatalysis needs to be followed by the appropriate development of efficient light sources with beneficial light penetration depths, where WLEs and technologies such as light guides (e.g. optical-fibers illumination[107]) can play an important role. The cost of the WLEs itself, their durability and the efficiency of energy transfer via inductions might be drawbacks of the BCR; nevertheless, our results show that the principle of internal illumination bears clear advantages over external light supply. Future research will focus on the identification of the best way to combine an internal light source with an efficient mixing of the reaction, both in view of efficiency and practicability.

Easier handling and scalability of BCR with higher volume is an advantage of this technology, as these bioreactors can be filled up to higher volume without influencing surface to volume ratio (while appropriately increasing the number of WLEs). This reactor concept is generally applicable for recently described whole-cell biotransformations[68, 108], keeping in mind that volatile substrates pose a problem. Other reactor concepts, such as capillary biofilm reactors operated at higher cell densities up to 52 g L^{-1} show another promising approach, but one of the bottlenecks for applications are the extreme long times for biofilm maturation (up to 5 weeks).[109] One of the concerns with cultivation set-ups for high cell density is the CO_2 supply across the gas-liquid interface, which could be problematic with longer BCR geometries. It should be noted, however, that the biotransformation does not require CO_2 itself. Moreover, the presence of the ene-reduction as a strong electron sink might alleviate the need of CO_2 fixation from a metabolic point of view.[110] While we indeed did not observe any positive effect of higher CO_2 supply or $NaHCO_3$ addition during small-scale biotransformation reactions (unpublished), this idea remains to be proven experimentally. Another problem that might limit the applicable length of the BCR could be the accumulation of oxygen, which could lead to photoinhibition.[111]

4.4. Conclusion

The strong light absorption of cyanobacteria is a main limiting factor for the scale-up of cyanobacterial biotransformations. Here we demonstrate that internal illumination in a bubble column reactor can alleviate this limitation. At a cell density of 2.4 g L^{-1}, internal illumination with 40 wireless light emitters in 200 mL reaction volume allowed to obtain a reaction rate of 3.7 mM h^{-1} and a specific activity of 32.5 U g_{DCW}^{-1}. An intensified reaction with stepwise feeding of 40 mM ran to completion: Isolation of 650 mg product (73% yield) underlined the practical usefulness of the approach. The fact that purification of the compound was not necessary highlight the practical advantages of cyanobacterial biotransformation. Compared to external source of light, illumination by floating wireless light emitters allowed a more than two-fold rate increase. The results demonstrate the principle of internal illumination as a means to overcome the intrinsic cell density limitation of cyanobacterial biotransformations, obtaining high reaction rates in a scalable photobioreactor.

4.5. Material and Methods

Chemicals. The substrate, 2-methylmaleimide (2-MM) was synthesized as previously described.[70] The product, 2-methylsuccinimide (2-MS) was obtained as a white powder from Chiracon GmbH (Luckenwalde, Germany). All other chemicals were purchased from Sigma-Aldrich (Steinheim, Germany) or Carl Roth (Karlsruhe, Germany) unless otherwise indicated.

Strains. All *Synechocystis* strains utilized are listed in **SI Table 3**.

Cultivation of *Synechocystis* strains. Seed cultures of *Synechocystis* were grown in liquid BG-11 medium (pH 8) supplemented with 50 µg mL^{-1} kanamycin in 300 mL Erlenmeyer flasks with a working volume of 100 mL. The cultures were maintained in a plant growth chamber (SWGC-1000, WISD lab instruments) fitted with white fluorescent lamps delivering a light intensity of 40-60 µE m^{-2} s^{-1}. The cultures were placed on a rotary shaker (140 rpm) under ambient CO_2 and 50% humidity and a temperature of 30 °C. Cell growth was monitored by measuring the optical density at 750 nm (OD_{750}). Upon reaching an OD_{750} 1-2,

the cells were harvested by centrifugation (24 °C, 15min, 3500 rpm), resuspended in fresh BG-11, and inoculated in gas washing tubes (V 200 mL) to an OD_{750} 0.1. The tubes were maintained in an aquarium regulated at 30 °C and illuminated with six fluorescent lamps delivering a light intensity of 200-250 µE m^{-2} s^{-1} (**SI Figure 27 b**). Aeration and mixing of the cultures were ensured by bubbling using an air pump (Boyu S-4000B pump) and filtered through a 0.2 µm filter to ensure the sterility.

Whole-cell Biotransformation. Upon reaching an OD_{750} 1-3, cells were harvested by centrifugation (24 °C, 15min, 3500 rpm). The pellet was resuspended in an appropriate volume of BG-11 to a specific OD_{750} and subsequently utilized in whole-cell biotransformations 10 mM 2-MM with a working volume of 200 mL (stock solution in BG-11). OD_{750} 10 corresponded to 2.4 g L^{-1} of cell density, as previously determined.[92] Reactions were performed using a bubble column reactor (BCR; φ_I = 5 cm, h = 50 cm) with a working volume of 200 to 800 mL fitted with emitting coils. Wireless light emitters (WLEs) in varying numbers were suspended in the reactor to provide internal illumination. The WLEs consist of a white LED plus a receiving coil inside a polycarbonate shell (**SI Figure 25 b**). Air was supplied by a pump (Boyu S-4000B) at a rate of 0.6 mL min^{-1}. A fan was utilized to provide cooling for reactions to keep the temperature at 30 °C. Reaction temperature was measured four times over the course of one hour, then again after 3.5 h and 20 h and was found to be stable and did not increase above 30 °C. Large-scale biotransformations with external illumination were performed by wrapping the BCR with LED stripes (BOXXX) (**SI Figure 31**). The light intensity was maintained constant as an internally illuminated reactor.

For small-scale biotransformation, the cells obtained from centrifugation were resuspended in fresh BG-11 to an OD_{750} of 20 and adjusted accordingly. Reactions were performed in 5 mL glass vials with a working volume of 1 mL and initiated with the addition of 10 mM 2-MM (stock solution: 100 mM in BG-11). The vials were placed in a bioreactor maintained at 30 °C (160 rpm) and equipped with LED lamps with an intensity of 200 µE m^{-2} s^{-1}. Aliquots (100 µL) of the reaction mixture were taken at several time points (0h, 2 min, 5 min, 10 min, 20 min, 1 h, 2 h, 3,5h, 5 h and 24 h) and immediately frozen in liquid nitrogen. Samples were stored at -20 °C prior to GC analysis. Specific activities were calculated at <10% substrate conversion.

GC Analysis. The substrate, 2-MM and its corresponding product, 2-MS were analyzed using GC-FID (GC-2010 Plus, Shimadzu, Japan) outfitted with a ZB-5 column. Samples (100 µL) were extracted with ethyl acetate containing 2 mM *n*-decanol as an internal standard. The organic phase was dried in anhydrous $MgSO_4$ and subsequently analyzed. The enantiomeric excess (%*ee*) of the obtained product after biotransformation was analyzed using chiral GC-FID (GC-2030, Shimadzu, Japan) equipped with a β–6TBDAc column. Detailed GC procedure is given in Table S2.

Determination of Light Intensity. The light intensity was measured using an LI-250A light meter (LICOR Biosciences, Hamburg, Germany) equipped with a spherical micro quantum sensor US-SQS/L (Walz, Effeltrich, Germany). Values were taken as an average (15 s) as well as a plot for 40 s (**SI Figure 26 a**).

Product Isolation. After the reaction, the mixture was extracted three times with ethyl acetate (1:1.33, v/v). The organic layer was dried in anhydrous $MgSO_4$ and evaporated in vacuo. The obtained product was analyzed using chiral GC-FID and ^{1}H and ^{13}C NMR.

Quantification of Chlorophyll a Content. The amount of chlorophyll a was determined as previously described.[92] A sample of cell culture (100 µL) with a known OD_{750} was pelleted, resuspended in 100 µL dH_2O and 900 µL methanol was added. Samples were briefly vortexed and incubated in darkness for 10 min. The absorption at 665 nm was measured and the amount of chlorophyll a was determined using the extinction coefficient ε = 78.74 L g^{-1} cm^{-1}.

5. Conclusion

This PhD thesis on photobiocatalytic reactions shed light on several important aspects of one of the key emerging topic for the synthesis of chemicals. Photobiocatalysis is a diverse field facing many challenges, but also showing lots of potential. The first part of this PhD study, the in vitro light-driven hydroxylation, explored the use of a novel photocatalyst for continuous H_2O_2 synthesis with immobilized unspecific peroxygenase (UPO) in organic medium. The photocatalyst, nitrogen doped carbon nanodots (N-CNDs) paired nicely with the calcium alginate enzyme entrapment, as the N-CNDs spread homogenously throughout the hydrophilic beads, but did not mix with the organic phase around it. This created a 2-in-1 heterogeneous photobiocatalyst and makes it easy to recover if desired. The hydrophilic beads also provided a suitable environment for the enzyme, shielding it from the organic surroundings. Being able to run the reaction in neat cyclohexane was an additional bonus, since the use of neat conditions reduces the complexity of the system, as the solvent is omitted all together. The performance of the system in the actual hydroxylation of cyclohexane, had two main characteristics: The low product formation rate and the remarkable robustness. The performance was heavily impacted by the amount of photocatalyst applied. The medium amount outperforming the low amount can be expected, but the reason for the slow reaction rate with the most photocatalyst is unclear. Decreasing bead size, led to lower immobilization yield, but performance in the reaction was not negatively impacted, hinting a mass transfer or H_2O_2 supply limitation. Increasing H_2O_2 formation by switching from 391 nm to 365 nm LEDs proved to decrease the system's stability, leading to lower product concentrations. Product absorption on the alginate beads was substantial, with more than half of the target product cyclohexanol being removed from the liquid phase. Alginate entrapped UPO can be used in non-polar organic medium, but UV light is a major cause for enzyme inactivation. In principle, N-CNDs are very useful for the application with alginate beads in organic solvents. However, their unfavorable absorption spectrum, makes them no good fit for UPO catalysis. While N-CNDs were indeed degraded under UV illumination, the limiting factor was enzyme inactivation, and not photocatalyst stability. From these results we can conclude, that the key factors are light intensity and wavelength, the photocatalyst-to-enzyme ratio and quality and amount of immobilization

carrier. In the end, the low product titers combined with the low price of the product cyclohexanol, which is after all a bulk chemical, disqualified it for the next step in the project, the upscaling of a photobiocatalytic reaction. Nevertheless, it was a proof-of-principle with the first published demonstration of photobiocatalysis in organic media.

For the upscaling of a light-driven biotransformation a fitting alternative was found in *Synechocystis* P_{cpcB}::*yqjM* reducing 2-methylmaleimide to (*R*)-2-methylsuccinimide. The low volatility of the compounds made it a suitable model reaction for the bubble column reactor (BCR) with wireless light emitters (WLEs). Screening the different reaction conditions, 2.4 g L^{-1} and 40 WLEs were found to deliver the best performance with a specific activity of 32.5 U g_{DCW}^{-1} and 3.7 mM h^{-1}, reaching complete conversion of the 10 mM substrate in 3.5 h. The control reactions with external illumination clearly showed the advantage of internal illumination by WLEs, especially at higher cell densities. Internally illuminated reactions at 2.4 g L^{-1} delivered 2.7-fold higher reaction rates than the externally illuminated one. Furthermore, it has to be mentioned that the 40 WLEs used in this study may not even be the optimum for cell density of 2.4 g L^{-1} yet and that using even more would further improve the reaction. The preparative reaction, with 650 mg pure (73% isolated yield) with a simple extraction shows one of the advantages of a cyanobacterial whole-cell application. The cells seem to stay mostly intact, are fully removed by centrifugation and only the desired product is extracted. These results are consistent with previous reports about high product purity and isolated yields when using cyanobacteria.[70] A major advantage of the WLE reactor is its scalability. The BCR was run at its lower limit of 200 mL, but can be filled up to 800 mL and the largest previously constructed BCR for WLEs even has a volume of 30 L.[112] At increasing scale however, the gas exchange will be more and more challenging as O_2 has to efficiently removed to avoid inhibition effects. The conclusion for this part of the thesis is, that WLE technology is well suited to run photobiotransformations in scalable reactors. Especially for high optical densities, the internal illumination proved to be very beneficial.

6. Outlook

Looking at future research on the here presented photobiotransformations there is a multitude of possibilities. For the UPO/N-CND part, a major challenge was UPO inactivation by UV light, as previously reported.[113] Therefore, using alternative photocatalysts which perform better under higher wavelength illumination could lead to some improvements. A recently published carbon nitride photocatalyst used with green light at 528 nm could be a feasible alternative.[114] Since most photocatalysts including N-CNDs consume O_2 for H_2O_2 formation, oxygen measurements can be a way to further explore the limitations of the system. Clark-type microsensors which have previously been used for O_2 measurements in alginate beads[115] and in deep eutectic solvents,[116] could be used to determine O_2 concentrations in the organic medium as well as in the N-CND-loaded alginate beads. Beyond photocatalysis for H_2O_2 formation, formate oxidase from *Aspergillus oryzae* (*Ao*FOx) is probably the most promising enzymatic alternative.[117] High atom efficiency and impressive turnover numbers (TONs) of 318,000 for both enzymes in the hydroxylation of ethylbenzene in a relatively unrefined system promise great potential. Another way could lead back to the roots: external addition of H_2O_2. Combined with new reactor types with excellent mixing properties like the rotating bed reactor, [118] this cost-effective and simple method could prove to deliver promising results once again. The issue of product absorption to the alginate beads can be tackled with alternative immobilization techniques, using different matrices with lower affinity to cyclohexanol and less solid material in the reaction. While for the here presented research, UPO provided by TU Delft was used, *Pichia pastoris* fermentation was also established in a bench-top multi-bioreactor system here at Aarhus University (see Technical Report in the Appendix). Therefore, enzyme supply for future research can be provided in-house. The protocol already produces good amounts of enzyme, but will be further optimized, especially regarding stirring and gas flow rates in the methanol feed phase.

The second part of the project, the use of WLEs for the upscaling and intensification of photobiotransformations led us to conclude that the WLE technology is suitable to tackle that challenge. Promising characteristics that warrant further research, especially on

applications with cyanobacteria are the high retained activity at high cell densities and easy downstream processing (DSP). Simple DSP is not only desirable for economic feasibility of a process, but also for its environmental sustainability. In this regard, cyanobacteria have an inherent advantage over heterotrophic expression hosts, as they grow on CO_2 as sole carbon source. However, a drawback in their cultivation is their slow growth reaching comparatively low cell densities.[69] It would be highly interesting to see if and how these effects weigh up against each other regarding the sustainability of cyanobacterial biotransformations. A comparative life cycle assessment could shed light on the sustainability aspects of the process. It could be assessed which specific activities and product formation rates are required to actually make the cyanobacterial approach more sustainable than using a heterotrophic host like *Escherichia coli*. The reactor system could also be applied with other substrates and cyanobacteria expressing different enzymes, like a P450 monooxygenase for the hydroxylation of cyclohexane. This reaction was previously optimized for a cell density of 1g L^{-1},[74] therefore it would be interesting to see how it performs with higher cell densities in the internally illuminated BCR. However, the volatility of substrate and product would require the addition of an off-gas condenser to the BCR. As it is still a young technology, so far only one other application of WLEs for photobiocatalysis was published.[98] The authors used the light dependent fatty acid decarboxylase (*Cv*FAP) with blue WLEs for the synthesis of diesel alkanes. In the highly turbid 50 g L^{-1} *E. coli* whole cell suspension, internal illumination proved to be very effective. Furthermore, the reactor used in the *Cv*FAP application belongs to the second generation of WLE reactors. In contrast to the reactor used in this thesis, it has the transmitting coils not fixed to its outside walls, but to a scaffold surrounding the reactor. This makes the reactor exchangeable, improves handling and increases flexibility. Another interesting development in the field is about wireless temperature sensors.[119] With inductive tracking the sensor's location in the measurement setup could be determined with an accuracy of 3 cm, opening possibilities for real time positional process monitoring. As photo(bio)catalysis continues to attract significant attention,[108] we can expect further spread and improvements of the WLE technology, and other innovative illumination technologies.

7. References

[1] M. Heining, A. Sutor, S. C. Stute, C. P. Lindenberger, R. Buchholz, *J. Appl. Phycol.* **2014**, *27*, 59-66 https://doi.org/10.1007/s10811-014-0290-x.

[2] T. Li, T. Lan, L. Wang, Y. Rao, in *Green Oxidation in Organic Synthesis*, **2019**, pp. 1-34, https://doi.org/10.1002/9781119304197.ch1.

[3] a) T. Punniyamurthy, S. Velusamy, J. Iqbal, *Chem. rev.* **2005**, *105*, 2329-2363 https://doi.org/10.1021/cr050523v; b) E. Roduner, W. Kaim, B. Sarkar, V. B. Urlacher, J. Pleiss, R. Gläser, W.-D. Einicke, G. A. Sprenger, U. Beifuß, E. Klemm, C. Liebner, H. Hieronymus, S.-F. Hsu, B. Plietker, S. Laschat, *ChemCatChem* **2013**, *5*, 82-112 https://doi.org/10.1002/cctc.201200266.

[4] M. T. Musser, in *Ullmann's Encyclopedia of Industrial Chemistry, Vol. 11*, 6 ed., Wiley-VCH Verlag GmbH & Co. KGaA., Weinheim, **2011**, pp. 49-60, https://doi.org/10.1002/14356007.a08_217.pub2.

[5] Y. Guo, T. Ying, X. Liu, B. Shi, Y. Wang, *Mol. Catal.* **2019**, *479* https://doi.org/10.1016/j.mcat.2019.110487.

[6] S. Bormann, A. Gomez Baraibar, Y. Ni, D. Holtmann, F. Hollmann, *Catal. Sci. Technol.* **2015**, *5*, 2038-2052 https://doi.org/10.1039/c4cy01477d.

[7] D. L. Craft, K. M. Madduri, M. Eshoo, C. R. Wilson, *Appl. Environ. Microbiol.* **2003**, *69*, 5983-5991 https://doi.org/10.1128/AEM.69.10.5983-5991.2003.

[8] J.-A. Stevenson, A. C. G. Westlake, C. Whittock, L.-L. Wong, *J. Am. Chem. Soc.* **1996**, *118*, 12846-12847 https://doi.org/10.1021/ja963087q.

[9] S. G. Bell, E. Orton, H. Boyd, J.-A. Stevenson, A. Riddle, S. Campbell, L.-L. Wong, *Dalton Trans.* **2003** https://doi.org/10.1039/b300869j.

[10] F. Xu, S. G. Bell, J. Lednik, A. Insley, Z. Rao, L. L. Wong, *Angew. Chem. Int. Ed.* **2005**, *44*, 4029-4032 https://doi.org/10.1002/anie.200462630.

[11] P. Meinhold, M. W. Peters, M. M. Chen, K. Takahashi, F. H. Arnold, *ChemBioChem* **2005**, *6*, 1765-1768 https://doi.org/10.1002/cbic.200500261.

[12] F. E. Zilly, J. P. Acevedo, W. Augustyniak, A. Deege, U. W. Hausig, M. T. Reetz, *Angew. Chem. Int. Ed.* **2011**, *50*, 2720-2724 https://doi.org/10.1002/anie.201006587.

[13] S. C. Maurer, K. Kühnel, L. A. Kaysser, S. Eiben, R. D. Schmid, V. B. Urlacher, *Adv. Synth. Catal.* **2005**, *347*, 1090-1098 https://doi.org/10.1002/adsc.200505044.

[14] D. Salamanca, R. Karande, A. Schmid, D. Dobslaw, *Appl. Microbiol. Biotechnol.* **2015**, *99*, 6889-6897 https://doi.org/10.1007/s00253-015-6599-9.

[15] S. Mordhorst, J. N. Andexer, *Nat. Prod. Rep.* **2020**, *37*, 1316-1333 https://doi.org/10.1039/D0NP00004C.

[16] S. Schmidt, C. Scherkus, J. Muschiol, U. Menyes, T. Winkler, W. Hummel, H. Groger, A. Liese, H. G. Herz, U. T. Bornscheuer, *Angew. Chem. Int. Ed.* **2015**, *54*, 2784-2787 https://doi.org/10.1002/anie.201410633.

[17] S. C. Maurer, H. Schulze, R. D. Schmid, V. Urlacher, *Adv. Synth. Catal.* **2003**, *345*, 802-810 https://doi.org/10.1002/adsc.200303021.

[18] D. Holtmann, F. Hollmann, *ChemBioChem* **2016**, *17*, 1391-1398 https://doi.org/10.1002/cbic.201600176.

[19] M. Hobisch, D. Holtmann, P. Gomez de Santos, M. Alcalde, F. Hollmann, S. Kara, *Biotechno.l Adv.* **2020**, 107615 https://doi.org/10.1016/j.biotechadv.2020.107615.

[20] M. Hofrichter, R. Ullrich, *Appl. Microbiol. Biotechnol.* **2006**, *71*, 276-288 https://doi.org/10.1007/s00253-006-0417-3.

[21] a) V. B. Urlacher, M. Girhard, *Trends Biotechnol.* **2019**, *37*, 882-897 https://doi.org/10.1016/j.tibtech.2019.01.001; b) R. Fasan, *ACS Catal.* **2012**, *2*, 647-666

https://doi.org/10.1021/cs300001x; c) M. Hofrichter, R. Ullrich, *Curr. Opin. Chem. Biol.* **2014**, *19*, 116-125 https://doi.org/10.1016/j.cbpa.2014.01.015; d) R. Ullrich, J. Nuske, K. Scheibner, J. Spantzel, M. Hofrichter, *Appl. Environ. Microbiol.* **2004**, *70*, 4575-4581 https://doi.org/10.1128/AEM.70.8.4575-4581.2004.

[22] N. C. Veitch, *Phytochemistry* **2004**, *65*, 249-259 https://doi.org/10.1016/j.phytochem.2003.10.022.

[23] a) D. S. Lee, A. Yamada, H. Sugimoto, I. Matsunaga, H. Ogura, K. Ichihara, S. Adachi, S. Y. Park, Y. Shiro, *J. Biol. Chem.* **2003**, *278*, 9761-9767 https://doi.org/10.1074/jbc.M211575200; b) M. Hofrichter, H. Kellner, M. J. Pecyna, R. Ullrich, in *Monooxygenase, Peroxidase and Peroxygenase Properties and Mechanisms of Cytochrome P450, Vol. 851*, 2015/05/24 ed., **2015**, pp. 341-368, https://doi.org/10.1007/978-3-319-16009-2_13.

[24] M. Hofrichter, H. Kellner, R. Herzog, A. Karich, C. Liers, K. Scheibner, V. W. Kimani, R. Ullrich, in *Grand Challenges in Fungal Biotechnology*, 1 ed., Springer, Cham, Berlin, **2020**, pp. 369-403, https://doi.org/10.1007/978-3-030-29541-7_14.

[25] R. Ullrich, M. Hofrichter, *Cell. Mol. Life. Sci.* **2007**, *64*, 271-293 https://doi.org/10.1007/s00018-007-6362-1.

[26] S. Peter, M. Kinne, X. Wang, R. Ullrich, G. Kayser, J. T. Groves, M. Hofrichter, *FEBS J.* **2011**, *278*, 3667-3675 https://doi.org/10.1111/j.1742-4658.2011.08285.x.

[27] E. Churakova, M. Kluge, R. Ullrich, I. Arends, M. Hofrichter, F. Hollmann, *Angew. Chem., Int. Ed.* **2011**, *50*, 10716-10719 https://doi.org/10.1002/anie.201105308.

[28] A. Gutierrez, E. D. Babot, R. Ullrich, M. Hofrichter, A. T. Martinez, J. C. del Rio, *Arch. Biochem. Biophys.* **2011**, *514*, 33-43 https://doi.org/10.1016/j.abb.2011.08.001.

[29] Y. Ni, E. Fernandez-Fueyo, A. Gomez Baraibar, R. Ullrich, M. Hofrichter, H. Yanase, M. Alcalde, W. J. van Berkel, F. Hollmann, *Angew. Chem. Int. Ed.* **2016**, *55*, 798-801 https://doi.org/10.1002/anie.201507881.

[30] J. Carro, P. Ferreira, L. Rodriguez, A. Prieto, A. Serrano, B. Balcells, A. Arda, J. Jimenez-Barbero, A. Gutierrez, R. Ullrich, M. Hofrichter, A. T. Martinez, *FEBS J.* **2015**, *282*, 3218-3229 https://doi.org/10.1111/febs.13177.

[31] R. Ullrich, M. Hofrichter, *FEBS Lett.* **2005**, *579*, 6247-6250 https://doi.org/10.1016/j.febslet.2005.10.014.

[32] M. Kluge, R. Ullrich, K. Scheibner, M. Hofrichter, *Green Chem.* **2012**, *14*, 440-446 https://doi.org/10.1039/C1GC16173C.

[33] I. Bassanini, E. E. Ferrandi, M. Vanoni, G. Ottolina, S. Riva, M. Crotti, E. Brenna, D. Monti, *Eur. J. Org. Chem.* **2017**, *2017*, 7186-7189 https://doi.org/10.1002/ejoc.201701390.

[34] a) D. H. Anh, PhD thesis thesis, International Graduate School of Zittau (Zittau), **2008**; b) D. H. Anh, R. Ullrich, D. Benndorf, A. Svatos, A. Muck, M. Hofrichter, *Appl. Environ. Microbiol.* **2007**, *73*, 5477-5485 https://doi.org/10.1128/AEM.00026-07.

[35] G. Grobe, R. Ullrich, M. J. Pecyna, D. Kapturska, S. Friedrich, M. Hofrichter, K. Scheibner, *AMB Express* **2011**, *1*, 31 https://doi.org/10.1186/2191-0855-1-31.

[36] J. Kiebist, K. U. Schmidtke, J. Zimmermann, H. Kellner, N. Jehmlich, R. Ullrich, D. Zander, M. Hofrichter, K. Scheibner, *ChemBioChem* **2017**, *18*, 563-569 https://doi.org/10.1002/cbic.201600677.

[37] R. Ullrich, M. Poraj-Kobielska, S. Scholze, C. Halbout, M. Sandvoss, M. J. Pecyna, K. Scheibner, M. Hofrichter, *J Inorg Biochem* **2018**, *183*, 84-93 https://doi.org/10.1016/j.jinorgbio.2018.03.011.

[38] E. D. Babot, J. C. del Rio, L. Kalum, A. T. Martinez, A. Gutierrez, *Biotechnol Bioeng* **2013**, *110*, 2323-2332 https://doi.org/10.1002/bit.24904.

[39] S. Peter, A. Karich, R. Ullrich, G. Gröbe, K. Scheibner, M. Hofrichter, *Journal of Molecular Catalysis B: Enzymatic* **2014**, *103*, 47-51 https://doi.org/10.1016/j.molcatb.2013.09.016.

[40] J. Carro, A. González-Benjumea, E. Fernández-Fueyo, C. Aranda, V. Guallar, A. Gutiérrez, A. T. Martínez, *ACS Catal.* **2019**, *9*, 6234-6242 https://doi.org/10.1021/acscatal.9b01454.

[41] A. González-Benjumea, J. Carro, C. Renau-Mínguez, D. Linde, E. Fernández-Fueyo, A. Gutiérrez, A. T. Martínez, *Catalysis Science & Technology* **2020** https://doi.org/10.1039/c9cy02332a.

[42] a) P. Gomez de Santos, F. V. Cervantes, F. Tieves, F. J. Plou, F. Hollmann, M. Alcalde, *Tetrahedron* **2019**, *75*, 1827-1831 https://doi.org/10.1016/j.tet.2019.02.013; b) P. Gomez de Santos, M. Cañellas, F. Tieves, S. H. H. Younes, P. Molina-Espeja, M. Hofrichter, F. Hollmann, V. Guallar, M. Alcalde, *ACS Catal.* **2018**, *8*, 4789-4799 https://doi.org/10.1021/acscatal.8b01004; c) C. P. Javier Martin-Diaz, Eva García-Ruiz, Patricia Molina-Espeja, Miguel Alcaldea, *Appl. Environ. Microbiol.* **2018**, *84*, 12; d) M. Ramirez-Escudero, P. Molina-Espeja, P. Gomez de Santos, M. Hofrichter, J. Sanz-Aparicio, M. Alcalde, *ACS Chem Biol* **2018**, *13*, 3259-3268 https://doi.org/10.1021/acschembio.8b00500; e) D. M. Mate, M. A. Palomino, P. Molina-Espeja, J. Martin-Diaz, M. Alcalde, *Prot. Eng., Des. Sel.* **2017**, *30*, 189-196 https://doi.org/10.1093/protein/gzw073; f) P. Molina-Espeja, M. Canellas, F. J. Plou, M. Hofrichter, F. Lucas, V. Guallar, M. Alcalde, *Chembiochem* **2016**, *17*, 341-349 https://doi.org/10.1002/cbic.201500493; g) P. Molina-Espeja, S. Ma, D. M. Mate, R. Ludwig, M. Alcalde, *Enzyme Microb. Technol.* **2015**, *73-74*, 29-33 https://doi.org/10.1016/j.enzmictec.2015.03.004; h) P. Molina-Espeja, E. Garcia-Ruiz, D. Gonzalez-Perez, R. Ullrich, M. Hofrichter, M. Alcalde, *Appl. Environ. Microbiol.* **2014**, *80*, 3496-3507 https://doi.org/10.1128/AEM.00490-14; i) J. Martin-Diaz, C. Paret, E. Garcia-Ruiz, P. Molina-Espeja, M. Alcalde, *Appl. Environ. Microbiol.* **2018**, *84* https://doi.org/10.1128/aem.00808-18.

[43] R. A. S. Fred van Rantwijk, *Current Opinion in Biotechnology* **2000**, *11*, 554-564

[44] F. Tieves, F. Tonin, E. Fernández-Fueyo, J. M. Robbins, B. Bommarius, A. S. Bommarius, M. Alcalde, F. Hollmann, *Tetrahedron* **2019**, *75*, 1311-1314 https://doi.org/10.1016/j.tet.2019.01.065.

[45] a) T. Krieg, S. Hüttmann, K.-M. Mangold, J. Schrader, D. Holtmann, *Green Chem.* **2011**, *13* https://doi.org/10.1039/c1gc15391a; b) A. E. W. Horst, S. Bormann, J. Meyer, M. Steinhagen, R. Ludwig, A. Drews, M. Ansorge-Schumacher, D. Holtmann, *Journal of Molecular Catalysis B: Enzymatic* **2016**, *133*, S137-S142 https://doi.org/10.1016/j.molcatb.2016.12.008.

[46] S. J. Freakley, S. Kochius, J. van Marwijk, C. Fenner, R. J. Lewis, K. Baldenius, S. S. Marais, D. J. Opperman, S. T. L. Harrison, M. Alcalde, M. S. Smit, G. J. Hutchings, *Nat Commun* **2019**, *10*, 4178 https://doi.org/10.1038/s41467-019-12120-w.

[47] W. Zhang, B. O. Burek, E. Fernandez-Fueyo, M. Alcalde, J. Z. Bloh, F. Hollmann, *Angew. Chem. Int. Ed.* **2017**, *56*, 15451-15455 https://doi.org/10.1002/anie.201708668.

[48] W. Zhang, E. Fernandez-Fueyo, Y. Ni, M. van Schie, J. Gacs, R. Renirie, R. Wever, F. G. Mutti, D. Rother, M. Alcalde, F. Hollmann, *Nature Catalysis* **2018**, *1*, 55-62 https://doi.org/10.1038/s41929-017-0001-5.

[49] S. J. Willot, E. Fernandez-Fueyo, F. Tieves, M. Pesic, M. Alcalde, I. Arends, C. B. Park, F. Hollmann, *ACS Catal* **2019**, *9*, 890-894 https://doi.org/10.1021/acscatal.8b03752.

[50] D. S. Choi, Y. Ni, E. Fernandez-Fueyo, M. Lee, F. Hollmann, C. B. Park, *ACS Catal.* **2017**, *7*, 1563-1567 https://doi.org/10.1021/acscatal.6b03453.

[51] a) M. Janssen, C. Müller, D. Vogt, *Green Chem.* **2011**, *13* https://doi.org/10.1039/c1gc15264e; b) A. Liese, L. Hilterhaus, *Chem Soc Rev* **2013**, *42*, 6236-6249 https://doi.org/10.1039/c3cs35511j.

[52] P. Molina-Espeja, P. Santos-Moriano, E. Garcia-Ruiz, A. Ballesteros, F. J. Plou, M. Alcalde, *Int J Mol Sci* **2019**, *20* https://doi.org/10.3390/ijms20071627.

[53] M. Poraj-Kobielska, S. Peter, S. Leonhardt, R. Ullrich, K. Scheibner, M. Hofrichter, *Biochemical Engineering Journal* **2015**, *98*, 144-150 https://doi.org/10.1016/j.bej.2015.02.037.

[54] E. Fernández-Fueyo, Y. Ni, A. Gomez Baraibar, M. Alcalde, L. M. van Langen, F. Hollmann, *Journal of Molecular Catalysis B: Enzymatic* **2016**, *134*, 347-352 https://doi.org/10.1016/j.molcatb.2016.09.013.
[55] M. C. R. Rauch, F. Tieves, C. E. Paul, I. W. C. E. Arends, M. Alcalde, F. Hollmann, *ChemCatChem* **2019**, *11*, 4519-4523 https://doi.org/10.1002/cctc.201901142.
[56] M. van Schie, J. D. Sporing, M. Bocola, P. Dominguez de Maria, D. Rother, *Green Chem.* **2021**, *23*, 3191-3206 https://doi.org/10.1039/d1gc00561h.
[57] Y. Ma, Y. Li, S. Ali, P. Li, W. Zhang, M. C. R. Rauch, S. J. P. Willot, D. Ribitsch, Y. H. Choi, M. Alcalde, F. Hollmann, Y. Wang, *ChemCatChem* **2019** https://doi.org/10.1002/cctc.201901842.
[58] S. Venkata Mohan, J. A. Modestra, K. Amulya, S. K. Butti, G. Velvizhi, *Trends Biotechnol.* **2016**, *34*, 506-519 https://doi.org/10.1016/j.tibtech.2016.02.012.
[59] B. H. H. Goh, H. C. Ong, M. Y. Cheah, W.-H. Chen, K. L. Yu, T. M. I. Mahlia, *Renewable and Sustainable Energy Reviews* **2019**, *107*, 59-74 https://doi.org/10.1016/j.rser.2019.02.012.
[60] S. Singh, B. N. Kate, U. C. Banerjee, *Critical Reviews in Biotechnology* **2008**, *25*, 73-95 https://doi.org/10.1080/07388550500248498.
[61] J. Hu, D. Nagarajan, Q. Zhang, J. S. Chang, D. J. Lee, *Biotechnol Adv* **2018**, *36*, 54-67 https://doi.org/10.1016/j.biotechadv.2017.09.009.
[62] a) F. Camacho, A. Macedo, F. Malcata, *Mar Drugs* **2019**, *17* https://doi.org/10.3390/md17060312; b) T. M. M. Bernaerts, L. Gheysen, I. Foubert, M. E. Hendrickx, A. M. Van Loey, *Biotechno.l Adv.* **2019**, *37* https://doi.org/10.1016/j.biotechadv.2019.107419.
[63] Y. Chisti, *Biotechno.l Adv.* **2007**, *25*, 294-306 https://doi.org/10.1016/j.biotechadv.2007.02.001.
[64] a) B. D. Fernandes, A. Mota, J. A. Teixeira, A. A. Vicente, *Biotechno.l Adv.* **2015**, *33*, 1228-1245 https://doi.org/10.1016/j.biotechadv.2015.03.004; b) M. Heining, R. Buchholz, *Biotechnol. J.* **2015**, *10*, 1131-1137 https://doi.org/10.1002/biot.201400572.
[65] a) E. T. Sero, N. Siziba, T. Bunhu, R. Shoko, E. Jonathan, *International Journal of Energy Research* **2020**, *44*, 5071-5092 https://doi.org/10.1002/er.5059; b) B. C. Benson, M. T. Gutierrez-Wing, K. A. Rusch, *Aquac. Eng.* **2007**, *36*, 198-211 https://doi.org/10.1016/j.aquaeng.2006.12.002; c) E. Franco-Lara, J. Havel, F. Peterat, D. Weuster-Botz, *Biotechnol. Bioeng.* **2006**, *95*, 1177-1187 https://doi.org/10.1002/bit.21086.
[66] J. Li, M. Stamato, E. Velliou, C. Jeffryes, S. N. Agathos, *J. Appl. Phycol.* **2014**, *27*, 75-86 https://doi.org/10.1007/s10811-014-0335-1.
[67] a) P. L. Gupta, S. M. Lee, H. J. Choi, *World. J. Microbiol. Biotechnol.* **2015**, *31*, 1409-1417 https://doi.org/10.1007/s11274-015-1892-4; b) C. U. Ugwu, H. Aoyagi, H. Uchiyama, *Bioresour Technol* **2008**, *99*, 4021-4028 https://doi.org/10.1016/j.biortech.2007.01.046.
[68] L. Schmermund, V. Jurkaš, F. F. Özgen, G. D. Barone, H. C. Büchsenschütz, C. K. Winkler, S. Schmidt, R. Kourist, W. Kroutil, *ACS Catal.* **2019**, *9*, 4115-4144 https://doi.org/10.1021/acscatal.9b00656.
[69] J. Jodlbauer, T. Rohr, O. Spadiut, M. D. Mihovilovic, F. Rudroff, *Trends Biotechnol.* **2021** https://doi.org/10.1016/j.tibtech.2020.12.009.
[70] K. Koninger, A. Gomez Baraibar, C. Mugge, C. E. Paul, F. Hollmann, M. M. Nowaczyk, R. Kourist, *Angew. Chem. Int. Ed.* **2016**, *55*, 5582-5585 https://doi.org/10.1002/anie.201601200.
[71] S. Böhmer, K. Köninger, Á. Gómez-Baraibar, S. Bojarra, C. Mügge, S. Schmidt, M. Nowaczyk, R. Kourist, *Catalysts* **2017**, *7*, 240 https://doi.org/10.3390/catal7080240.
[72] H. C. Büchsenschütz, V. Vidimce-Risteski, B. Eggbauer, S. Schmidt, C. K. Winkler, J. H. Schrittwieser, W. Kroutil, R. Kourist, *ChemCatChem* **2019**, *12*, 726-730 https://doi.org/10.1002/cctc.201901592.
[73] A. Sengupta, A. V. Sunder, S. V. Sohoni, P. P. Wangikar, *J. Biotechnol.* **2019**, *289*, 1-6 https://doi.org/10.1016/j.jbiotec.2018.11.002.

[74] A. Hoschek, J. Toepel, A. Hochkeppel, R. Karande, B. Buhler, A. Schmid, *Biotechnol. J.* **2019**, *14*, 1800724 https://doi.org/10.1002/biot.201800724.
[75] M. Hobisch, M. M. C. H. van Schie, J. Kim, K. Røjkjær Andersen, M. Alcalde, R. Kourist, C. B. Park, F. Hollmann, S. Kara, *ChemCatChem* **2020**, *12*, 4009-4013 https://doi.org/10.1002/cctc.202000512.
[76] J. Dong, E. Fernandez-Fueyo, F. Hollmann, C. E. Paul, M. Pesic, S. Schmidt, Y. Wang, S. Younes, W. Zhang, *Angew. Chem. Int. Ed.* **2018**, *57*, 9238-9261 https://doi.org/10.1002/anie.201800343.
[77] a) M. Patzold, S. Siebenhaller, S. Kara, A. Liese, C. Syldatk, D. Holtmann, *Trends Biotechnol.* **2019**, *1768*, 1-17 https://doi.org/10.1016/j.tibtech.2019.03.007; b) S. Kara, A. Liese, in *Industrial Enzyme Applications*, 1 ed. (Ed.: O. M. Andreas Vogel), Wiley-VCH Verlag GmbH & Co. KGaA, **2019**
[78] Y. Wang, D. Lan, R. Durrani, F. Hollmann, *Curr Opin Chem Biol* **2017**, *37*, 1-9 https://doi.org/10.1016/j.cbpa.2016.10.007.
[79] a) J. S. Dordick, M. A. Marletta, A. M. Klibanov, *Proc Natl Acad Sci U S A* **1986**, *83*, 6255-6257 https://doi.org/10.1073/pnas.83.17.6255; b) J. S. Dordick, M. A. Marletta, A. M. Klibanov, *Biotechnol Bioeng* **1987**, *30*, 31-36 https://doi.org/10.1002/bit.260300106.
[80] B. O. Burek, S. Bormann, F. Hollmann, J. Z. Bloh, D. Holtmann, *Green Chem.* **2019**, *21*, 3232-3249 https://doi.org/10.1039/c9gc00633h.
[81] a) D. I. Perez, M. M. Grau, I. W. Arends, F. Hollmann, *Chem Commun (Camb)* **2009**, 6848-6850 https://doi.org/10.1039/b915078a; b) E. Churakova, I. W. C. E. Arends, F. Hollmann, *ChemCatChem* **2013**, *5*, 565-568 https://doi.org/10.1002/cctc.201200490; c) I. Zachos, S. K. Gassmeyer, D. Bauer, V. Sieber, F. Hollmann, R. Kourist, *Chem Commun (Camb)* **2015**, *51*, 1918-1921 https://doi.org/10.1039/c4cc07276f.
[82] P. Adlercreutz, in *Organic Synthesis with Enzymes in Non-Aqueous Media* (Eds.: G. Carrea, S. Riva), Wiley-VCH Verlag GmbH & Co. KGaA, **2008**, https://doi.org/https://doi.org/10.1002/9783527621729.ch1.
[83] L. Fernandez-Arrojo, B. Rodriguez-Colinas, P. Gutierrez-Alonso, M. Fernandez-Lobato, M. Alcalde, A. O. Ballesteros, F. J. Plou, *Process Biochem.* **2013**, *48*, 677-682 https://doi.org/10.1016/j.procbio.2013.02.015.
[84] J. Kim, S. H. Lee, F. Tieves, D. S. Choi, F. Hollmann, C. E. Paul, C. B. Park, *Angew. Chem. Int. Ed.* **2018**, *57*, 13825-13828 https://doi.org/10.1002/anie.201804409.
[85] W. Zhang, A. Bariotaki, I. Smonou, F. Hollmann, *Green Chem.* **2017**, *19*, 2096-2100 https://doi.org/10.1039/c7gc00539c.
[86] M. Hobisch, J. Spasic, L. Malihan-Yap, G. D. Barone, K. Castiglione, P. Tamagnini, S. Kara, R. Kourist, *ChemSusChem* **2021**
[87] P. Anastas, N. Eghbali, *Chem. Soc. Rev.* **2010**, *39*, 301-312 https://doi.org/10.1039/b918763b.
[88] a) F. Jüttner, R. Hans, *Appl. Microbiol. Biotechnol.* **1986**, *25*, 52-54 https://doi.org/10.1007/bf00252512; b) K. Nakamura, R. Yamanaka, K. Tohi, H. Hamada, *Tetrahedron Lett.* **2000**, *41*, 6799-6802 https://doi.org/10.1016/s0040-4039(00)01132-1; c) J. Havel, D. Weuster-Botz, *Eng. Life Sci.* **2006**, *6*, 175-179 https://doi.org/10.1002/elsc.200620909; d) T. Utsukihara, W. Chai, N. Kato, K. Nakamura, C. A. Horiuchi, *J. Mol. Catal. B: Enzym.* **2004**, *31*, 19-24 https://doi.org/10.1016/j.molcatb.2004.06.002; e) M. Górak, E. Żymańczyk-Duda, *Green Chem.* **2015**, *17*, 4570-4578 https://doi.org/10.1039/c5gc01195g; f) H. Hamada, Y. Kondo, K. Ishihara, N. Nakajima, H. Hamada, R. Kurihara, T. Hirata, *J. Biosci. Bioeng.* **2003**, *96*, 581-584 https://doi.org/10.1016/s1389-1723(04)70154-1; g) K. Nakamura, R. Yamanaka, *Tetrahedron: Asymmetry* **2002**, *13*, 2529-2533 https://doi.org/10.1016/s0957-4166(02)00683-3; h) S. Rasoul-Amini, E. Fotooh-Abadi, Y. Ghasemi, *J. Appl. Phycol.* **2010**, *23*, 975-981 https://doi.org/10.1007/s10811-010-9625-4; i) K. Shimoda, N. Kubota, H. Hamada,

M. Kaji, T. Hirata, *Tetrahedron: Asymmetry* **2004**, *15*, 1677-1679 https://doi.org/10.1016/j.tetasy.2004.04.024; j) T. Takemura, K. Akiyama, N. Umeno, Y. Tamai, H. Ohta, K. Nakamura, *J. Mol. Catal. B: Enzym.* **2009**, *60*, 93-95 https://doi.org/10.1016/j.molcatb.2009.03.017; k) R. Yamanaka, K. Nakamura, A. Murakami, *AMB Express* **2011**, *1*, 24 https://doi.org/10.1186/2191-0855-1-24; l) R. Yamanaka, K. Nakamura, M. Murakami, A. Murakami, *Tetrahedron Lett.* **2015**, *56*, 1089-1091 https://doi.org/10.1016/j.tetlet.2015.01.092; m) M. T. Yazdi, H. Arabi, M. A. Faramarzi, Y. Ghasemi, M. Amini, S. Shokravi, F. A. Mohseni, *Phytochemistry* **2004**, *65*, 2205-2209 https://doi.org/10.1016/j.phytochem.2004.05.015; n) B. Zyszka, M. Aniol, J. Lipok, *Microb. Cell Fact.* **2017**, *16*, 136 https://doi.org/10.1186/s12934-017-0752-3; o) B. Zyszka-Haberecht, A. Poliwoda, J. Lipok, *Appl. Microbiol. Biotechnol.* **2018**, *102*, 7097-7111 https://doi.org/10.1007/s00253-018-9109-z.

[89] A. Hoschek, B. Bühler, A. Schmid, *Angew. Chem. Int. Ed.* **2017**, *56*, 15146-15149 https://doi.org/10.1002/anie.201706886.

[90] A. Berepiki, J. R. Gittins, C. M. Moore, T. S. Bibby, *Synth. Biol.* **2018**, *3*, ysy009 https://doi.org/10.1093/synbio/ysy009.

[91] H. C. Büchsenschütz, V. Vidimce-Risteski, B. Eggbauer, S. Schmidt, C. K. Winkler, J. H. Schrittwieser, W. Kroutil, R. Kourist, *ChemCatChem* **2020**, *12*, 726-730

[92] L. Assil-Companioni, H. C. Büchsenschütz, D. n. Solymosi, N. G. Dyczmons-Nowaczyk, K. K. Bauer, S. Wallner, P. Macheroux, Y. Allahverdiyeva, M. M. Nowaczyk, R. Kourist, *ACS Catal.* **2020**, *10*, 11864-11877

[93] C. J. Knoot, J. Ungerer, P. P. Wangikar, H. B. Pakrasi, *J Biol Chem* **2018**, *293*, 5044-5052 https://doi.org/10.1074/jbc.R117.815886.

[94] a) Z. Gao, H. Zhao, Z. Li, X. Tan, X. Lu, *Energy Environ. Sci.* **2012**, *5*, 9857-9865; b) S. A. Angermayr, A. D. van der Woude, D. Correddu, A. Vreugdenhil, V. Verrone, K. J. Hellingwerf, *Biotechnol. Biofuels* **2014**, *7*, 99 https://doi.org/10.1186/1754-6834-7-99; c) J. E. Chaves, P. Rueda-Romero, H. Kirst, A. Melis, *ACS Synth. Biol.* **2017**, *6*, 2281-2292; d) J. W. Oliver, I. M. Machado, H. Yoneda, S. Atsumi, *Proc. Natl. Acad. Sci. U. S. A.* **2013**, *110*, 1249-1254 https://doi.org/10.1073/pnas.1213024110.

[95] Y. Allahverdiyeva, H. Mustila, M. Ermakova, L. Bersanini, P. Richaud, G. Ajlani, N. Battchikova, L. Cournac, E. M. Aro, *Proc. Natl. Acad. Sci. U. S. A.* **2013**, *110*, 4111-4116 https://doi.org/10.1073/pnas.1221194110.

[96] a) J. C. Ogbonna, H. Yada, H. Masui, H. Tanaka, *J. Ferment. Bioeng.* **1996**, *82*, 61-67 https://doi.org/10.1016/0922-338x(96)89456-6; b) I. S. Suh, S. B. Lee, *J. Appl. Phycol.* **2001**, *13*, 381-388 https://doi.org/10.1023/a:1017979431852; c) I. S. Suh, S. B. Lee, *Biotechnol. Bioeng.* **2003**, *82*, 180-189 https://doi.org/10.1002/bit.10558.

[97] M. Heining, A. Sutor, S. C. Stute, C. P. Lindenberger, R. Buchholz, *J. Appl. Phycol.* **2014**, *27*, 59-66 https://doi.org/10.1007/s10811-014-0290-x.

[98] H. T. Duong, Y. Wu, A. Sutor, B. O. Burek, F. Hollmann, J. Z. Bloh, *ChemSusChem* **2021**, *14*, 1053-1056 https://doi.org/10.1002/cssc.202002957.

[99] J. Kauny, P. Setif, *Biochim. Biophys. Acta* **2014**, *1837*, 792-801 https://doi.org/10.1016/j.bbabio.2014.01.009.

[100] K. Ogawa, K. Yoshikawa, F. Matsuda, Y. Toya, H. Shimizu, *J. Biosci. Bioeng.* **2018**, *126*, 596-602 https://doi.org/10.1016/j.jbiosc.2018.05.015.

[101] L. Assil-Companioni, H. C. Buchsenschutz, D. Solymosi, N. G. Dyczmons-Nowaczyk, K. K. F. Bauer, S. Wallner, P. Macheroux, Y. Allahverdiyeva, M. M. Nowaczyk, R. Kourist, *ACS Catal.* **2020**, *10*, 11864-11877 https://doi.org/10.1021/acscatal.0c02601.

[102] N. Wan, D. M. DeLorenzo, L. He, L. You, C. M. Immethun, G. Wang, E. E. Baidoo, W. Hollinshead, J. D. Keasling, T. S. Moon, *Biotechnol. Bioeng.* **2017**, *114*, 1593-1602

[103] A. Makowka, L. Nichelmann, D. Schulze, K. Spengler, C. Wittmann, K. Forchhammer, K. Gutekunst, *Mol. Plant* **2020**, *13*, 471-482 https://doi.org/https://doi.org/10.1016/j.molp.2020.02.002.
[104] A. Hoschek, B. Buhler, A. Schmid, *Biotechnol. Bioeng.* **2019**, *116*, 1887-1900 https://doi.org/10.1002/bit.27006.
[105] A. C. Apel, C. E. Pfaffinger, N. Basedahl, N. Mittwollen, J. Göbel, J. Sauter, T. Brück, D. Weuster-Botz, *Algal Res.* **2017**, *25*, 381-390 https://doi.org/10.1016/j.algal.2017.06.004.
[106] L. Bähr, A. Wüstenberg, R. Ehwald, *J. Appl. Phycol.* **2015**, *28*, 783-793 https://doi.org/10.1007/s10811-015-0614-5.
[107] C.-Y. Chen, J.-S. Chang, *Process Biochem.* **2006**, *41*, 2041-2049 https://doi.org/10.1016/j.procbio.2006.05.005.
[108] L.-E. Meyer, B. E. Eser, S. Kara, *Curr. Opin. Green Sustain. Chem.* **2021**, *31* https://doi.org/10.1016/j.cogsc.2021.100496.
[109] A. Hoschek, I. Heuschkel, A. Schmid, B. Buhler, R. Karande, K. Buhler, *Bioresour. Technol.* **2019**, *282*, 171-178 https://doi.org/10.1016/j.biortech.2019.02.093.
[110] a) P. Erdrich, H. Knoop, R. Steuer, S. Klamt, *Microb. Cell. Fact.* **2014**, *13*, 128 https://doi.org/10.1186/s12934-014-0128-x; b) M. Faizi, R. Steuer, *Microb. Cell. Fact.* **2019**, *18*, 165 https://doi.org/10.1186/s12934-019-1209-7.
[111] A. Hoschek, A. Schmid, B. Bühler, *ChemCatChem* **2018**, *10*, 5366-5371 https://doi.org/10.1002/cctc.201801262.
[112] M. Heining, PhD thesis, Friedrich-Alexander-Universität Erlangen (Nurenberg), **2016**.
[113] B. O. Burek, S. R. de Boer, F. Tieves, W. Y. Zhang, M. van Schie, S. Bormann, M. Alcalde, D. Holtmann, F. Hollmann, D. W. Bahnemann, J. Z. Bloh, *ChemCatChem* **2019**, *11*, 3093-3100 https://doi.org/10.1002/cctc.201900610.
[114] L. Schmermund, S. Reischauer, S. Bierbaumer, C. K. Winkler, A. Diaz-Rodriguez, L. J. Edwards, S. Kara, T. Mielke, J. Cartwright, G. Grogan, B. Pieber, W. Kroutil, *Angew. Chem. Int. Ed.* **2021**, *60*, 6965-6969 https://doi.org/10.1002/anie.202100164.
[115] M. Sonderholm, K. N. Kragh, K. Koren, T. H. Jakobsen, S. E. Darch, M. Alhede, P. O. Jensen, M. Whiteley, M. Kuhl, T. Bjarnsholt, *Appl Environ Microbiol* **2017**, *83* https://doi.org/10.1128/AEM.00113-17.
[116] N. Zhang, F. Steininger, L.-E. Meyer, K. Koren, S. Kara, *ACS Sustainable Chemistry & Engineering* **2021**, *9*, 8347-8353 https://doi.org/10.1021/acssuschemeng.1c03547.
[117] F. Tieves, S. J. Willot, M. van Schie, M. C. R. Rauch, S. H. H. Younes, W. Zhang, J. Dong, P. Gomez de Santos, J. M. Robbins, B. Bommarius, M. Alcalde, A. S. Bommarius, F. Hollmann, *Angew. Chem. Int. Ed.* **2019**, *58*, 7873-7877 https://doi.org/10.1002/anie.201902380.
[118] J. Johannsen, F. Meyer, C. Engelmann, A. Liese, G. Fieg, P. Bubenheim, T. Waluga, *AIChE J.* **2021**, *67* https://doi.org/10.1002/aic.17158.
[119] D. Demetz, A. Sutor, *Sensors* **2021**, *21* https://doi.org/10.3390/s21124201.
[120] R. Y. Stanier, R. Kunisawa, M. Mandel, G. Cohen-Bazire, *Bacteriol. Rev.* **1971**, *35*, 171–205
[121] L. Assil-Companioni, H. C. Buchsenschutz, D. Solymosi, N. G. Dyczmons-Nowaczyk, K. K. F. Bauer, S. Wallner, P. Macheroux, Y. Allahverdiyeva, M. M. Nowaczyk, R. Kourist, *ACS Catal.* **2020**, *10*, 11864-11877 https://doi.org/10.1021/acscatal.0c02601.
[122] M. Heining, R. Buchholz, *Biotechnol. J.* **2015**, *10*, 1131-1137 https://doi.org/10.1002/biot.201400572.

8. Supplementary Information

8.1. SI Article I[1]

8.1.1. Hydroxylation of cyclohexane with alginate beads and H_2O_2 addition

The peak at 10.9 min clearly shows successful cyclohexanol production in cyclohexane as reaction medium, using PaDa-I entrapped in calcium alginate beads.

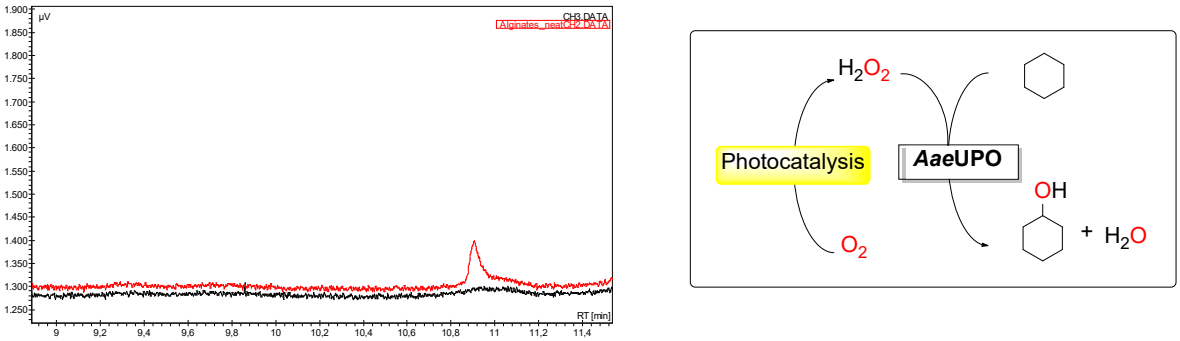

Figure 11. Chromatogram of the hydroxylation of neat cyclohexane with alginate entrapped *Aae*UPO PaDa-I. 5 mL cyclohexane, 1 g alginate beads (37.9 U), 30 °C, magnetic stirring at 500 rpm. Addition of H_2O_2 (3.5 µL, 3.5%) every hour for 7 h, overnight without extra addition of H_2O_2. Black: 0 h, red 24 h. Retention time cyclohexanol: 10.9 min (slightly different retention time than in **Figure 19** due to several column changes between this measurement and the other two).

[1] Chapter 8.1 is taken from the publication 'Solvent-free Photobiocatalytic Hydroxylation of Cyclohexane' (Hobisch *et al.*, *ChemCatChem* 12, 2020, 4009–4013) except for the page layout and small stylistic alterations without changing the main content.

8.1.2. Measurement of Philips light bulb emission spectrum

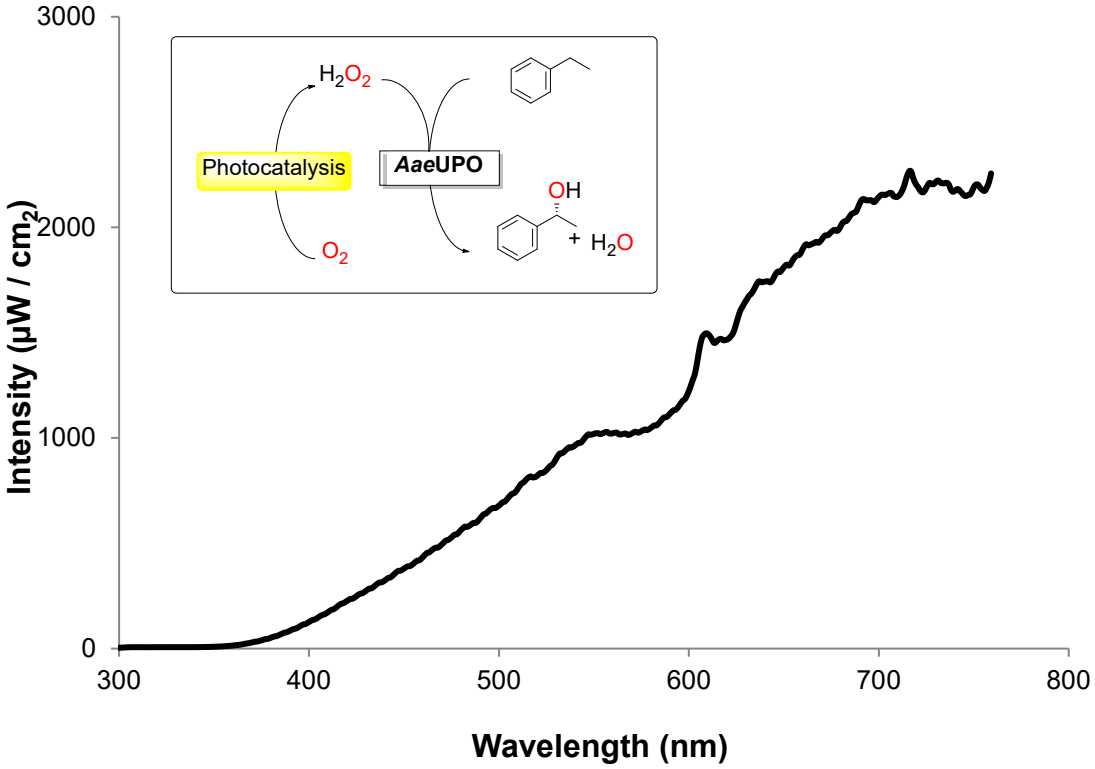

Figure 12. The light intensity of homemade white light setup used in ethylbenzene reactions with N-CNDs. The measurement was performed with a distance of 45 cm between the calibrated spectrometer and light bulb.

8.1.3. N-CND reaction under anaerobic conditions

After attempting the N-CND and UPO catalyzed hydroxylation of ethylbenzene under anaerobic conditions, only trace amounts of product were found. This clearly indicates that O_2 is essential for the reaction.

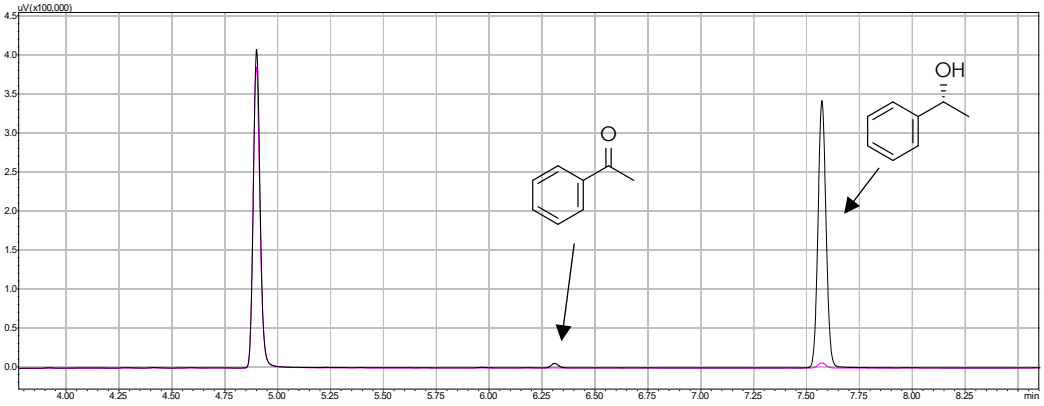

Figure 13. GC chromatogram of the photooxidation reactions under aerobic (black) and anaerobic (pink) conditions. Reaction conditions: UPO (100 nM), ethyl benzene (50 mM), N-CND (5 mg mL^{-1}), KPi buffer pH 7.0 (100 mM), 30 °C, magnetic stirring at 600 rpm, white light bulb for 24 hours. Retention times: Octanol (internal standard): 4.8 min., acetophenone: 6.3 min., and *(R)*-(1)-phenyl ethanol 7.6 min.

8.1.4. Hydroxylation of ethylbenzene with H_2O^{18}

The hydroxylation of ethylbenzene in KPi buffer made with H_2O^{18} yielded no heavier product in the GC-MS analysis, only the regular 122 g mol^{-1} product was detected. That means that the oxygen for the hydroxylation reaction is not derived from water.

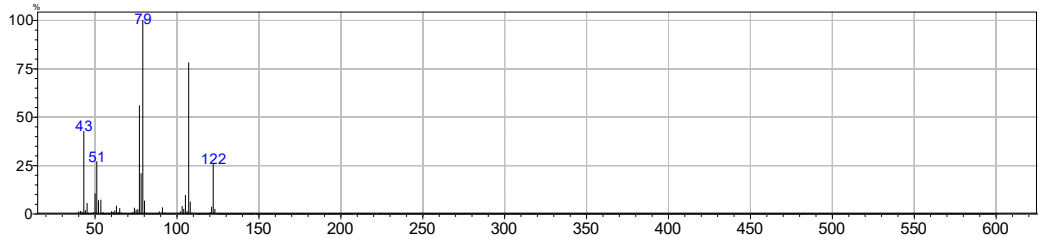

Figure 14. GC-MS analysis of the hydroxylation of ethylbenzene to phenyl ethanol by PaDa-I and N-CNDs with H_2O^{18}. Mass of product: with O^{16} 122 g mol^{-1}, with O^{18} 124 g mol^{-1}.

8.1.5. EPR Spectroscopy

EPR spectroscopy of N-CNDs under white light illumination showed clear signs for the presence of hydroxyl radicals ($HO^{\bullet}$).

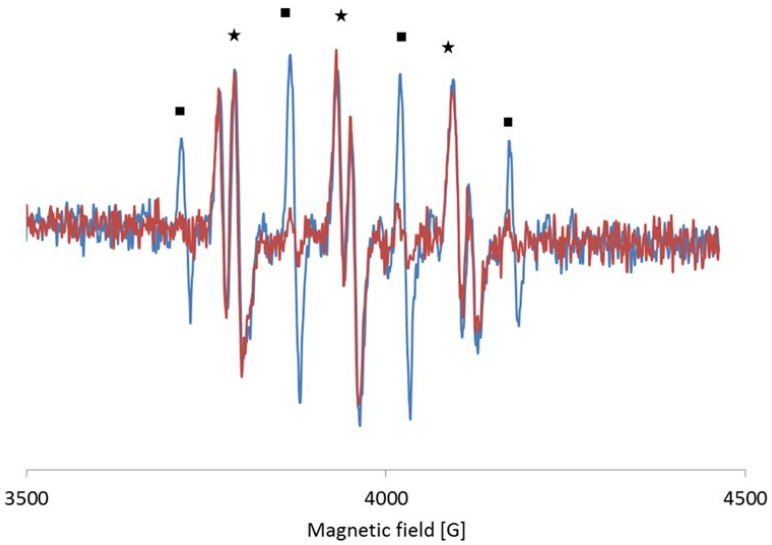

Figure 15. Electron paramagnetic resonance (EPR) spectrogram of N-CNDs under white light illumination (blue, with squares) and in darkness (red, with stars).

8.1.6. N-CND degradation by light

The recorded absorption spectrum of N-CNDs showed substantial degradation caused by UV illumination. In dark conditions, no degradation was observed, even when H_2O_2 was added to the solution.

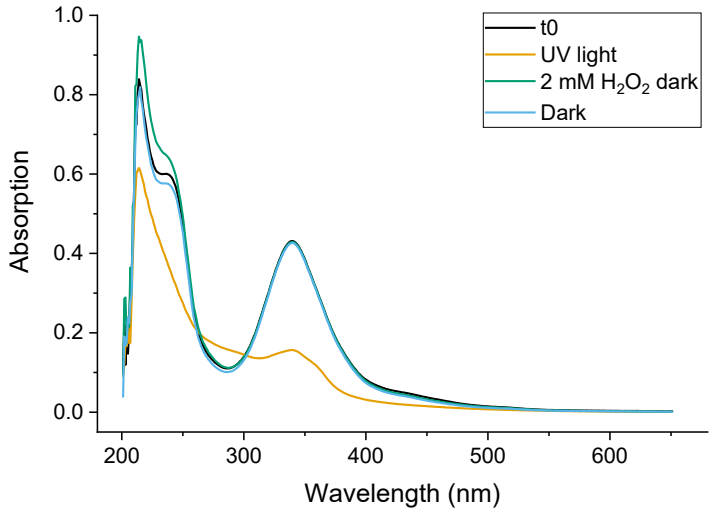

Figure 16. Absorption spectrum analysis of N-CNDs under different conditions. Black: time 0 sample (without H_2O_2); blue: dark conditions, time 24 h; green: dark conditions, time 24 h, in the presence of 2 mM H_2O_2; orange: UV-LED illumination, time 24 h.

8.1.7. Measurement of LED emission spectra

Blue and UV LEDs were considered as light sources. Emission peaks at 450 nm and 391 nm and irradiance flux densities of 193.5 W m^{-2} and 41.5 W m^{-2} were found, respectively. As the UV LEDs showed an emission closer to the main absorption peak of the N-CNDs, they were selected to run the reaction. Under UV illumination, the N-CND loaded alginate beads were fluorescent.

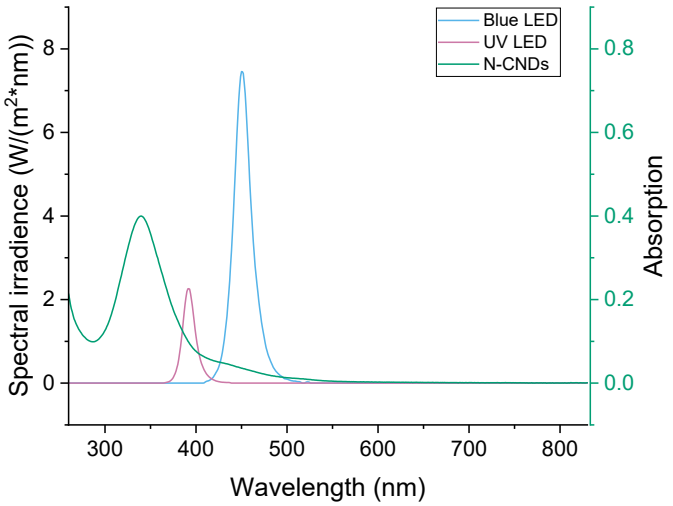

Figure 17. Emission spectra of different LED strips (blue and UV light) and the absorption spectrum of N-CNDs.

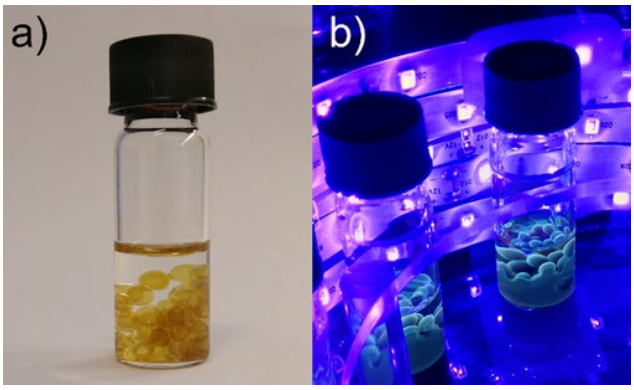

Figure 18. *Aae*UPO PaDa-I alginate beads (0.8 g) with N-CNDs (4 mg) in cyclohexane shortly after mixing (a) and during the reaction under UV LED illumination (b).

8.1.8. Light driven hydroxylation of ethylbenzene

GC analysis of the hydroxylation of ethylbenzene shows an excellent enantioselectivity with an *ee* of 99%. This indicates that the reaction is indeed run by the enzyme and not by the photocatalyst.

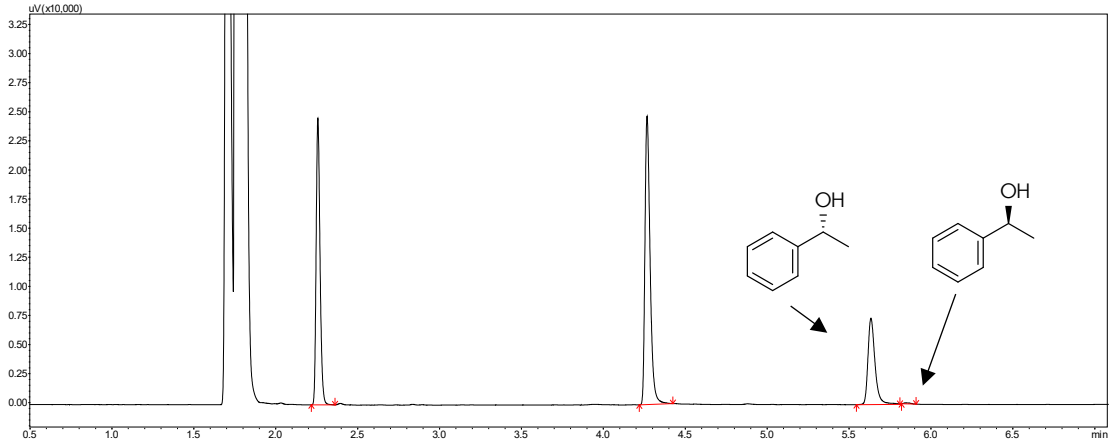

Figure 19. GC chromatogram of *Aae*UPO PaDa-I and N-CND driven hydroxylation of ethylbenzene. Retention time of (*R*)-1-phenyl ethanol: 5.6 min, (*S*)-1-phenyl ethanol: 5.8 min

8.1.9. Light driven hydroxylation of cyclohexane

This exemplary chromatogram of the hydroxylation of cyclohexane to cyclohexanol shows clear separations of all peaks of interest.

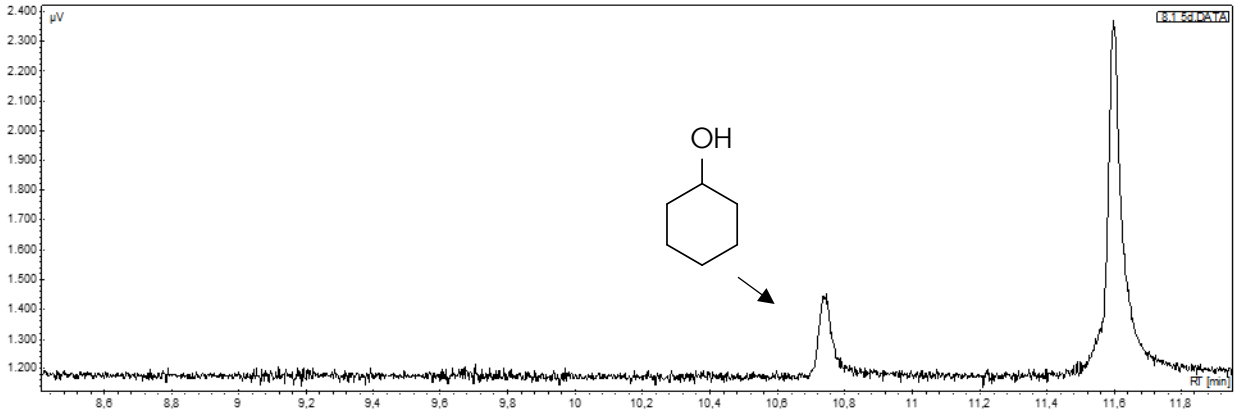

Figure 20. Exemplary GC chromatogram of neat cyclohexane hydroxylation with N-CNDs and AaeUPO PaDa-I alginate beads under UV illumination. Reaction: N-CND to enzyme ratio 8:1 (mg:nmol), time 5 days. Retention times: cyclohexanone 9.66 min, cyclohexanol 10.75 min, and dodecane (internal standard) 11.6 min.

8.1.10. Light driven hydroxylation with smaller alginate beads

The hydroxylation of cyclohexane with N-CNDs and smaller PaDa-I alginate beads (diameter ~1 mm), produced 2.25 mM cyclohexanol in four days. As the bigger beads (diameter ~3 mm) provided a very similar reaction rate (**Figure 3**), but used three times more enzyme, a mass transfer limitation is most likely the rate limiting step of the reaction. Besides cyclohexanol also 0.06 mM of the overoxidation product cyclohexanone were detected (**Figure 21**). That this was not the case for the previously run reactions, is due to different detection limits of the used GCs.

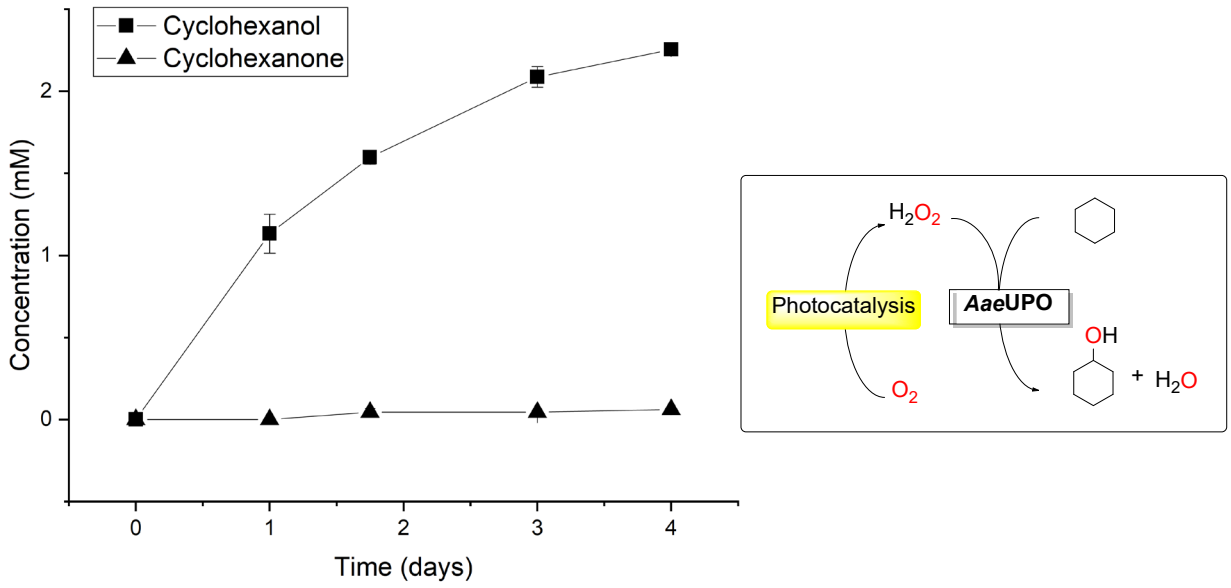

Figure 21. UV light driven hydroxylation of cyclohexane using N-CNDs and smaller PaDa-I alginate beads (diameter ~1 mm).

8.1.11. Light driven hydroxylation of cyclopentane

Cyclopentane was also hydroxylated using PaDa-I and N-CNDs. Cyclopntane was apparently a worse substrate than cyclohexane, a maximum of 1 mM cyclopentanol was produced over 4 days. No cyclopentanone was detected, most likely due to the very low cyclopentanol concentration.

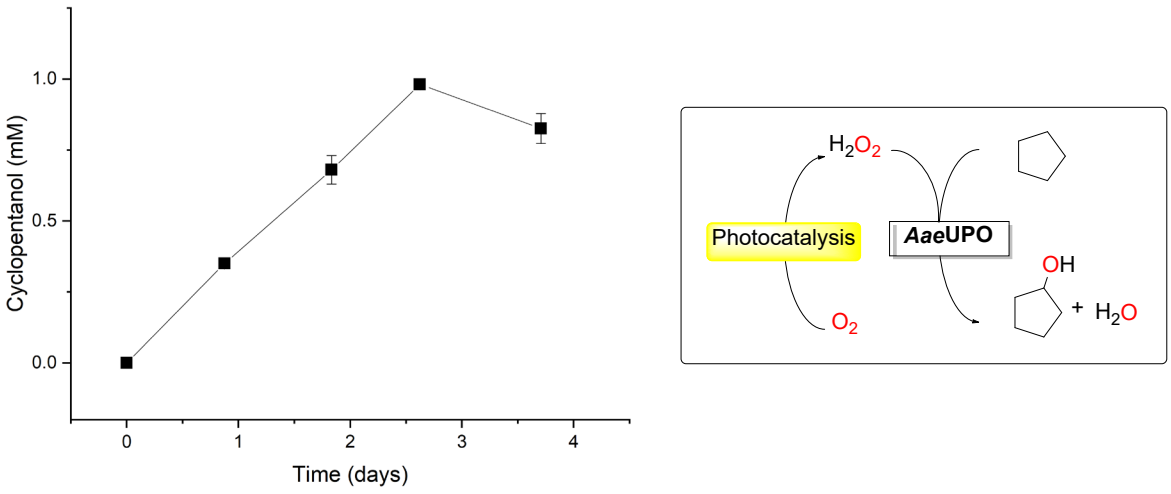

Figure 22. UV light driven hydroxylation of neat cyclopentane using N-CNDs and smaller PaDa-I alginate beads.

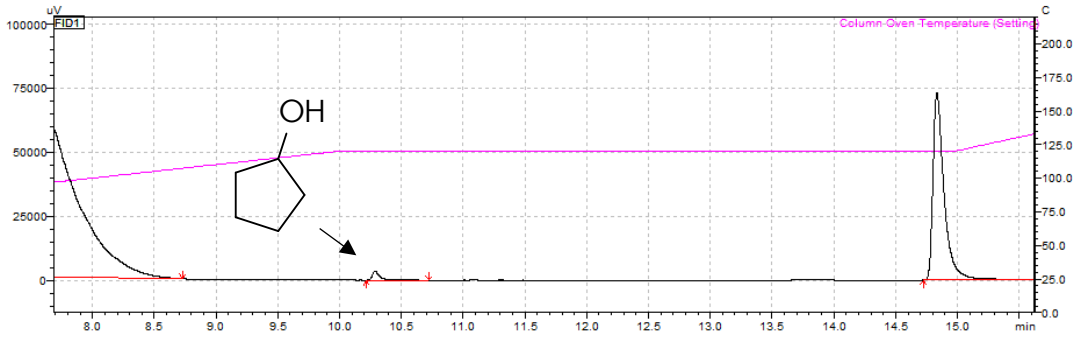

Figure 23. Exemplary GC chromatogram of neat cyclopentane hydroxylation with N-CNDs and AaeUPO PaDa-I alginate beads under UV illumination. Reaction: N-CND to enzyme ratio 8:1 (mg:nmol), time days. Retention times: cyclopentanone 8.83 min, cyclopentanol 10.28 min, and dodecane (internal standard) 14.84 min.

8.1.12. Product absorption on alginate beads

When 0.5 mL cyclohexane with 20 mM cyclohexanol and cyclohexanone was incubated with 0.5 g calcium alginate beads,

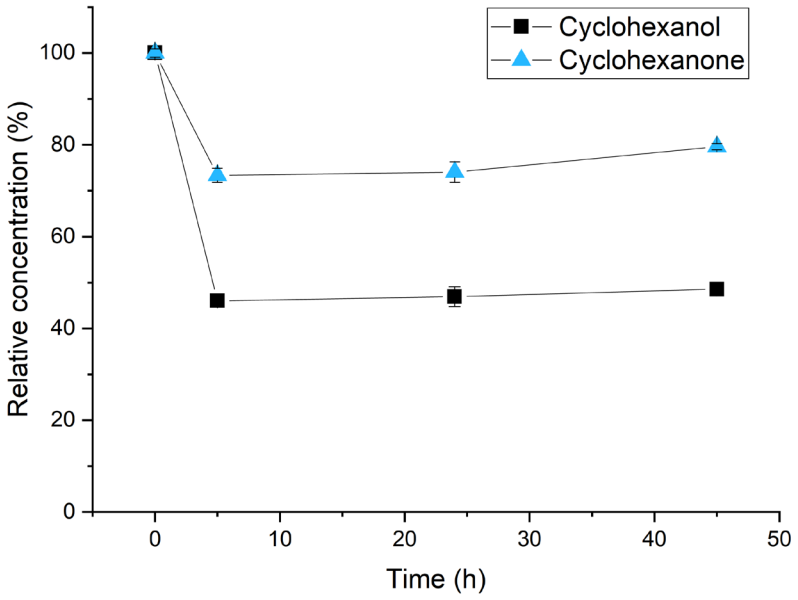

Figure 24. Absorption of 20 mM cyclohexanol and cyclohexanone in cyclohexane to calcium alginate beads. (0.5 g beads, 0.5 mL cyclohexane with products, 30 °C, 800 rpm)

8.2. SI Article II[2]

8.2.1. Strains

Table 3. Cyanobacteria strains utilized in this work.

Strains	Description	Reference
Synechocystis sp. PCC 6803 WT	Wild type cyanobacterium *Synechocystis sp.* PCC 6803	[120]
Synechocystis sp. PCC 6803 $P_{cpcB::}$yqjM	Transgenic *Synechocystis sp.* PCC 6803 constructed in WT background harboring the gene *yqjM* from *Bacillus subtilis* under the control of the P_{cpcB} promoter in the genome locus *slr0168*	[121]
Synechocystis sp. PCC 6803 $P_{psbA2::}$yqjM	Transgenic *Synechocystis sp.* PCC 6803 constructed in WT background harboring the gene *yqjM* from *Bacillus subtilis* under the control of the promoter P_{psbA2} in the genome locus *slr0168*	[121]

[2] Chapter 8.2 is taken from the publication 'Internal Illumination to Overcome the Cell Density Limitation in the Scale-up of Whole-cell Photobiocatalysis' (Hobisch *et al.*, *ChemSusChem*, 2021, in press) except for the page layout and small stylistic alterations without changing the main content.

8.2.2. GC methods

Table 4. Gas Chromatography Flame Ionization Detector Method.

Achiral GC-FID (GC-2010 Plus, Shimadzu, Japan)		
Column	Phase	ZB-5 (5% phenyl, 95% dimethyl polysiloxane)
	Dimension	Length = 30 m; Film Thickness = 0.25 μm; Inner Diameter = 0.32 mm
	Temperature	100 °C
FID Detector	Temperature	320 °C
	Air flowrate	400 mL min^{-1}
	H_2 flowrate	40 mL min^{-1}
Injection port	Volume	1.0 μL
	Carrier Gas	N_2 (1.5 mL min^{-1})
	Temperature	230 °C
	Split Ratio	20
Temperature	Program	80 °C for 1 min; 2) 80-160 °C (50 °C min^{-1}); 3) 160-220 (15 °C min^{-1}); 4) 220-300 °C (50 °C min^{-1}) and 5) 300 °C for 3.8 min
The percent enantiomeric excess (% *ee*) was determined using Chiral GC-FID as detailed below: **Chiral GC-FID** (GC-2030 Plus, Shimadzu, Japan)		
Column	Phase	β-6TBDAc (Column ID: 23254-3)
	Dimension	Length = 50 m; Film Thickness = 0.25 μm; Inner Diameter = 0.25 mm
	Temperature	180 °C
FID Detector	Temperature	250 °C
	Air flowrate	200 mL min^{-1}
	H_2 flowrate	32 mL min^{-1}
Injection port	Volume	1.0 μL
	Carrier Gas	N_2 (24 mL min^{-1})
	Temperature	230
	Split Ratio	100
Temperature	Program	180 °C (2 min); 2) 220 °C (5 °C min^{-1} for 3min)

8.2.3. Light intensity measurements in the BCR

The light intensity in the cyanobacterial mixture was determined using an LI-250A light meter (LI-COR Biosciences UK Ltd, Cambridge, United Kingdom) with a US-SQS/L light sensor (Waltz, Effeltrich, Germany) submerged at a depth of 5 cm from the surface in the center of the reactor.

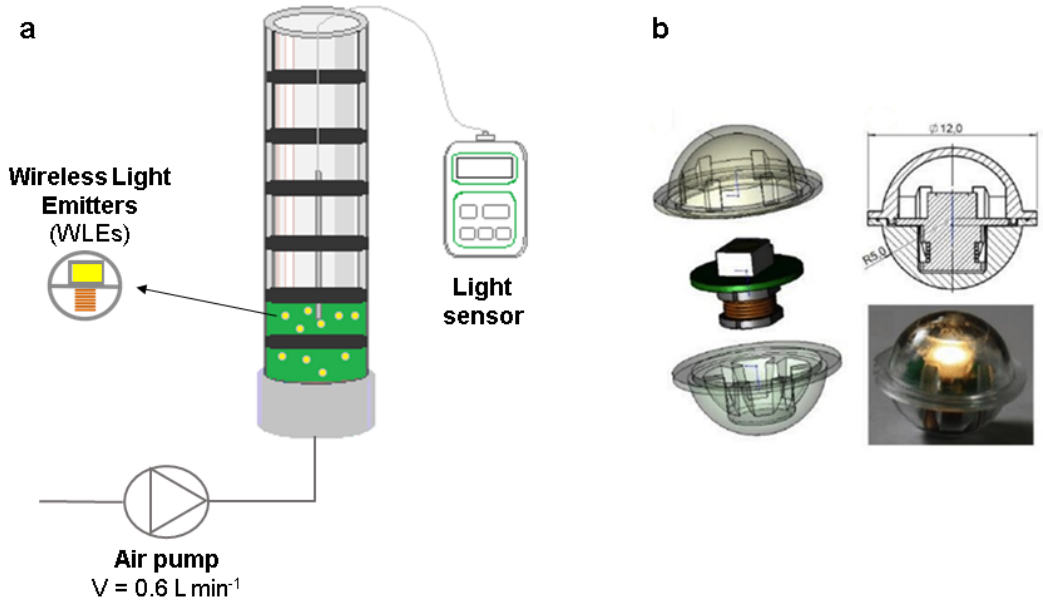

Figure 25. a) Schematic illustration of the Bubble Column Reactor with a working volume of 200 mL cyanobacterial mixture, air was delivered using a pump at a flowrate of 0.6 L min-1; b) Wireless Light Emitters (WLEs) utilized for internal illumination in the BCR. [122]

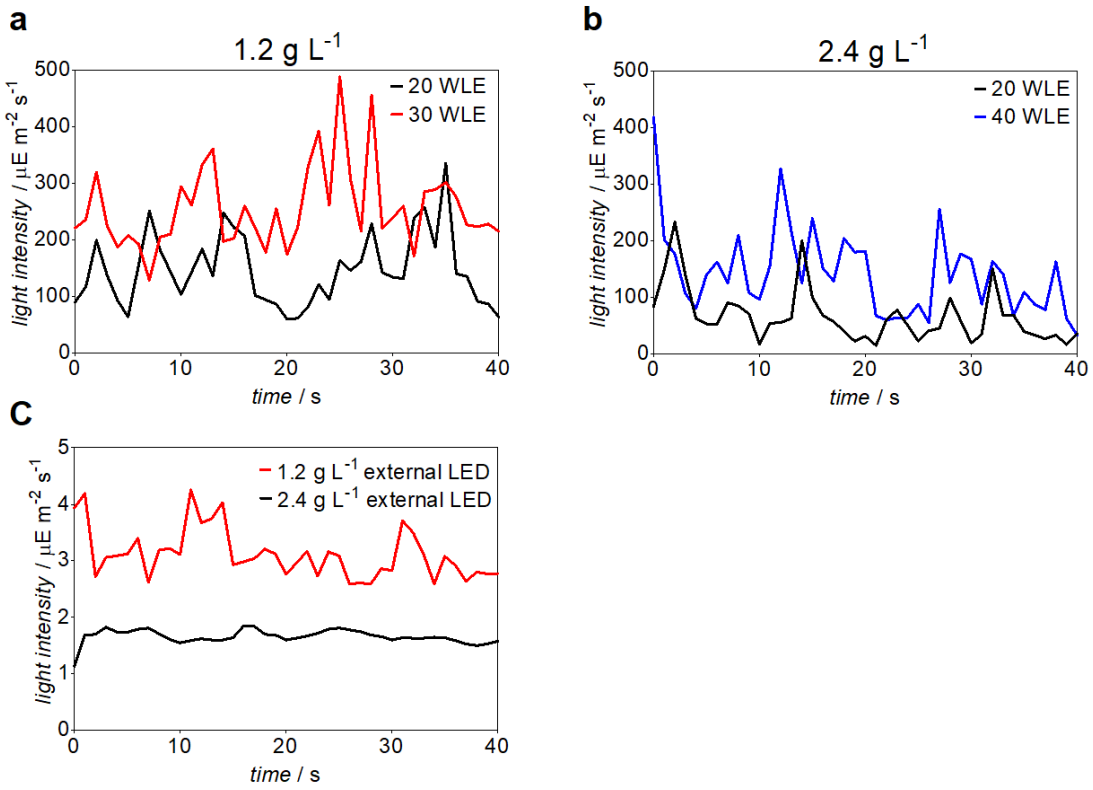

Figure 26. Light Intensity Measurements inside BCR with a) internal illumination at cell density 1.2 g L^{-1}; b) internal illumination at cell density 2.4 g L^{-1}; c) external illumination provided by LED strips.

Table 5. Average light intensity in BCR

Conditions	Average light intensity [µE m^{-2} s^{-1}]
BG11 WLE 40	302.3
BG11 external LED stripes	300.5
0.48 g L^{-1} WLE 20	145.1
0.48 g L^{-1} WLE 30	238.1
0.48 g L^{-1} WLE 40	268.4
1.2 g L^{-1} WLE 20	76.3
1.2 g L^{-1} WLE 40	142.3
2.4 g L^{-1} WLE 40	60.7
1.2 g L^{-1} external LED stripes	3.01
2.4 g L^{-1} external LED stripes	1.66

Synechocystis was cultivated in an aquarium-type reactor at 30 °C using a heater (Thermo Fisher Scientific, Waltham, USA). Each gas washing tube contains 200 mL of cell culture supplemented with 50 µg mL^{-1} of kanamycin as a selectable marker. The cells were allowed to grow to an OD_{750} of 1-3, harvested by centrifugation (24 °C, 15min, 3500 rpm) and subsequently utilized in whole-cell light driven biotransformations. The OD_{750} 10 corresponded to 2.4 g L^{-1} of cell density as previously determined.[121] For this cell density, measured chlorophyll a content was in the range of 29-31 µg mL^{-1}.

a

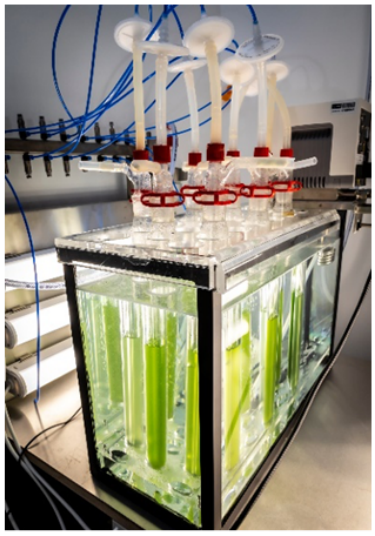

b

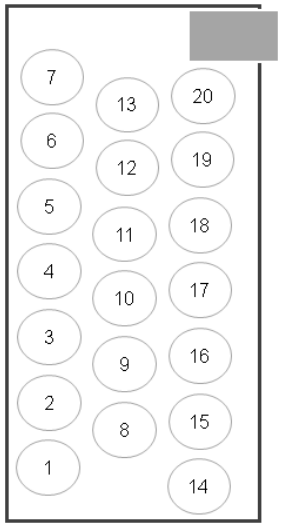

Slot #	Light Intensity	Slot #	Light Intensity
1	207.8	11	243.1
2	230.6	12	232.4
3	249.9	13	211.9
4	256.1	14	220.0
5	250.3	15	222.7
6	239.6	16	227.0
7	220.4	17	223.5
8	218.7	18	220.7
9	232.7	19	208.8
10	240.0	20	197.48

Light Intensity in µE m^{-2} s^{-1}

Figure 27. a) Cultivation of Synechocystis in gas washing tubes in an aquarium maintained at 30 °C, air was delivered using a pump and passed through 0.2 µm filters; b) Light intensity measurements for each tube (measured in water).

8.2.4. Synthesis of 2-Methylmaleimide

2-Methylmaleimide was synthesized as described elsewhere.[70] In a typical reaction, citranoic anhydride (89 mmol) and ammonium acetate (178 mmol) were reacted in acetic acid (40 mL). The mixture was allowed to heat under reflux for 2.5 h. After the reaction, the solvent was partially removed in vacuo. The remaining solution was mixed with 100 mL of saturated NaCl and 40 mL of water. The solution was then extracted with ethyl acetate (8 x 25 mL). The crude product was purified by silica column chromatography using a mobile phase of 5:1 (Cyclohexane: Ethyl acetate) obtaining a white solid product (3.5 g, 35.3% yield).

^{1}H NMR (300 MHz, DMSO-*d6*) δ 10.73 (s, br, 1H, NH), δ 6.54-6.56 (m, 1H, =CH-), δ 1.94 (J_{HH}=1.5 Hz, d, 3H, CH_3,)

^{13}C NMR (300 MHz, $CDCl_3$) δ 10.377, δ 128.166, δ 146.129, δ 172.422, δ 173.310

8.2.5. 2-MS Extraction and characterization

Optically pure (> 99% ee) 2-MS was isolated as a solid powder (157.4 mg, 71% yield). The product was analyzed by ^{1}H and ^{13}C NMR.

^{1}H NMR (300 MHz, $CDCl_3$) δ 7.86 (s, br, 1H, NH), δ 3.02–2.81 (m, 2H, –CH_2-), δ 2.46-2.23 (m, 1H, -CH-), δ 1.41–1.28 (m, 3H, –CH_3)

^{13}C NMR (300 MHz, $CDCl_3$) δ 17.098, δ 36.768, δ 38.194, δ 176.618, δ 180.920

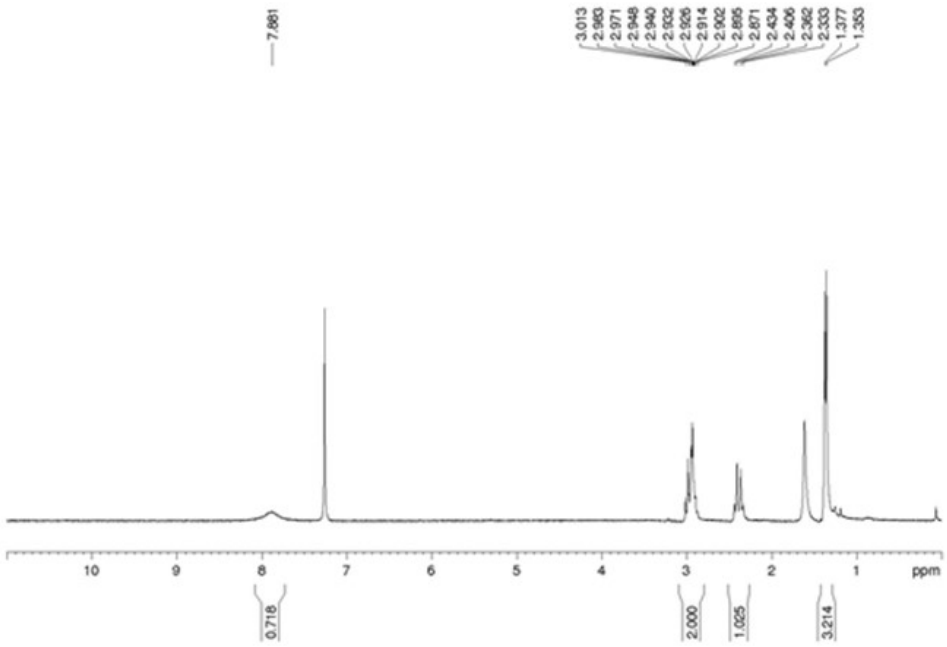

Figure 28. [1]H NMR of 2-MS obtained after whole-cell biotransformation.

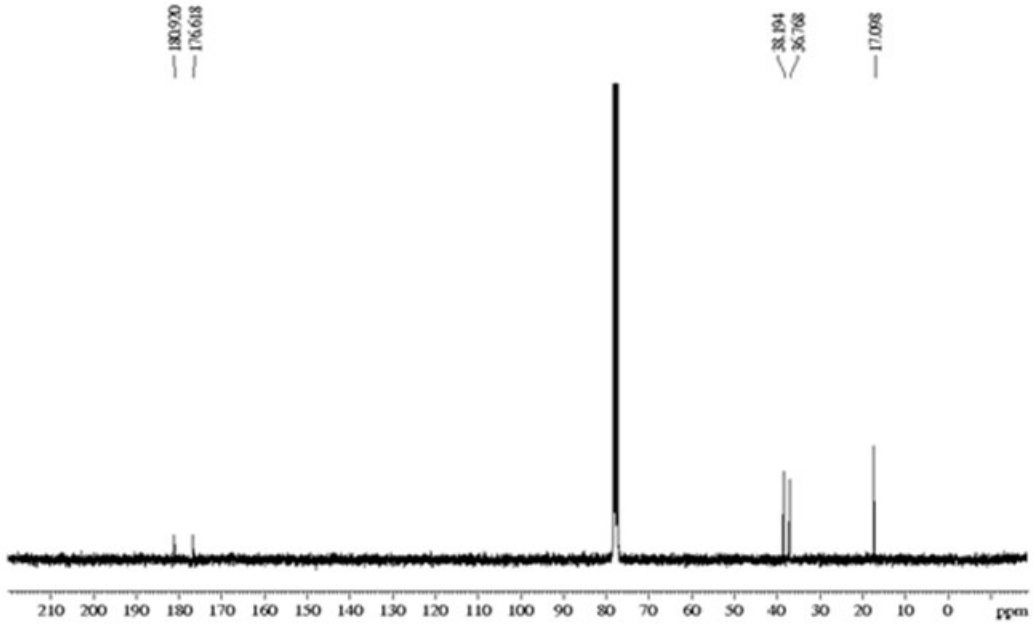

Figure 29. [13]C NMR of 2-MS obtained after whole-cell biotransformation.

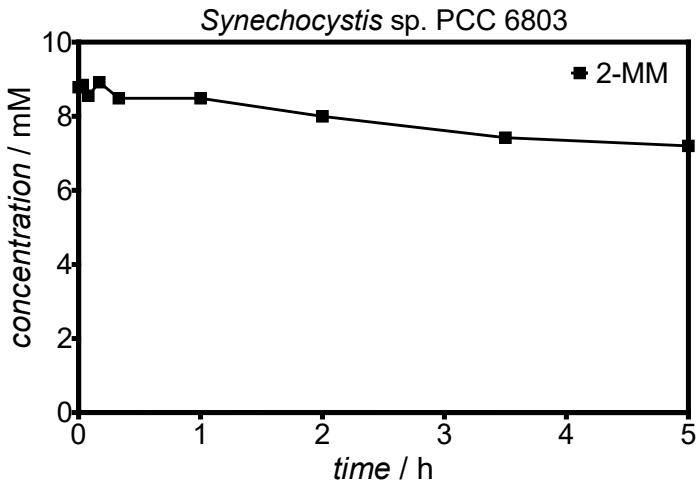

Figure 30. Consumption of 2-MM substrate over time by Synechocystis sp. PCC 6803 WT (1.2 g L^{-1}, 200 mL, 10 mM 2-methylmaleimide, 0.6 L min^{-1} airflow, 40 WLEs).

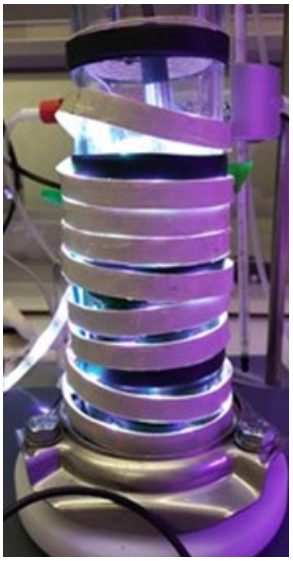

Figure 31. External illumination of BCR provided by LED strips (BOXXX).

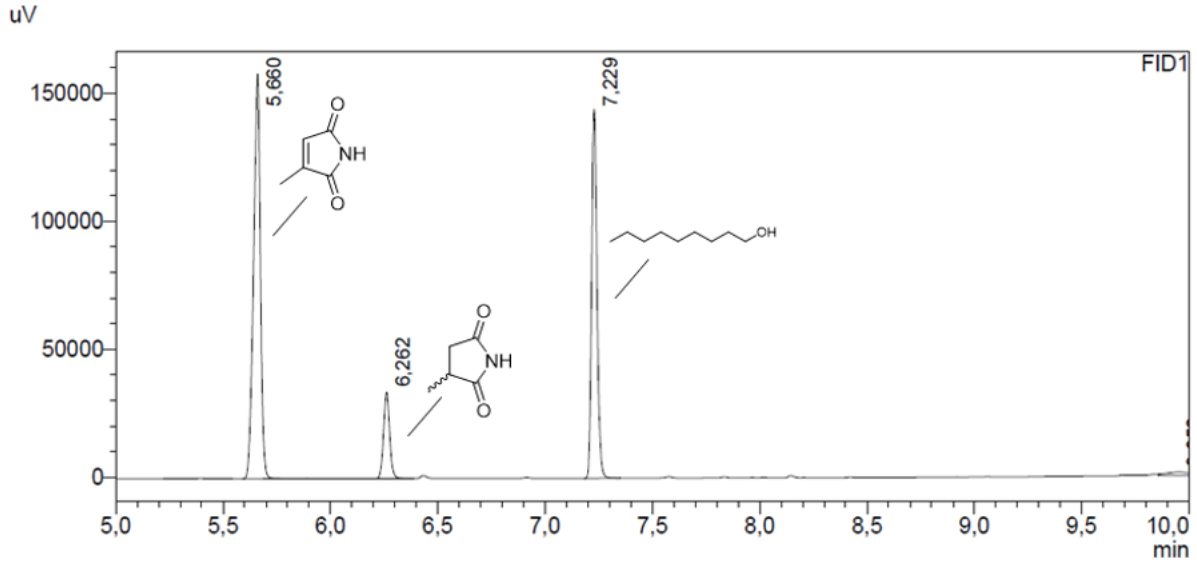

Figure 32. Example GC-Chromatogram with 2-MM substrate (ret. time 5.660 min) and 2-MS product (ret. time 6.262 min). n-decanol (ret. time 7.229 min) was used as an internal standard.

8.2.6. Measurement of emission spectrum

The emission spectrum of a white WLE was measured with a MSC15 spectrometer (Gigahertz-Optik, Türkenfeld, Germany).

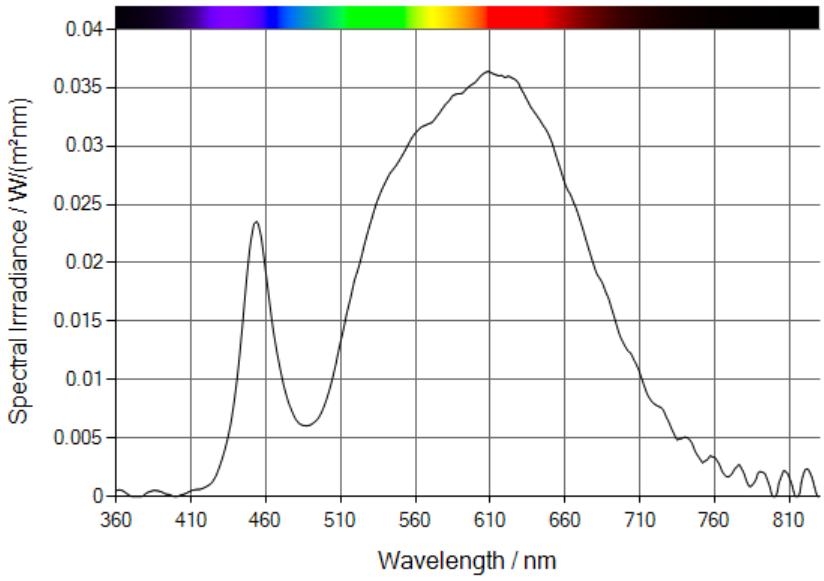

Figure 33. Emission spectrum of a white WLE.

9. Appendix

9.1. Review

Recent developments in the use of peroxygenases – Exploring their high potential in selective oxyfunctionalisations

Markus Hobisch, Dirk Holtmann, Patricia Gomez de Santos, Miguel Alcalde, Frank Hollmann, Selin Kara, Biotechnol. Adv., 2020, 107615, DOI: 10.1016/j.biotechadv.2020.107615

9.2. Technical Report

Automated Feeding and Fermentation Phase Transitions for the Production of Unspecific Peroxygenase by *Pichia pastoris*

Markus Hobisch, Selin Kara, bioRxiv, 2021, preprint, DOI: 10.1101/2021.07.29.454275

Biotechnology Advances xxx (xxxx) xxxx

Contents lists available at ScienceDirect

Biotechnology Advances

journal homepage: www.elsevier.com/locate/biotechadv

Recent developments in the use of peroxygenases – Exploring their high potential in selective oxyfunctionalisations

Markus Hobisch[a], Dirk Holtmann[b], Patricia Gomez de Santos[c], Miguel Alcalde[c,d], Frank Hollmann[e], Selin Kara[a,*]

[a] Department of Engineering, Biocatalysis and Bioprocessing Group, Aarhus University, Gustav Wieds Vej 10, Aarhus C 8000, Denmark
[b] Institute of Bioprocess Engineering and Pharmaceutical Technology, University of Applied Sciences Mittelhessen, Wiesenstr. 14, Gießen 35390, Germany
[c] Department of Biocatalysis, Institute of Catalysis, CSIC, C/Marie Curie 2, Madrid 28049, Spain
[d] EvoEnzyme S.L, C/ Marie Curie 2, Madrid 28049, Spain
[e] Department of Biotechnology, Biocatalysis Group, Delft University of Technology, Van der Maasweg 9, Delft 2629 HZ, The Netherlands

ARTICLE INFO

Keywords:
Oxidation chemistry
Oxyfunctionalisation
Fungal enzyme
Oxygenase
Peroxygenase

ABSTRACT

Peroxygenases are an emerging new class of enzymes allowing selective oxyfunctionalisation reactions in a cofactor-independent way different from well-known P450 monooxygenases. Herein, we focused on recent developments from organic synthesis, molecular biotechnology and reaction engineering viewpoints that are devoted to bring these enzymes in industrial applications. This covers natural diversity from different sources, protein engineering strategies for expression, substrate scope, activity and selectivity, stabilisation of enzymes via immobilisation, and the use of peroxygenases in low water media. We believe that peroxygenases have much to offer for selective oxyfunctionalisations and we have much to study to explore the full potential of these versatile biocatalysts in organic synthesis.

1. Introduction

Biocatalysis is steadily gaining importance in pharmaceutical and industrial chemistry. Especially the high stereo- and regioselectivity of many wild type or tailor-made enzymes is mostly valued. Furthermore, the excellent rate accelerations exceeded by enzymes are very beneficial for many processes as they allow for significantly lower reaction temperatures as compared to many heterogeneous and homogeneous catalysts. (Burek et al., 2019) Analysing the use of enzymes in the chemical industry (Sheldon and Woodley, 2018; Truppo, 2017; Woodley, 2019; Woodley, 2020) it becomes clear that enzymes are applied for a very limited range of production processes. Besides the widespread hydrolases, alcohol dehydrogenases, transaminases and imine reductases are receiving increased interest for the chemical and pharmaceutical production. (Huisman and Collier, 2013; Huisman et al., 2010) Selective oxidation chemistry or even selective oxyfunctionalisation of non-activated C–H-, C–C-, or C = C-bonds remains a white spot on the map of industrial biocatalysis with only a few examples from the pharmaceutical industry. This is astonishing insofar as especially in this area the selectivity benefits of enzymes can fully deploy.

Amongst the oxygenases (E.C. 1.13 and E.C. 1.14), the heme-containing monooxygenases (P450 monooxygenases) are the most popular and best-known catalysts giving access to regio- and stereoselective hydroxylation, epoxidation and heteroatom oxygenation reactions. (Bormann et al., 2015) Given this enormous potential of P450s, the question of why these reactions are not more widespread, especially on industrial scale, suggests itself. Widely discussed reasons are the (i) limited availability of the enzyme, (ii) low substrate loadings, (iii) cofactor dependency of the P450s as well as the so-called (iv) *Oxygen Dilemma*. (Holtmann and Hollmann, 2016) While the first three reasons can certainly be solved by means of molecular biology and technical systems, the last factor (*Oxygen Dilemma*) is more difficult to address. Fe-dependent monoxygenases essentially rely on single electron transfer steps. Hence the hydride provided by NAD(P)H cannot directly reduce the monooxygenases' active sites requiring a relays system to transform the hydride transfer into two successive single electron transfer steps. For this, mediator molecules such as ferredoxins or flavins are used. In their reduced (radical) form, they are however, also prone to direct electron transfer to dissolved O_2. Since (in contrast to e.g. the reaction of O_2 with NAD(P)H) this reaction is spin-allowed, it also occurs at high rates. As a consequence, a significant portion of the reducing equivalents theoretically provided by NAD(P)H does not reach the monooxygenases' active sites but is wasted in a futile reaction with

* Corresponding author.
E-mail address: selin.kara@eng.au.dk (S. Kara).

https://doi.org/10.1016/j.biotechadv.2020.107615
Received 10 February 2020; Received in revised form 10 August 2020; Accepted 14 August 2020

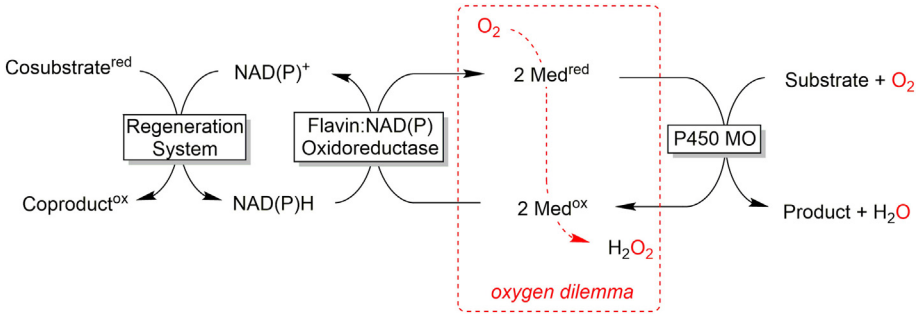

Fig. 1. *Oxygen Dilemma of P450 monooxygenase reactions.* As NAD(P)H cannot directly reduce the (Fe-containing) monooxygenases' active sites redox mediators are necessary to transform the (NAD(P)H-dependent) hydride transfer into two successive single electron transfer steps. The reduced mediators (radicals) however also react spontaneously with dissolved O_2 eventually yielding H_2O_2. This results in a futile uncoupling of the regeneration reaction from the monooxygenation reaction.

O_2 (eventually yielding H_2O_2, Fig. 1).

The final consequence thereof is that the reaction systems tend to be inefficient in terms of turnover numbers of the monooxygenase (*i.e.* moles of product formed per mole of monooxygenase) and hydroxylation (mono-oxygenase) efficiency (*i.e.* the proportion of reducing equivalents provided by the cosubstrate that are productively used for substrate turnover). An alternative class of enzymes that circumvents the *Oxygen Dilemma* are the fungal peroxygenases. These enzymes are structurally related to the aforementioned P450 monooxygenases insofar as they also contain the heme prosthetic group coordinated by a cysteine ligand and therefore, in principle, give access to the same enormous range of reactions and products. In contrast to P450 monooxygenases, peroxygenases do not catalyse the reductive activation of molecular oxygen but rather directly use hydrogen peroxide to form the catalytically active oxyferryl. (Wang et al., 2017) In fact, there do exist bacterial P450 peroxygenases (*i.e.* fed by H_2O_2) which limit their activity to the α-selective hydroxylation of long fatty acids. (Munro et al., 2018; Onoda et al., 2018; Xu et al., 2017) Thus, the *Oxygen Dilemma* can be avoided in general. The aim of the current contribution therefore was to review the current state of the art in practical application of fungal peroxygenases. In particular, the catalysed reactions and substrate scope, applied expression systems, protein engineering approaches to optimise the peroxygenases, reaction engineering as well as the immobilisation techniques will be addressed.

2. Natural diversity and protein engineering

The first reported true heme-thiolate peroxygenase isolated from an edible mushroom that produces white rot, the peroxygenase from *Agrocybe aegerita* (*Aae*UPO) (Ullrich et al., 2004), represents to date the main model enzyme for all peroxygenase chemistry (Hofrichter et al., 2015). After its initial misclassification as an unusual alkaline lignin peroxidase, later as a haloperoxidase, it was referred to as an aromatic peroxygenase (APO), and finally recognised as unspecific peroxygenase (UPO) constituting the first member of a new sub-subclass of oxidoreductases (EC 1.11.2.1). Four other enzymes are part of this subclass: myeloperoxidase (EC 1.11.2.2; $Cl^- + H_2O_2 + H^+ \rightarrow HClO + H_2O$) (Klebanoff, 2005), plant seed peroxygenase (EC 1.11.2.3; $R_1H + R_2OOH \rightarrow R_1OH + R_2OH$) (Hanano et al., 2006), fatty acid peroxygenase (EC 1.11.2.4; fatty acid + $H_2O_2 \rightarrow$ 3- or 2-hydroxy fatty acid + H_2O) (Lee et al., 2003) and 3-methyl-L-tyrosine peroxygenase (EC 1.11.2.5; 3-methyl-L-tyrosine + $H_2O_2 \rightarrow$ 3-hydroxy-5-methyl-L-tyrosine + H_2O) (Tang et al., 2012).

UPO is able to insert oxygen into non-activated C-H (both in aliphatic and aromatic compounds), being more enantio- than regioselective and it can be considered a *Swiss Army knife* for oxyfunctionalisation chemistry whose promiscuity is reflected by its extensive portfolio of transformations (see section 3 on Substrate Scope). Despite its broad substrate specificity (over 400 compounds already described), the peroxygenase sole catalytic requirement is hydrogen peroxide, which acts as both the final electron acceptor and the oxygen donor. The resting state heme binds hydrogen peroxide and through a short-lived compound 0, forms the key intermediate compound I. This strong oxidant can then directly interact with the substrate, forming compound II and subsequently releasing the hydroxylated product. (Hofrichter et al., 2020) While showing a similar chemistry as P450 monooxygenases, UPOs have much less requirements to perform complex oxyfunctionalisation chemistry with high efficiency, in the absence of expensive redox cofactors or auxiliary flavoproteins, being highly active and extracellular secreted enzymes. More significantly, UPOs escape from the O_2 uncoupling which for P450s represents a recurrent problem as up to 90% of all the reducing equivalents provided by the sacrificial substrate can be wasted in the futile uncoupling reaction (the *Oxygen Dilemma*). Given that UPOs can carry out one-electron oxidations (as general peroxidases) and two-electron oxidations (the base for oxyfunctionalisation chemistry), they are considered, from a catalytic point of view the "missing link" between P450s and the classical chloroperoxidase from *Caldariomyces fumago* (*Cfu*CPO, EC 1.11.1.10) –heme-thiolate containing enzyme with a Cys residue as axial ligand of the heme– as well as with general peroxidases with a His residue as axial ligand. As heme thiolate peroxidases, *Cfu*CPO and UPO share an overall similar reaction mechanism, but *Cfu*CPO cannot perform oxygenations of alicyclic/aromatic rings or *n*-alkanes like UPO.

In terms of natural diversity, over 4,000 putative peroxygenase sequences from different fungi have been deposited in the genomic databases, with the characterisation of the following wild type UPOs (*i.e.* produced from the natural fungus): the original *Agrocybe aegerita* –*Aae*UPO– (Ullrich et al., 2004), *Agrocybe parasitica* -*Apa*UPO- (Hofrichter et al., 2015), *Coprinellus radians* –*Cra*UPO–, *Coprinopsis verticillata* –*Cve*UPO– (Anh, 2008; Anh et al., 2007), *Marasmius rotula* –*Mro*UPO– (Gröbe et al., 2011), *Chaetomium globosum* –*Cgl*UPO– (Kiebist et al., 2017), *Marasmius wettsteinii* –*Mwe*UPO– (Ullrich et al., 2018) and *Psathyrella aberdarensis* –*Pab*UPO– (Hofrichter et al., 2020). Given their widespread distribution in fungi, UPOs have been phylogenetically sorted into family I (short peroxygenases) and family II (long peroxygenases). Short UPOs with molecular weights of ~26 kDa (like *Mro*UPO or *Cgl*UPO), are broadly found throughout the fungal kingdom. They are dimeric proteins with a histidine residue as a charge stabiliser at the active site and lack intramolecular disulfide bridges, although they do establish an intermolecular disulfide bridge to connect both monomers. By contrast, long UPOs with molecular weights of ~44 kDa (like *Aae*UPO or *Pab*UPOs) are found in basidiomycetes and ascomycetes, and they are monomeric with an internal disulfide bridge and an arginine residue as a charge stabiliser (Hofrichter et al., 2015). Both families have highly conserved sequences at the active site (*i.e.* -EHD-S-E- and -EGD-S-R-E for short and long UPOs, respectively). The composition, dimensions and conformation of heme access channel between the short and long clades are reflected in their distinct substrate profiles and functions, Table 1. (Hofrichter et al., 2020) Short UPOs heme access channel is upholstered by flexible aliphatic amino acids and is shorter but wider compared with that of long UPOs, which is translated for the former into a preference for bulky substrates like steroids (Kiebist et al., 2019). Conversely, long UPO's channel is formed by rigid aromatic amino acids, which determine a substrate preference towards

Table 1
General comparison between *Mro*UPO (short clade) and *Aae*UPO (long clade).

	UPO Family	
Clade/UPO	Short/*Mro*UPO	Long/*Aae*UPO
Molecular weight	29 kDa	44.4 kDa
pI	6.41	5.77
Conformation	Dimeric	Monomeric
Disulfide bridges	Intermolecular to connect monomers	C-terminal
Hydrophobic amino acids lining the channel	Aliphatic amino acids	Aromatic amino acids
Charge stabiliser	Histidine 86	Arginine 189
Other examples	*Mwe*UPO, *Cgl*UPO	*Pab*UPOs, *Cra*UPO, r*Cci*UPO

smaller aromatic substrates (Fig. 2). The role of UPO in nature remains uncertain, with several activities proposed, including the synthesis of metabolites, detoxification processes and the lignin degradation by its *O*-demethylation activity. (Hofrichter et al., 2015)

The main hurdle for a new peroxygenase-based chemistry is the production and engineering of UPO in efficient recombinant expression systems. Indeed, the heterologous functional expression of UPOs is the main bottleneck for their industrial application. Missing chaperones along with different post-translational modifications (glycosylation, disulfide bridge, N- and C- terminal processing) among natural and heterologous hosts are high hurdles that must be avoided with only a few successful examples hitherto described in the literature: the evolved *Aae*UPO mutant (called PaDa-I variant) and the offspring of variants commercialised by EvoEnzyme (Gomez de Santos et al., 2018; Gomez de Santos et al., 2019; Martin-Diaz et al., 2018; Mate et al., 2017; Molina-Espeja et al., 2016; Molina-Espeja et al., 2014; Molina-Espeja et al., 2015; Ramirez-Escudero et al., 2018), as well as the UPOs developed by Novozymes heterologously expressed in *Aspergillus oryzae*: UPO from *Coprinopsis cinerea* (r*Cci*UPO) (Babot et al., 2013) and UPO from an undetermined mould (rNOVO) (Peter et al., 2014). Besides, very recently *Mro*UPO (Carro et al., 2019) and *Collariella virescens* UPO (*Cvir*UPO) (González-Benjumea et al., 2020) have been reported to be expressed in *Escherichia coli*. Similarly, *Cfu*CPO also suffers the same expression problems as UPO, with only one heterologous expression system developed in the filamentous fungi *Aspergillus niger* (10 mg/L), as well as some strain engineering in the original fungus to enhance production up to remarkable levels of 1.95 g/L. (Buchhaupt et al., 2011; Conesa et al., 2001)

Within the wish list for UPOs protein engineers we can find: the modification of selectivity, the enhancement of the turnover numbers in a given process, the removal of the unwanted peroxidase activity during oxyfunctionalisation reactions, to stop overoxidation reactivities, to improve oxidative stability as well as its performance in the presence of organic co-solvents and/or at high temperatures. As mentioned above, for all these goals, it is first necessary to heterologously and functionally express the enzyme in a host suited to sculpture its properties by directed evolution (Molina-Espeja et al., 2017). To date, the most successful case story of UPO engineering has been achieved with the *Aae*UPO, which was first heterologously functional expressed in *Saccharomyces cerevisiae* and *Pichia pastoris* (*Komagataella phaffii*) after several rounds of laboratory directed evolution (Molina-Espeja et al., 2014). With expression levels of 8 mg L^{-1} in *S. cerevisiae* and above 200 mg L^{-1} in *P. pastoris* in a bioreactor (Molina-Espeja et al., 2015), the highly active and stable *Aae*UPO secretion variant (PaDa-I) was subjected to new directed evolution campaigns aimed at producing, with high efficiency, from agrochemicals (1-naphthol) (Molina-Espeja et al., 2016) to human drug metabolites (Gomez de Santos et al., 2018; Gomez de Santos et al., 2019). Moreover, the PaDa-I variant was studied by structured-guided evolution and neutral genetic drift in an attempt to make a breakdown of the peroxygenase and peroxidase activities, as well as to expand its substrate promiscuity and stability (Martin-Diaz et al., 2018; Mate et al., 2017). Within this framework, the crystal structure of PaDa-I was solved at a resolution of 1.5 Å. Exhaustive soaking experiments with a panel of peroxidase and peroxygenase substrates combined with the construction of mutant libraries demonstrated an exceptional dynamic trafficking through the heme channel as the main driving force for the substrate promiscuity of PaDa-I (Ramirez-Escudero et al., 2018). Taken together, these findings are opening a new venue for future protein engineering towards more regio- and enantioselective variants by combining computational and directed

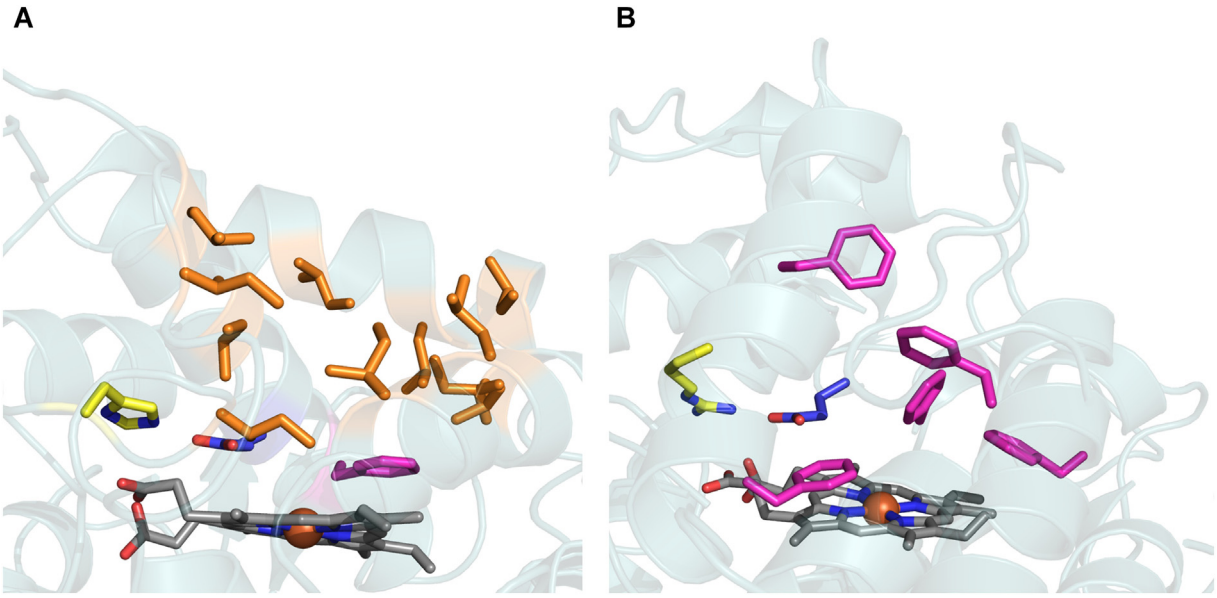

Fig. 2. Heme access channel of (A) *Mro*UPO (short UPO family) and (B) *Aae*UPO (long UPO family). Glutamic acid from the acid base pair is depicted in blue (Glu157 in *Mro*UPO and Glu196 in *Aae*UPO) and charge stabiliser amino acid is colored in yellow (His86 in *Mro*UPO and Arg189 in *Aae*UPO). Heme access channel lining amino acids are represented in orange (hydrophobic aliphatic in *Mro*UPO) and in pink (hydrophobic aromatic in *Aae*UPO). The models were visualised with Pymol (http://pymol.org) using the crystal structure of *Mro*UPO at a resolution of 1.83 Å (PDB ID: 5FUJ) and *Aae*UPO at a resolution of 2.19 Å (PDB ID: 2YOR). (For interpretation of the references to color in this figure legend, the reader is referred to the web version of this article.)

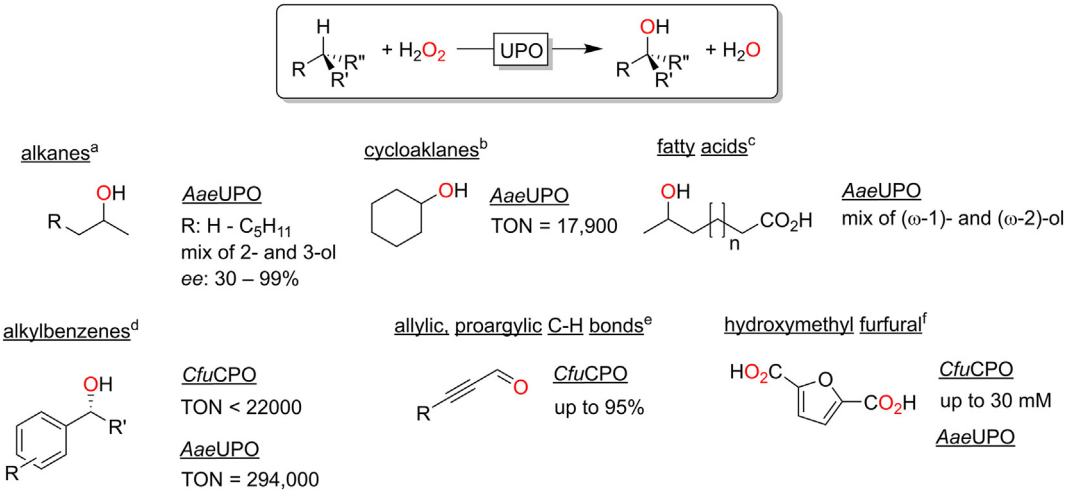

Fig. 3. Selection of hydroxylation products obtained with peroxygenases. a) (Peter et al., 2011); b) (Churakova et al., 2011); c) (Gutierrez et al., 2011); d) (Ni et al., 2016; Park and Clark, 2006; Zaks and Dodds, 1995); e) (Hu and Hager, 1998); f) (Carro et al., 2015; van Deurzen et al., 2006)

evolution approaches.

3. Substrate scope

Peroxygenases rely on Compound I as the actual oxidant in their catalytic mechanism. This puts peroxygenases in mechanistic relationship to the well-known P450 monooxygenases. (Fasan, 2012; Hofrichter and Ullrich, 2014; Urlacher and Girhard, 2019) Therefore, it is not very astonishing that peroxygenases have been applied for a broad range of P450-like oxidation and oxyfunctionalisation reactions. The current scope and limitations will be outlined in the following:

3.1. Peroxygenase-catalysed hydroxylation of aliphatic C-H bonds

A representative selection of peroxygenase-catalysed hydroxylation of sp^3-hybridised C-H bonds is shown in Fig. 3.

In the late 1990s, *Cfu*CPO had been in focus of research (see section 2 on Natural Diversity and Protein Engineering). From the known substrate scope, however, it becomes clear that *Cfu*CPO exhibits significant activity only on activated C-H-bonds such as benzylic, allylic or propargylic C-H bonds. Also the turnover numbers (TONs, $mol_{product} \cdot mol_{enzyme}^{-1}$) of *Cfu*CPO observed in these experiments predominantly lie in the several hundreds to few thousands range. The more recent peroxygenases such as the one from *Agrocybe aegerita* (*Aae*UPO) exhibit significantly higher activity. Hydroxylation of non-activated (cyclo-)alkanes is possible with these enzymes thereby opening up a range of possible applications in the synthesis of (chiral) fine chemicals and even bulk chemicals.

Nevertheless, the current (wild-type) peroxygenases also frequently face issues of poor selectivity: The hydroxylation of CH_3- or CH_2-groups, for example, is frequently accompanied by overoxidation. In other words, the initially formed (chiral) alcohol is in some cases is further oxidised to the corresponding ketones, aldehydes or carboxylic acids (Fig. 4). In the oxidation of cyclohexane, for example, *Aae*UPO predominantly forms the cyclohexanol whereas *Mro*UPO forms the ketone in higher concentrations. (Peter et al., 2014)

Chemoselectivity issues are frequently observed in the hydroxylation of activated (benzylic or allylic) C-H bonds. The conversion of alkenes, for example, frequently yields mixtures of epoxides and allylic hydroxylation products (Fig. 5). Allylic methyl groups, however, appear to be non-reactive. Similar observations had also been made with *Cfu*CPO. (Zaks and Dodds, 1995)

It is also interesting to note that e.g. in case of *Aae*UPO-catalysed hydroxylation reactions of alkyl aromatics the chemoselectivity very much depends on the structure of the starting material. The hydroxylation of ethyl benzene for example yields almost exclusively (*R*)-1-phenyl ethanol (and traces of the overoxidation product) while the conversion of toluene yields a complex mixture of benzyl alcohol and various over oxidation- and ring hydroxylation products (Fig. 5). (Ullrich and Hofrichter, 2005)

Finally, also the **regioselectivity** of peroxygenase-catalysed hydroxylation reactions is worth discussing. The peroxygenases available today exhibit a very broad selectivity spectrum for example for the hydroxylation of fatty acids (Fig. 6). While *Aae*UPO prefers subterminal hydroxylation, the UPO from *Marasmius rotula* (*Mro*UPO) also exhibits significant activity on the terminal CH_3-group as well as α-oxidation followed by decarboxylation (fatty-acid shortening). (Olmedo et al., 2017) Some recently reported P450 peroxygenases prefer C-H-bonds closer to the carboxylate group. Among them, the P450 peroxygenase OleT yields terminal alkenes from fatty acids, presumably via α-hydroxylation followed by decarboxylation. (Zachos et al., 2015)

3.2. Peroxygenase-catalysed hydroxylation of aromatic C-H bonds

A range of preparatively very relevant aromatic hydroxylation reactions using peroxygenases have been reported in recent years. Apparently, only the new, true peroxygenases such as *Aae*UPO are efficient in this reaction. Fig. 7 gives an overview over the variety of products obtainable via peroxygenase-catalysis.

The mechanism of peroxygenase-catalysed aromatic hydroxylation has been investigated intensively by Hofrichter and co-workers (Barková et al., 2011; Hofrichter and Ullrich, 2014; Kluge et al., 2009) and appears to proceed in most cases via an aromatic epoxide intermediate, which then spontaneously rearranges to the corresponding phenol (Fig. 8).

Though already today, a broad range of interesting aromatic hydroxylation reactions are possible, there are nevertheless also a range of challenges that need to be addressed. One of them is the above-mentioned chemoselectivity issue in the hydroxylation of alkyl benzenes (Fig. 5). Another issue is the peroxidase-activity of peroxygenases (Fig. 9). In other words, the phenol (originating from the aromatic hydroxylation reaction) can serve as substrate for a peroxygenase, which through its peroxidase activity (one electron oxidation reaction) undergo an H-atom-abstraction reaction yielding phenoxy radicals. The latter are rather reactive and undergo spontaneous polymerisation reactions, which obviously in most cases are not desired. One possibility to alleviate this polymerisation reaction is to administer radical scavengers to the reaction mixture. Ascorbic acid, for example, is

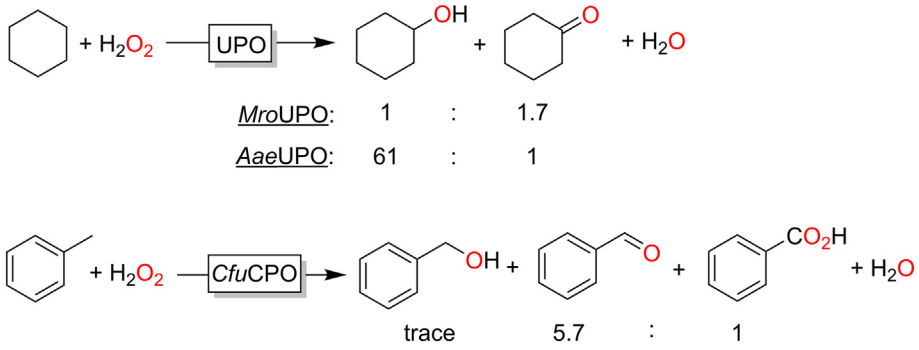

Fig. 4. Overoxidation issues observed in peroxygenase-catalysed hydroxylation of C-H bonds. Depending on the UPO used, the oxidation of cyclohexane yields either predominantly cyclohexanol or cyclohexanone. (Peter et al., 2014) Using *Cfu*CPO for the hydroxylation of toluene, Dodds and coworkers observed significant overoxidation of the initial benzyl alcohol to the aldehyde and acid. (Zaks and Dodds, 1995)

frequently used to suppress the polymerisation reaction.

More elegantly, Alcalde and co-workers have shown that protein engineering in principle can yield peroxygenase mutants with drastically reduced peroxidase activity. (Molina-Espeja et al., 2016)

3.3. Peroxygenase-catalysed epoxidation reactions

The chemical versatility of epoxides as starting materials for a myriad of synthetic transformations has ever since motivated research on *Cfu*CPO and, more recently, on *Aae*UPO-catalysed epoxidation reactions. As can be seen from Fig. 10, *Aae*UPO appears to be the more suitable catalyst for this reaction (as judged by the turnover numbers reported). Even though it appears that epoxidation reactions have not been in focus of the ongoing research efforts for *Aae*UPO.

One major limitation of peroxygenases *en route* to truly applicable epoxidation catalysts is the frequently observed poor chemoselectivity of the reaction also yielding the allylic hydroxylation products. Furthermore, gaining control over the stereo- and (in case of starting materials containing several C=C-double bonds) regioselectivity (Fig. 11). This issue has been studied extensively by Hofrichter and coworkers. (Peter et al., 2013)

3.4. Peroxygenase-catalysed sulfoxidation reactions

In terms of classical, oxygen transfer reactions, finally, also peroxygenase-catalysed sulfoxidation reactions are worth being mentioned here. In contrast to the aforementioned hydroxylation – and epoxidation reactions, *Cfu*CPO truly excels as catalyst as usually very high turnover numbers are reported for this type of reaction (Fig. 12). It is also worth mentioning that overoxidation to the corresponding sulfones is generally not observed.

While *Cfu*CPO has been studied extensively, to the best of our knowledge, only one analytical study on *Aae*UPO-catalysed sulfoxidation (albeit reporting excellent enantioselectivities and conversions) has been published yet. (Bassanini et al., 2017)

3.5. Miscellaneous

Both, *Cfu*CPO and *Aae*UPO had first been reported as haloperoxidases catalysing the H_2O_2-driven oxidation of halides to the corresponding hypohalites. For quite some time, this has been regarded as a synthetically less relevant reaction (because the hypohalite diffuses out of the enzyme active site and undergoes chemical, non-selective transformations). In recent years, the synthetic value, however, is increasingly recognised leading to a range of interesting transformations (Fig. 13). In this respect it is worth mentioning that the classical heme-dependent peroxidases are nowadays increasingly being complemented by the (more H_2O_2-robust) vanadium-dependent haloperoxidases.

4. Reaction and medium engineering approaches

The following parts focus on the specific applications of peroxygenases. Firstly, we discuss the essential but also destructive reaction component H_2O_2 and photobiocatalysis as a possible solution for this challenge. Secondly, enzyme immobilisation approaches followed for peroxygenases are introduced, as it can increase enzyme stability and

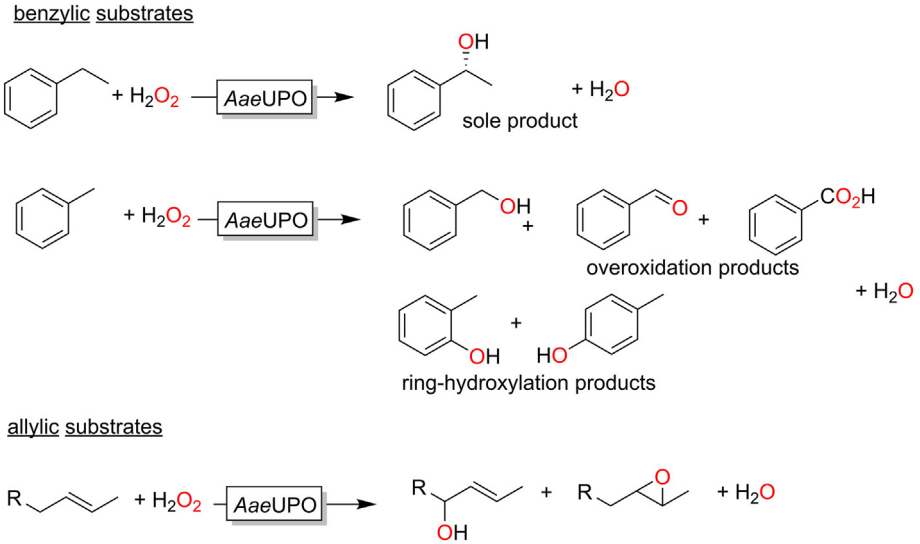

Fig. 5. Selectivity issues observed in *Aae*UPO-catalysed hydroxylation reactions of activated (benzylic or allylic substrates). (Peter et al., 2013; Ullrich and Hofrichter, 2005)

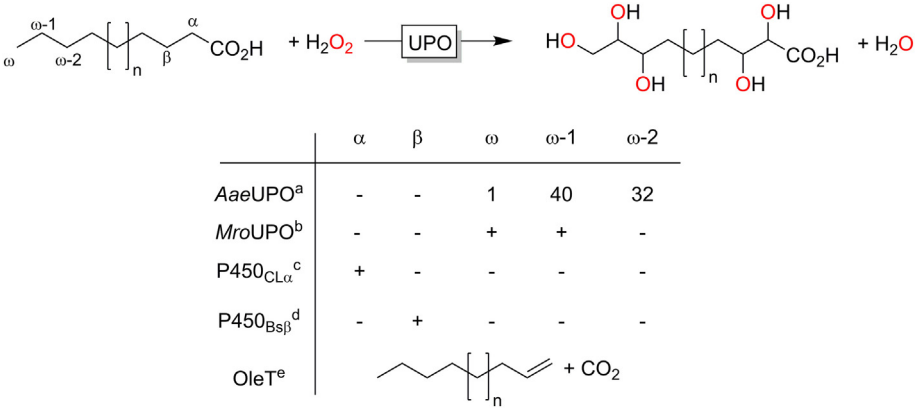

	α	β	ω	ω-1	ω-2
*Aae*UPO[a]	-	-	1	40	32
*Mro*UPO[b]	-	-	+	+	-
$P450_{CL\alpha}$[c]	+	-	-	-	-
$P450_{Bs\beta}$[d]	-	+	-	-	-
OleT[e]					

Fig. 6. Regioselectivity of some peroxygenases in the conversion of fatty acids. a) (Gutierrez et al., 2011); b) (Olmedo et al., 2016); c) (Girhard et al., 2007); d) (Paul et al., 2014); e) (Zachos et al., 2015).

facilitate reuse of the biocatalyst. At last, a second important aspect of economic feasibility is discussed: Volumetric productivity. This part is on the increase of substrate loading for hydrophobic peroxygenase substrates by using non-conventional media, which may in turn, necessitates the use of immobilised enzymes for increased stability.

4.1. H_2O_2 challenge and photobiocatalysis

The use of hydrogen peroxide (H_2O_2) needed at stoichiometric amounts for enzymatic oxidation reactions (e.g. peroxidase-, peroxygenase catalysed) faces the challenge of heme oxidation leading to enzyme inactivation. To alleviate this limitation, several strategies have been developed for *in situ* supply of H_2O_2. Those include enzymatic production using glucose oxidase (Fred van Rantwijk, 2000) or formate oxidase (Tieves et al., 2019), electrochemistry (Horst et al., 2016; Krieg et al., 2011), chemical catalysis (Freakley et al., 2019) and photocatalysis.

Light-driven methods generally rely on a photocatalyst that, when excited by light, can oxidise an electron donor and can transfer the reducing equivalents to oxygen, generating H_2O_2 (Fig. 14).

One of the first published examples of this light-driven approach was the use of *Aae*UPO in combination with flavin adenine mononucleotide (FMN) as photocatalyst and ethylenediaminetetraacetic acid (EDTA) as co-substrate. This system was able to hydroxylate a range of alkylic and aromatic substrates and to catalyse the epoxidation reaction of styrene and some of its derivatives. (Churakova et al., 2011)

Later on, an approach with higher atom efficiency was reported by Zhang *et al.* using gold loaded rutile titanium dioxide (Au-TiO_2) as photocatalyst and methanol as sacrificial electron donor, in combination with the engineered *Aae*UPO PaDa-I. Upon illumination with visible light, full conversion of the model substrate ethylbenzene (15 mM) was reached within 72 hours and (*R*)-1-phenylethanol was produced with high selectivity (98.2% *ee*). In line with the previously discussed substrate scope of *Aae*UPO, they were also able to hydroxylate other alkanes producing only minor amounts of the corresponding ketone as side product. In ^{1}H-NMR analysis, they found methanol was photocatalytically oxidised not only to formaldehyde, but also subsequently to formate. When using formaldehyde and formate as electron donors and comparing it to methanol, the authors reported H_2O_2 formation rates to be 75% higher and reaction rates to be 32% and 18% higher, respectively. (Zhang et al., 2017) One interesting prospective of using Au-TiO_2 is that due to its water oxidation activity, also water as sacrificial electron donor for the *in situ* generation of H_2O_2 comes into reach. While the hydroxylation of ethylbenzene achieved lower yields than with co-substrate, a linear correlation between concentration of photocatalyst and concentration of acetophenone, the over-oxidised side product was observed. This prompted the researchers to extend the photocatalytic reaction with a second enzyme.

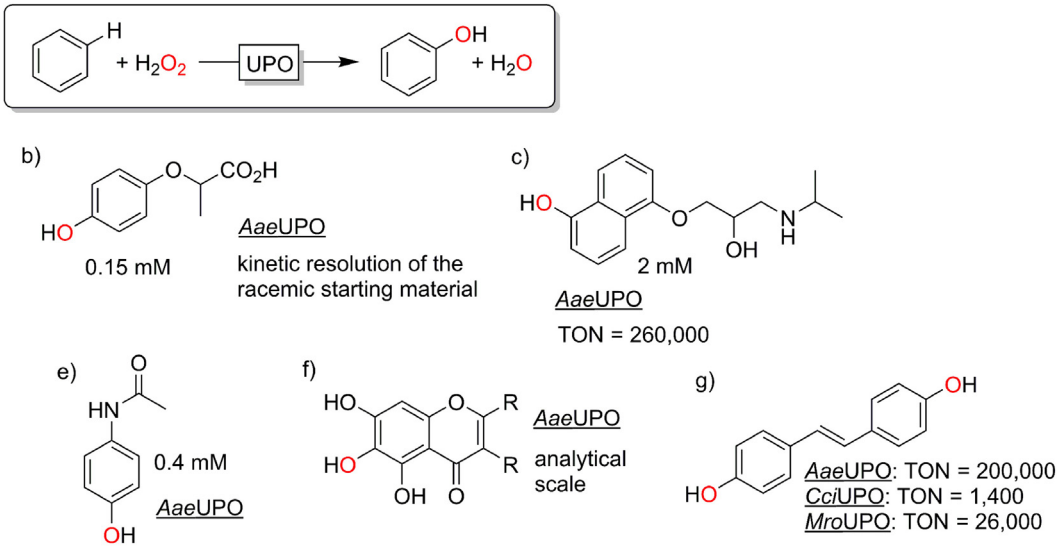

Fig. 7. Selection of peroxygenase-catalysed aromatic hydroxylation products. a) (Molina-Espeja et al., 2016; Ullrich and Hofrichter, 2005); b) (Kinne et al., 2008); c) (Gomez de Santos et al., 2018; Kinne et al., 2009); d) (Kinne et al., 2009); e) (Poraj-Kobielska et al., 2011); f) (Barková et al., 2011); g) (Aranda et al., 2018).

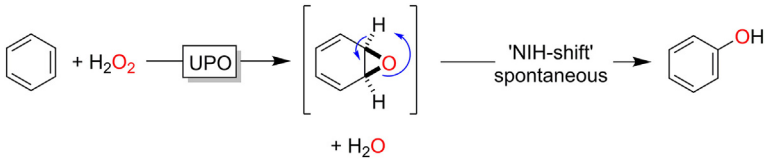

Fig. 8. Mechanism of the peroxygenase-catalysed hydroxylation proceeding via an intermediate arene oxide, which spontaneously rearranges into the corresponding phenol (NIH-shift).

Phenylethanol was oxidised to acetophenone by PaDa-I and rutile Au-TiO_2, which was then converted to (*R*)- *and* (*S*)-phenyl ethylamine by addition of ω-transaminases from *Aspergillus terreus* and *Bacillus megaterium*, respectively. Similarly, they oxidised toluene to benzaldehyde and then added benzaldehyde lyase from *Pseudomonas fluorescence* to perform a benzoin condensation, yielding (*R*)-benzoin. Overall, artificial cascade pathways could be successfully demonstrated initiated with photobiocatalytic oxyfunctionalisation step. Promising results were also achieved with carbon nanodots (CNDs) as non-metal photocatalysts. The combination of PaDa-I, CNDs and FMN yielded a higher initial rate (0.81 $mM{\cdot}h^{-1}$ vs 0.16 $mM{\cdot}h^{-1}$) and higher enzyme TONs (100,000 vs 21,000) when compared with Au-TiO_2. Furthermore, Au-$BiVO_4$ and g-C_3N_4 were investigated for their applicability with PaDa-I. While Au-$BiVO_4$ yielded comparably low product formation, g-C_3N_4 produced more overoxidation products. (Zhang et al., 2018)

While the system using Au-TiO_2 worked well, the reaction proceeded quite slowly, reaching full conversion of 15 mM after 72 h. (Zhang et al., 2018) This was partially due to the fact that the photocatalyst can only be excited by light below 413 nm, which makes up only 0.7% of the light emitted by the lamp used. (Zhang et al., 2017) An effort to accelerate this PaDa-I reaction by expanding the usable spectrum of visible light was made by Willot *et al.,* using a combination of three photosensitizers covering a wide range of wavelengths. They were applied in combination with a formate dehydrogenase (*Cb*FDH from *Candida boidinii*) reducing NAD^+ to NADH and oxidising formate to carbon dioxide. The produced NADH was used by the excited photocatalysts (FMN, phenosafranine and methylene blue) to produce H_2O_2, which was then utilised by PaDa-I to hydroxylate ethylbenzene (10 mM). After only four hours, full conversion to 10 mM (*R*)-1-phenylethanol was achieved. While the reaction proceeded remarkably fast, its robustness was lacking. Especially the photocatalyst FMN and *Cb*FDH were rather unstable, exhibiting turnover numbers of only 649 and 135, respectively. (Willot et al., 2019)

Also for *Cfu*CPO photocatalytic H_2O_2 supply systems were reported. One approach used FMN as a photocatalyst and EDTA or formate as an electron donor for the enantioselective sulfoxidation of thioanisole to the (*R*)-sulfoxide. While formate would pose a more environmentally benign co-substrate compared to EDTA, it lowered the enantioselectivity (78% *ee*, > 99% *ee* with using EDTA). (Perez, D.I. et al., 2009) The reason was attributed to binding of the formate to the heme-iron as suggested by crystallographic data, which was shown for CPO-catalysed epoxidation of limonene. (Águila et al., 2008)

Another photobiocatalytic application of *Aae*UPO added electrochemistry to the system. Choi *et al.* demonstrated the hydroxylation of ethylbenzene using single walled carbon nanotube (SWNT) electrodes. To reduce the overpotential required to reduce O_2 and produce H_2O_2 the SWNTs were hybridised with lumichrome, a flavin derivative. When exposed to visible light this treatment facilitated the transfer of electrons to O_2, reducing the required overpotential substantially, which resulted in a more energy efficient H_2O_2 synthesis. (Choi et al., 2017)

The choice of *the in situ* H_2O_2 generation system will also influence the overall environmental impact of the oxyfunctionalisation system. Sacrificial electron donors such as methanol or formate generate less and less problematic wastes than e.g. EDTA or TRIS. Essentially waste-free systems based on H_2 (Al Shameri et al., 2020)), water oxidation or renewable electricity will be preferable. These systems, however, also need to enable robust UPO catalysis at scale as well. Considering that enzyme production is a major contributor to the environmental impact of biocatalytic processes (Delgove et al., 2019; Tieves et al., 2019) those systems enabling the highest biocatalyst utilisation will be the 'greenest'. Comparative life cycle assessments investigating this issue would be helpful to guide future research and industrial applications.

4.2. Strategies for peroxygenase immobilisation

While photocatalytic provision of H_2O_2 has been explored using alternative photocatalyst and cosubstrates, it remains as a challenge to develop peroxygenase-catalysed biotransformations with high productivity and low cost contribution of the enzyme. Robust heterogeneous biocatalysts, that are stable at process conditions and that can be recovered and reused, may result in process simplification and reduced processing time combined with a higher product quality and a smaller environmental footprint. Enzyme immobilisation in turn enables the use of non-conventional media for biocatalysis as it restricts conformational mobility and avoids consequent unfolding allowing highly productive biocatalysis in non-aqueous media.

However, the need for enzyme immobilisation has to be assessed carefully, as described below, before making the decision. Based on the TON achievable, a judgement can be made if there is a need for enzyme immobilisation or not. It was proposed that if the TON is too low, immobilisation is not economically viable due to the cost of most of the solid supports, unless they come from a waste stream.(Janssen et al., 2011; Liese and Hilterhaus, 2013) On the other hand, if the TON is very high with a free enzyme or if the product is highly expensive, making a cost contribution of the enzyme < 0.05% compared to overall operational costs, then there is no need to immobilise the enzyme. Hence, if the TON value lies in between these borders, then enzyme immobilisation is recommended. The following parts summarizes the studies on immobilisation of UPOs with the aim to have quantitative comparisons mainly on TON values.

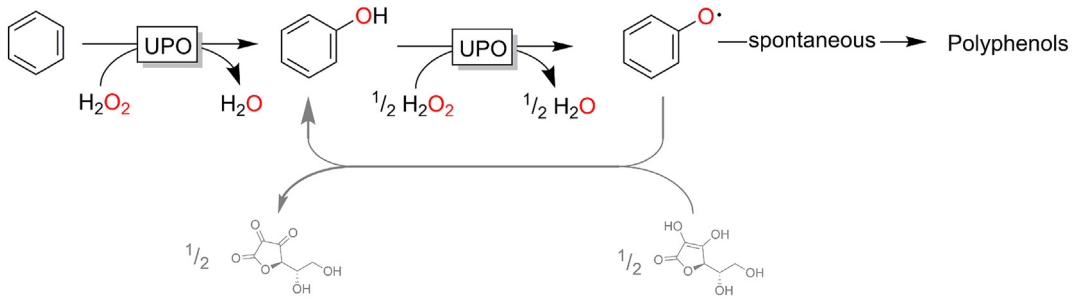

Fig. 9. Peroxidase activity of peroxygenases as a challenge for the hydroxylation of aromatic compounds.

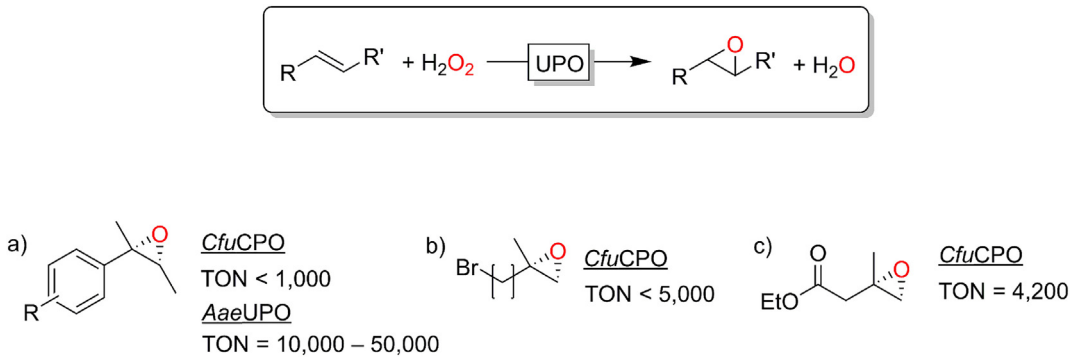

Fig. 10. Selection of peroxygenase-catalysed epoxidation reactions. a) (Kluge et al., 2012; Lakner et al., 1997; Rauch et al., 2019); b) (Lakner et al., 1997); c) (Dexter et al., 1995)

To immobilise *Cfu*CPO various carriers have been used so far (Table 2). For instance copolymer hydrogel membranes made from poly (hydroxypropyl methacrylate-co-polyethyleneglycole-methacrylate) (p (HPMA-co-PEG-MA)). While this covalent immobilisation led to an increase in the K_M from 24.6 to 47.3 μM in comparison to the free enzyme, it also provided increased stability. The immobilised enzyme exhibited increased robustness against higher temperatures, increased storage stability and excellent operational reusability with no activity loss over 9 cycles and only 27% loss first after 25 cycles. (Bayramoglu et al., 2011) Interesting results were published for the adsorptive immobilisation of *Cfu*CPO on mesoporous silica. (Águila et al., 2011) The immobilisation resulted not only in enhanced stability, like a four- to five fold increase of the TON, it also led to a nine-fold increase of the turnover frequency (k_{cat}). Similar results were reported for adsorptive *Cfu*CPO immobilisation in TiO_2 nanotubes. Not only the stability, but also the k_{cat} was increased, even by a factor of 16. The authors attributed this to a confinement effect that reduces enzyme unfolding. (Muñoz-Guerrero et al., 2015) The molecular understanding of this effect needs to be improved. It has been shown that if an enzyme is deposited in a tight pore or shares a larger pore with many other enzymes, its folded structure I favoured over its unfolded form, which increases thermal stability and activity.(Ping et al., 2004; Ping et al., 2003; Ravindra et al., 2004). A carrier-free approach for *Cfu*CPO immobilisation is aggregation and crosslinking. Co-precipitating the enzyme with pentaethylenehexaneamine (PEHA, works as amine donor) yielded a recovered activity of 68% and a biocatalyst more stable towards elevated temperature and inactivation by H_2O_2 compared to the free enzyme. (Perez, D. et al., 2009)

Looking at Table 2, it is evident that CPOs in general and *Cfu*CPO in particular are well-established biocatalysts as they were used in numerous immobilisation experiments with a wide variety of carrier materials. However, on the immobilisation of UPOs, there are dramatically few publications. Covalent immobilisation of *Aae*UPO on methacrylate polymer was used to increase enzyme stability in the photobiocatalytic oxidation of ethylbenzene. The removal of the enzyme from the oxidative influence of the used TiO_2 photocatalyst proved beneficial for the reaction's robustness as the enzyme's TON was increased by a factor of eight. (Zhang et al., 2018) A particularly sophisticated approach, published by Molina et al., was the directed unique-point covalent immobilisation (DUCI) of *Aae*UPO. For this the previously produced mutant PaDa-I (Ramirez-Escudero, M. et al., 2018) was further modified to carry one Cys residue on the enzyme surface opposite to the entrance of the active site. This Cys was then used for the covalent attachment of the enzyme to two different carriers (epoxy polymethylacrylate and agarose). While for both carriers the recovered activity was around 15%, further experiments with the agarose preparation showed increased robustness against acetonitrile and pH greater than 5 and improved temperature stability. (Molina-Espeja

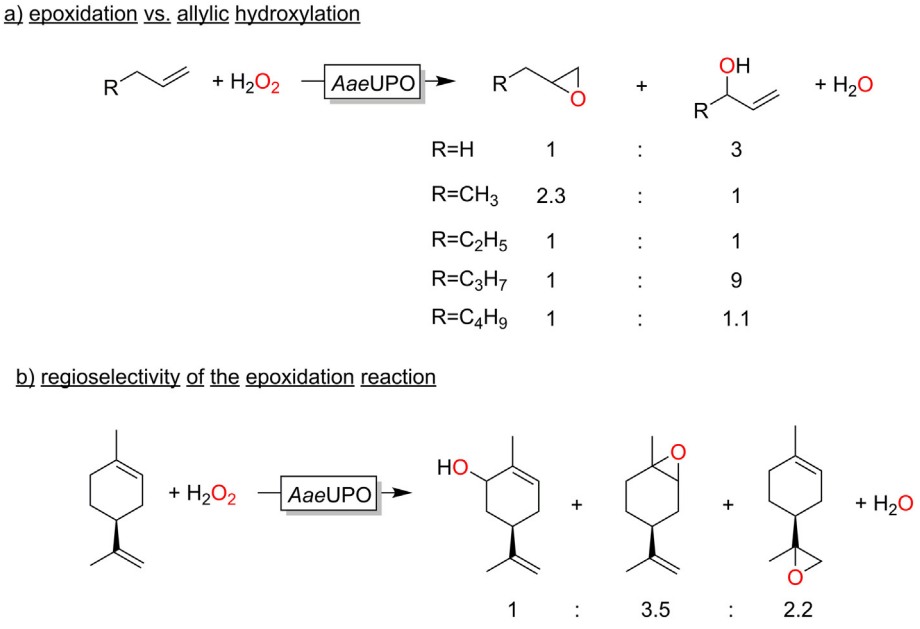

Fig. 11. Selectivity issues observed for the peroxygenase-catalysed epoxidation reaction at the example of *Aae*UPO. (Peter et al., 2013)

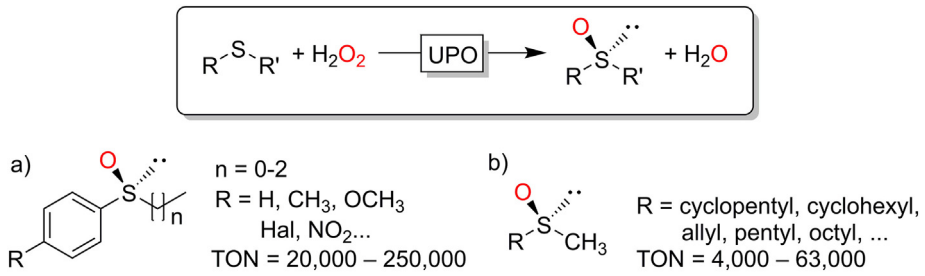

Fig. 12. *Cfu*CPO-catalysed sulfoxidation reactions. a) (Churakova et al., 2013; Kohlmann et al., 2009; Luetz et al., 2004; Perez et al., 2009b; van Deurzen et al., 1997); b) (Colonna et al., 1997; Vargas et al., 1999)

et al., 2019) The only carrier-free immobilisation approach published for UPOs was the encapsulation of *Mro*UPO and *Aae*UPO in PVA/PEG gel. While the kinetic parameters K_M and k_{cat} for the substrates diclofenac, dimethylene-5-nitrobenzene and 1,4-dimethoxybenzene were hardly influenced by the entrapment an interesting effect was reported for the storage of the immobilised enzyme. While the activity towards NBD decreased already after six days of storage in potassium phosphate buffer at pH 7, the storage in non-polar solvents (hexane, cyclohexane) increased the activity by up to 190% after 1 day and still showed 30% higher activity than the fresh preparation after 160 days. A possible explanation for this increase in activity is that the unipolar solvent makes the rather polar immobilisation matrix more accessible for rather non-polar substrates like NBD. Furthermore, the entrapped *Aae*UPO was used for diclofenac hydroxylation in a stirred tank reactor with a continuous H_2O_2 feed, where it showed a 60-fold improved TON of 61,041, compared to < 1,000 for the free enzyme. (Poraj-Kobielska et al., 2015)

Due to the inconsistent nature of the published data on the various techniques, it is not possible to point out any general recommendations for peroxygenase immobilisation, but the wide variety of the reported methods, can still give valuable input for new immobilisation approaches. There is little research available on immobilisation of *Aae*UPO; however, we believe that the high biocatalytic potential of *Aae*UPO will lead to more studies exploring its immobilisation for operational stability in the near future.

4.3. Peroxygenases in non-conventional media

In biocatalysis, many interesting substrates are rather hydrophobic and exhibit low water solubility. Therefore, use of non-conventional media like organic solvents or neat substrate (solvent-free) conditions are a possibility to increase substrate loadings and therefore productivity. One example for such an approach is the use of *Aae*UPO for ethylbenzene hydroxylation. At first free *Aae*UPO in combination with an alcohol oxidase from *Pseudomonas putida* (*Pp*AOx) for continuous H_2O_2 production from methanol was used in a two-liquid phase system

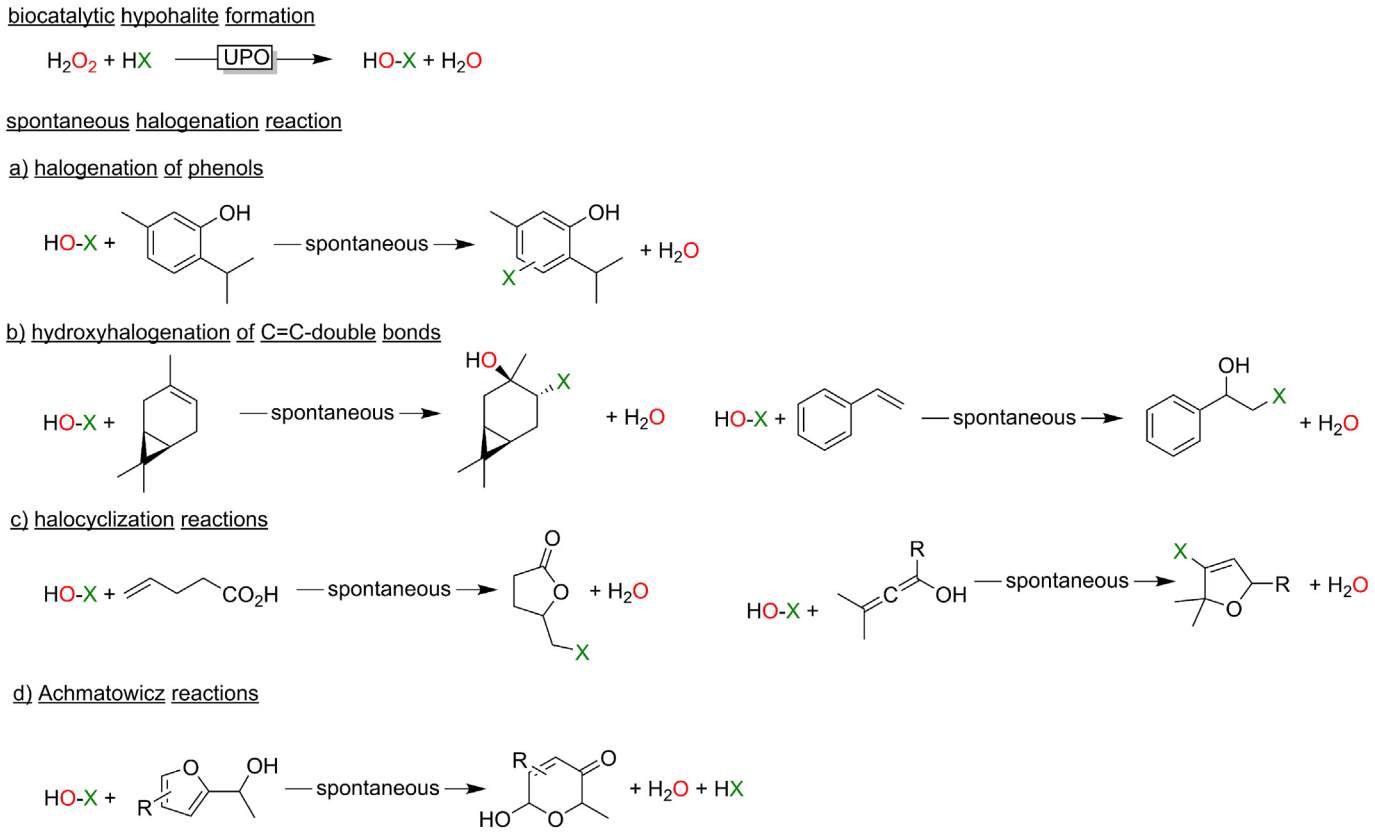

Fig. 13. Chemoenzymatic transformations based on a peroxidase-catalysed hypohalite formation followed by a chemical follow-up reaction. a) (Fernández-Fueyo et al., 2015; Frank et al., 2016; Getrey et al., 2014) b) (Dong et al., 2017; Kaup et al., 2007) c) (Naapuri et al., 2017; Younes et al., 2020); d) (Deska et al., 2018; Thiel et al., 2014).

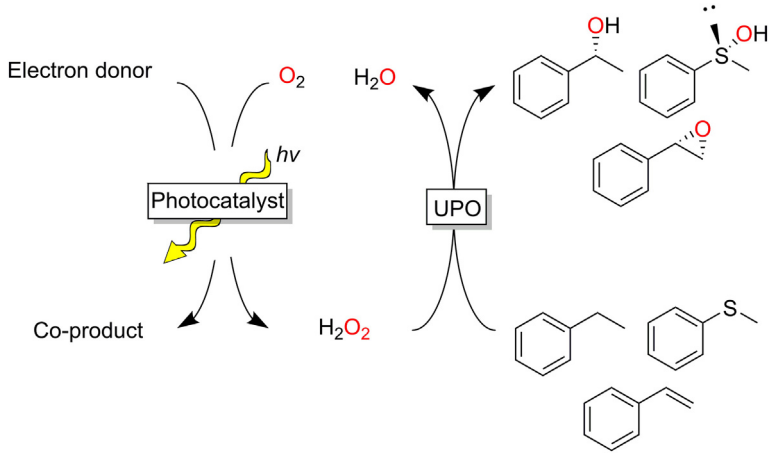

Fig. 14. Photocatalytic *in situ* synthesis of H_2O_2 for peroxygenase catalysis.

Table 2
Overview for immobilisation of peroxygenases.

Enzyme	Carrier (Interaction)	Immobilisation yield	Recovered activity	Reaction catalysed	Remarks	Ref.
Carrier-bound approaches						
*Cfu*CPO	Aminopropyl glass (covalent)	91%		TMPD oxidation	Improved storage stability	(Kadima and Pickard, 1990)
*Cfu*CPO	Methacrylate polymer (covalent)	n.d.	83%	Monochloro-dimedon chlorination	Storage and thermal stability increased	(Bayramoglu et al., 2011)
*Cfu*CPO	Mesoporous silica (covalent)	11%	n.d.	Azo dye oxidation	Increased temperature stability and k_{cat}/K_M	(Guerrero et al., 2012)
*Cfu*CPO	Mesoporous silica (adsorptive)	80%	n.d.	Styrene oxidation	Increased stability against temperature and acetonitrile	(Águila et al., 2011)
*Cfu*CPO	Magnetic beads (covalent)	n.d.	58%	Monochloro-dimedon chlorination	Improved thermal and storage stability	(Bayramoğlu et al., 2008)
*Cfu*CPO	Chitosan (covalent)	n.d.	n.d.	Monochloro-dimedon chlorination	Improved thermal and oxidative stability	(Zhang et al., 2009)
*Cfu*CPO	Agarose (adsorptive)	75%	50%	Monochloro-dimedon chlorination	Increased stability against *tert*-butyl hydroperoxide	(Pešić et al., 2012)
*Cfu*CPO	Agarose (covalent)	94%	55%	Monochloro-dimedon chlorination		(Pešić et al., 2012)
*Cfu*CPO	TiO_2 nanotubes (adsorptive)	35%	26%	Styrene epoxidation	Increased k_{cat} and operational stability	(Muñoz-Guerrero et al., 2015)
*Aae*UPO	Methacrylate polymers (covalent)	n.d.	4%	Ethylbenzene hydroxylation	Used in neat substrate	(Fernández-Fueyo et al., 2016)
*Aae*UPO	Methacrylate polymers (covalent)	n.d.	n.d.	Photo-biocatalytic ethylbenzene hydroxylation	8x increase of TON compared to free enzyme	(Zhang et al., 2018)
*Aae*UPO	Agarose (covalent)	n.d.	15%	Styrene epoxidation	Increased stability against acetonitrile, high temperature, high pH	(Molina-Espeja et al., 2019)
*Aae*UPO	Polyacryl (covalent)	72.8%	3%	Styrene epoxidation	Up to 360 mM product	(Rauch et al., 2019)
Carrier-free approaches						
CfuCPO	Aggregation and cross linking	n.d.	68%	Thioanisole oxidation	Higher tolerance against H_2O_2, temperature and pH	(Perez et al., 2009a)
*Mro*UPO/ *Aae*UPO	PVA/PEG Gel (entrapment)	n.d.	86%	Diclofenac oxidation	60 fold increase in TON, storage in cyclohexane increased activity	(Poraj-Kobielska et al., 2015)
*Aae*UPO	Calcium alginate entrapment	81%	-	Hydroxylation of cyclohexane and cyclopentane	Entrapment enabled light driven solvent free alkane hydroxylation	(Hobisch et al., 2020)

TMPD: N,N,N',N'-tetramethyl-p-phenylenediamine

(2LPS), where the aqueous phase holds the enzymes and the organic phase serves as a product sink and substrate reservoir. This approach suffered from poor enzyme stability and ethylbenzene hydroxylation ceased after 24 h. In an effort to increase stability, the enzymes were covalently immobilised on Relizyme™ HA 403/M resin to use them in neat substrate conditions. However, this combination only yielded trace amounts of the hydroxylated product. (Ni et al., 2016) The use of immobilised *Aae*UPO with a portion wise addition of *tert*-butyl hydroperoxide in neat ethylbenzene was the next approach. In a reaction volume of 250 mL 40 mM enantiopure (*R*)-1-phenylethanol was produced in three hours, which corresponded to a TON of 67,500 for *Aae*UPO. (Fernández-Fueyo et al., 2016) In a recently published article, an immobilised preparation of *Aae*UPO was employed in the epoxidation of neat styrene derivatives using a continuous feed of *tert*-butyl hydroperoxide (^{tert}BuOOH). Besides several successful epoxidations performed this way in 1.5 ml vials, the epoxidation of *cis*-β-methylstyrene was realised on a 10 mL scale using an exponential ^{tert}BuOOH feed. The peroxide still caused major enzyme inactivation, but with resupplying fresh enzyme three times, a (1*R*,2*S*)-β-methylstyrene oxide concentration of 360 mM was obtained. This reaction was also extended

to a chemoenzymatic cascade by adding methylamine to the mix to produce (pseudo)ephedrine. (Rauch et al., 2019) In a recent study, we investigated the hydroxylation of cyclohexane and showed in a solvent screening that the use of neat reaction media, was the simplest and the most efficient approach to follow. (Hobisch et al., 2020) *Aae*UPO was applied for hydroxylation reactions in neat cyclohexane whereby H_2O_2 was generated *in situ*, catalysed by nitrogen-doped carbon nanodots (N-CNDs) under UV-LED illumination. *Aae*UPO entrapment in alginate beads enabled the product formation in the neat reaction medium, otherwise not possible with the free enzyme. The absorption of hydrophilic N-CNDs into the water-rich alginate beads containing *Aae*UPO created a 2-in-1 heterogeneous photobiocatalyst. Although the activity was rather low (0.08 $mM_{product} \cdot \mu M_{UPO}^{-1} \cdot h^{-1}$) the product formation was linear for up to seven days. Herein, the enzyme-to-photocatalyst ratio played an important role for product concentration, which needs further evaluations.

For *Cfu*CPO there was an interesting application reported combining a 2LPS with thioanisole as the organic phase and *Cfu*CPO, FMN and EDTA running the photocatalytic H_2O_2 production in the aqueous phase. After a monophasic sulfoxidation of thioanisole did not prove very productive, this 2LPS was evaluated. Its effect was an increase in the product formation time from 2 h of the monophasic system to over 24 h. Adding vigorous agitation to increase the interfacial area between the phases, resulted in an eight-fold increase of the initial rate, but also in an end of the sulfoxidation reaction after 2–3 h. To provide sufficient surface area for mass transfer between the phases, sulfosuccinate was used as a surfactant for more stable emulsion at reduced stirring. This resulted in a decrease of the initial rate, but in turn the reaction was sustained for over 20 h and yielded 45 mM (*R*)-methyl phenyl sulfoxide (> 96% *ee*). (Churakova et al., 2013) While Churakova et al. did not further investigate the cause for *Cfu*CPO inactivation in the 2LPS, a previous publication by Park & Clark elucidates this question. The authors studied the inactivation of *Cfu*CPO in a 2LPS oxidation of toluene and xylene and found that the main cause for activity loss was oxidative destruction of the heme. Optimization of the buffer pH and addition of *t*-butyl alcohol as radical scavenger improved the total turnover numbers by up to 110%. Neither denaturation nor aggregation of the apoenzyme seemed to play a major role in enzyme inactivation. (Park and Clark, 2006)

Furthermore, PaDa-I was used in hydroxylation and epoxidation reactions containing natural deep eutectic solvents (NADES). While utilising several different electron bond donors, these NADES were all based on choline chloride as electron bond acceptor. That was essential, since a choline chloride oxidase was used for continuous H_2O_2 supply. Applying this system, 22.43 mM (*R*)-1-phenylethanol and 8.68 mM cis-β-methylstyrene oxide were produced equalling 224,300 and 86,800 TONs for UPO respectively. Among others, the researchers found that using 50% (v/v) NADES in the reaction mixture increased process stability. (Ma et al., 2020)

As of yet there are not many published applications of peroxygenases in non-conventional media. The ever-rising interest in reactions catalysed by this enzyme group will certainly be a driving force behind application-oriented research towards alternative reaction media. Since many UPO substrates are rather hydrophobic, especially neat substrate applications are a promising approach that should be further pursued. A neat system could dramatically increase substrate and subsequently product titers.

5. Perspectives

Since their discovery, peroxygenases have attracted a great deal of interest in the biocatalysis community. The simplicity of the reactions owing to independency to external redox cofactors (and hence the regeneration methods) and auxiliary proteins is a big advantage. This easiness and the wide range of H_2O_2-dependent reactions catalysed by peroxygenases make them promising catalysts for preparative oxyfunctionalisation chemistry. We are convinced that the knowledge and experiences gained during the past two decades will be helpful to explore the potential of peroxygenases further for: (i) Discovery of new peroxygenases, (ii) high-throughput screening strategies for engineered peroxygenase variants, (iii) enhancement of operational stability (via protein engineering and/or immobilisation), (iv) use of non-conventional media for higher substrate loadings and product titers, and (v) heterogenisation of biocatalysts by immobilisation for continuous applications. Herein, collaborative activities between protein engineers, organic chemists and process engineers can bring UPO catalysed reactions to a next level making them attractive for technical applications with more focus on truly interesting and high yield conversions.

Acknowledgements

This project has received funding from the European Union's Horizon 2020 research and innovation program under the Marie Skłodowska-Curie grant agreement No 764920. MA and PGS thank the FPI fellowship BES-2017-080040, the Spanish Government Project PID2019-106166RB-I00-Oxywave, and the Comunidad de Madrid Synergy CAM project Y2018/BIO-4738-EVOCHIMERA-CM. FH gratefully acknowledges support by The Netherlands Organisation for Scientific Research through a VICI grant (no. 724.014.003) and the European Research Commission (ERC consolidator grant No 648026).

References

Águila, S., Vazquez-Duhalt, R., Tinoco, R., Rivera, M., Pecchi, G., Alderete, J.B., 2008. Stereoselective oxidation of R-(+)-limonene by chloroperoxidase from Caldariomyces fumago. Green Chem. 10 (6) 10.1039/b719992a.

Águila, S., Vazquez-Duhalt, R., Covarrubias, C., Pecchi, G., Alderete, J.B., 2011. Enhancing oxidation activity and stability of iso-1-cytochrome c and chloroperoxidase by immobilization in nanostructured supports. J. Mol. Catal. B Enzym. 70 (3-4), 81–87 10.1016/j.molcatb.2011.02.008.

Al Shameri, A., Willot, S.J.-P., Paul, C.E., Hollmann, F., Lauterbach, L., 2020. Chemical Communications. 10.1039/D0CC03229H.

Anh, D.H., 2008. Novel extracellular haloperoxidase-peroxygenases from the coprophilous fungi Coprinus radians and Coprinus verticillatus: production, purification and biochemical characterization. International Graduate School of Zittau, Zittau.

Anh, D.H., Ullrich, R., Benndorf, D., Svatoš, A., Muck, A., Hofrichter, M., 2007. The Coprophilous Mushroom Coprinus radians Secretes a Haloperoxidase That Catalyzes Aromatic Peroxygenation. Appl. Environ. Microbiol. 73 (17), 5477–5485 10.1128/aem.00026-07.

Aranda, C., Ullrich, R., Kiebist, J., Scheibner, K., del Río, J.C., Hofrichter, M., Martínez, A.T., Gutiérrez, A., 2018. Selective synthesis of the resveratrol analogue 4,4′-dihydroxy-trans-stilbene and stilbenoids modification by fungal peroxygenases. Catal. Sci. Technol. 8 (9), 2394–2401.

Babot, E.D., del Río, J.C., Kalum, L., Martínez, A.T., Gutiérrez, A., 2013. Oxyfunctionalization of aliphatic compounds by a recombinant peroxygenase from Coprinopsis cinerea. Biotechnol. Bioeng. 110 (9), 2323–2332.

Barková, K., Kinne, M., Ullrich, R., Hennig, L., Fuchs, A., Hofrichter, M., 2011. Regioselective hydroxylation of diverse flavonoids by an aromatic peroxygenase. Tetrahedron 67 (26), 4874–4878.

Bassanini, I., Ferrandi, E.E., Vanoni, M., Ottolina, G., Riva, S., Crotti, M., Brenna, E., Monti, D., 2017. Peroxygenase-catalyzed enantioselective sulfoxidations. Eur. J. Org. Chem. 2017 (47), 7186–7189.

Bayramoğlu, G., Kiralp, S., Yilmaz, M., Toppare, L., Arıca, M.Y., 2008. Covalent immobilization of chloroperoxidase onto magnetic beads: Catalytic properties and stability. Biochem. Eng. J. 38 (2), 180–188.

Bayramoglu, G., Altintas, B., Yilmaz, M., Arica, M.Y., 2011. Immobilization of chloroperoxidase onto highly hydrophilic polyethylene chains via bio-conjugation: catalytic properties and stabilities. Bioresour. Technol. 102 (2), 475–482.

Bormann, S., Gomez Baraibar, A., Ni, Y., Holtmann, D., Hollmann, F., 2015. Specific oxyfunctionalisations catalysed by peroxygenases: opportunities, challenges and solutions. Catal. Sci. Technol. 5 (4), 2038–2052.

Buchhaupt, M., Ehrich, K., Huttmann, S., Guder, J., Schrader, J., 2011. Over-expression of chloroperoxidase in Caldariomyces fumago. Biotechnol. Lett. 33 (11), 2225–2231.

Burek, B.O., Bormann, S., Hollmann, F., Bloh, J.Z., Holtmann, D., 2019. Hydrogen peroxide driven biocatalysis. Green Chem. 21 (12), 3232–3249.

Carro, J., Ferreira, P., Rodriguez, L., Prieto, A., Serrano, A., Balcells, B., Arda, A., Jimenez-Barbero, J., Gutierrez, A., Ullrich, R., Hofrichter, M., Martinez, A.T., 2015. 5-hydroxymethylfurfural conversion by fungal aryl-alcohol oxidase and unspecific peroxygenase. FEBS J. 282 (16), 3218–3229.

Carro, J., González-Benjumea, A., Fernández-Fueyo, E., Aranda, C., Guallar, V., Gutiérrez, A., Martínez, A.T., 2019. Modulating fatty acid epoxidation vs hydroxylation in a fungal peroxygenase. ACS Catal. 9 (7), 6234–6242.

Choi, D.S., Ni, Y., Fernandez-Fueyo, E., Lee, M., Hollmann, F., Park, C.B., 2017.

Photoelectroenzymatic oxyfunctionalization on flavin-hybridized carbon nanotube electrode platform. ACS Catal. 7 (3), 1563–1567.
Churakova, E., Kluge, M., Ullrich, R., Arends, I., Hofrichter, M., Hollmann, F., 2011. Specific photobiocatalytic oxyfunctionalization reactions. Angew. Chem. Int. Ed. 50 (45), 10716–10719.
Churakova, E., Arends, I.W.C.E., Hollmann, F., 2013. Increasing the productivity of peroxidase-catalyzed oxyfunctionalization: A case study on the potential of two-liquid-phase systems. ChemCatChem 5 (2), 565–568.
Colonna, S., Gaggero, N., Carrera, G., Pasta, P., 1997. A new enzymatic enantioselective synthesis of dialkyl sulfoxides catalysed by monooxygenases. Chem. Commun. 5, 439–440.
Conesa, A., van De Velde, F., van Rantwijk, F., Sheldon, R.A., van Den Hondel, C.A., Punt, P.J., 2001. Expression of the Caldariomyces fumago chloroperoxidase in Aspergillus niger and characterization of the recombinant enzyme. J. Biol. Chem. 276 (21), 17635–17640.
Delgove, M.A.F., Laurent, A.B., Woodley, J.M., De Wildeman, S.M.A., Bernaerts, K.V., van der Meer, Y., 2019. A prospective life cycle assessment (LCA) of monomer synthesis: Comparison of biocatalytic and oxidative chemistry. ChemSusChem 12(7), 1349-1360.
Deska, J., Blume, F., Sprengart, P., 2018. Lipase-induced oxidative Furan rearrangements. Synlett 29 (10), 1293–1296.
van Deurzen, M.P.J., Remkes, I.J., van Rantwijk, F., Sheldon, R.A., 1997. Chloroperoxidase catalyzed oxidations in t-butyl alcohol/water mixtures. J. Mol. Catal. A Chem. 117 (1-3), 329–337.
van Deurzen, M.P.J., van Rantwijk, F., Sheldon, R.A., 2006. Chloroperoxidase-catalyzed oxidation of 5-hydroxymethylfurfural. J. Carbohydr. Chem. 16 (3), 299–309.
Dexter, A.F., Lakner, F.J., Campbell, R.A., Hager, L.P., 1995. Highly Enantioselective Epoxidation of 1,1-Disubstituted Alkenes Catalyzed by Chloroperoxidase. J. Am. Chem. Soc. 117 (23), 6412–6413.
Dong, J.J., Fernandez-Fueyo, E., Li, J., Guo, Z., Renirie, R., Wever, R., Hollmann, F., 2017. Halofunctionalization of alkenes by vanadium chloroperoxidase from Curvularia inaequalis. Chem. Commun. (Camb.) 53 (46), 6207–6210.
Fasan, R., 2012. Tuning P450 Enzymes as Oxidation Catalysts. ACS Catal. 2 (4), 647–666.
Fernández-Fueyo, E., van Wingerden, M., Renirie, R., Wever, R., Ni, Y., Holtmann, D., Hollmann, F., 2015. Chemoenzymatic Halogenation of Phenols by using the Haloperoxidase fromCurvularia inaequalis. ChemCatChem 7 (24), 4035–4038.
Fernández-Fueyo, E., Ni, Y., Gomez Baraibar, A., Alcalde, M., van Langen, L.M., Hollmann, F., 2016. Towards preparative peroxygenase-catalyzed oxyfunctionalization reactions in organic media. J. Mol. Catal. B Enzym. 134, 347–352.
Frank, A., Seel, C.J., Groll, M., Gulder, T., 2016. Characterization of a Cyanobacterial Haloperoxidase and Evaluation of its Biocatalytic Halogenation Potential. Chembiochem 17 (21), 2028–2032.
Freakley, S.J., Kochius, S., van Marwijk, J., Fenner, C., Lewis, R.J., Baldenius, K., Marais, S.S., Opperman, D.J., Harrison, S.T.L., Alcalde, M., Smit, M.S., Hutchings, G.J., 2019. A chemo-enzymatic oxidation cascade to activate C-H bonds with in situ generated H2O2. Nat. Commun. 10(1), 4178.
Fred van Rantwijk, R.A.S., 2000. Selective oxygen transfer catalysed by heme peroxidases: synthetic and mechanistic aspects. Curr. Opin. Biotechnol. 11, 554–564.
Getrey, L., Krieg, T., Hollmann, F., Schrader, J., Holtmann, D., 2014. Enzymatic halogenation of the phenolic monoterpenes thymol and carvacrol with chloroperoxidase. Green Chem. 16 (3), 1104–1108.
Girhard, M., Schuster, S., Dietrich, M., Durre, P., Urlacher, V.B., 2007. Cytochrome P450 monooxygenase from Clostridium acetobutylicum: a new alpha-fatty acid hydroxylase. Biochem. Biophys. Res. Commun. 362 (1), 114–119.
Gomez de Santos, P., Cañellas, M., Tieves, F., Younes, S.H.H., Molina-Espeja, P., Hofrichter, M., Hollmann, F., Guallar, V., Alcalde, M., 2018. Selective Synthesis of the Human Drug Metabolite 5′-Hydroxypropranolol by an Evolved Self-Sufficient Peroxygenase. ACS Catal. 8 (6), 4789–4799.
Gomez de Santos, P., Cervantes, F.V., Tieves, F., Plou, F.J., Hollmann, F., Alcalde, M., 2019. Benchmarking of laboratory evolved unspecific peroxygenases for the synthesis of human drug metabolites. Tetrahedron 75 (13), 1827–1831.
González-Benjumea, A., Carro, J., Renau-Mínguez, C., Linde, D., Fernández-Fueyo, E., Gutiérrez, A., Martínez, A.T., 2020. Fatty acid epoxidation by Collariella virescens peroxygenase and heme-channel variants. Catal. Sci. Technol. 10, 717–725 10.1039/c9cy02332a.
Gröbe, G., Ullrich, R., Pecyna, M.J., Kapturska, D., Friedrich, S., Hofrichter, M., Scheibner, K., 2011. High-yield production of aromatic peroxygenase by the agaric fungus Marasmius rotula. AMB Express 1 (1), 31.
Guerrero, E., Aburto, P., Terrés, E., Villegas, O., González, E., Zayas, T., Hernández, F., Torres, E., 2012. Improvement of catalytic efficiency of chloroperoxidase by its covalent immobilization on SBA-15 for azo dye oxidation. J. Porous. Mater. 20 (2), 387–396.
Gutierrez, A., Babot, E.D., Ullrich, R., Hofrichter, M., Martinez, A.T., del Rio, J.C., 2011. Regioselective oxygenation of fatty acids, fatty alcohols and other aliphatic compounds by a basidiomycete heme-thiolate peroxidase. Arch. Biochem. Biophys. 514 (1-2), 33–43.
Hanano, A., Burcklen, M., Flenet, M., Ivancich, A., Louwagie, M., Garin, J., Blée, E., 2006. Plant Seed Peroxygenase Is an Original Heme-oxygenase with an EF-hand Calcium Binding Motif. J. Biol. Chem. 281 (44), 33140–33151.
Hobisch, M., van Schie, M.M.C.H., Kim, J., Andersen, K.R., Alcalde, M., Kourist, R., Park, C.B., Hollmann, F., Kara, S., 2020. Solvent-Free Photobiocatalytic Hydroxylation of Cyclohexane. ChemCatChem.
Hofrichter, M., Ullrich, R., 2014. Oxidations catalyzed by fungal peroxygenases. Curr. Opin. Chem. Biol. 19, 116–125.
Hofrichter, M., Kellner, H., Pecyna, M.J., Ullrich, R., 2015. Fungal Unspecific Peroxygenases: Heme-Thiolate Proteins That Combine Peroxidase and Cytochrome P450 Properties. In: Hrycay, E.G., Bandiera, S.M. (Eds.), Monooxygenase, Peroxidase and Peroxygenase Properties and Mechanisms of Cytochrome P450. Springer International Publishing, Cham, pp. 341–368.
Hofrichter, M., Kellner, H., Herzog, R., Karich, A., Liers, C., Scheibner, K., Kimani, V.W., Ullrich, R., 2020. Fungal Peroxygenases: A Phylogenetically Old Superfamily of Heme Enzymes with Promiscuity for Oxygen Transfer Reactions. In: Grand Challenges in Fungal Biotechnology, pp. 369–403.
Holtmann, D., Hollmann, F., 2016. The Oxygen Dilemma: A Severe Challenge for the Application of Monooxygenases? ChemBioChem 17 (15), 1391–1398.
Horst, A.E.W., Bormann, S., Meyer, J., Steinhagen, M., Ludwig, R., Drews, A., Ansorge-Schumacher, M., Holtmann, D., 2016. Electro-enzymatic hydroxylation of ethylbenzene by the evolved unspecific peroxygenase of Agrocybe aegerita. J. Mol. Catal. B Enzym. 133, S137–S142.
Hu, S., Hager, L.P., 1998. Unusual propargylic oxidations catalyzed by chloroperoxidase. Biochem. Biophys. Res. Commun. 253 (2), 544–546.
Huisman, G.W., Collier, S.J., 2013. On the development of new biocatalytic processes for practical pharmaceutical synthesis. Curr. Opin. Chem. Biol. 17 (2), 284–292.
Huisman, G.W., Liang, J., Krebber, A., 2010. Practical chiral alcohol manufacture using ketoreductases. Curr. Opin. Chem. Biol. 14 (2), 122–129.
Janssen, M., Müller, C., Vogt, D., 2011. Recent advances in the recycling of homogeneous catalysts using membrane separation. Green Chem. 13 (9).
Kadima, T.A., Pickard, M.A., 1990. Immobilization of Chloroperoxidase on Aminopropyl-Glass. Appl. Environ. Microbiol. 56 (11), 5.
Kaup, B.A., Piantini, U., Wust, M., Schrader, J., 2007. Monoterpenes as novel substrates for oxidation and halo-hydroxylation with chloroperoxidase from Caldariomyces fumago. Appl. Microbiol. Biotechnol. 73 (5), 1087–1096.
Kiebist, J., Schmidtke, K.U., Zimmermann, J., Kellner, H., Jehmlich, N., Ullrich, R., Zänder, D., Hofrichter, M., Scheibner, K., 2017. A Peroxygenase from Chaetomium globosum Catalyzes the Selective Oxygenation of Testosterone. ChemBioChem 18 (6), 563–569.
Kiebist, J., Hofrichter, M., Zuhse, R., Scheibner, K., 2019. Oxyfunctionalization of pharmaceuticals by fungal peroxygenases. In: Grundwal, P. (Ed.), Pan Standford Series on Biocatalysis. Pan Stanford Publishing.
Kinne, M., Ullrich, R., Hammel, K.E., Scheibner, K., Hofrichter, M., 2008. Regioselective preparation of (R)-2-(4-hydroxyphenoxy)propionic acid with a fungal peroxygenase. Tetrahedron Lett. 49 (41), 5950–5953.
Kinne, M., Poraj-Kobielska, M., Aranda, E., Ullrich, R., Hammel, K.E., Scheibner, K., Hofrichter, M., 2009. Regioselective preparation of 5-hydroxypropranolol and 4'-hydroxydiclofenac with a fungal peroxygenase. Bioorg. Med. Chem. Lett. 19 (11), 3085–3087.
Klebanoff, S.J., 2005. Myeloperoxidase: friend and foe. J. Leukoc. Biol. 77 (5), 598–625.
Kluge, M., Ullrich, R., Dolge, C., Scheibner, K., Hofrichter, M., 2009. Hydroxylation of naphthalene by aromatic peroxygenase from Agrocybe aegerita proceeds via oxygen transfer from H2O2 and intermediary epoxidation. Appl. Microbiol. Biotechnol. 81 (6), 1071–1076.
Kluge, M., Ullrich, R., Scheibner, K., Hofrichter, M., 2012. Stereoselective benzylic hydroxylation of alkylbenzenes and epoxidation of styrene derivatives catalyzed by the peroxygenase of Agrocybe aegerita. Green Chem. 14 (2), 440–446.
Kohlmann, C., Greiner, L., Leitner, W., Wandrey, C., Lutz, S., 2009. Ionic liquids as performance additives for electroenzymatic syntheses. Chemistry 15 (43), 11692–11700.
Krieg, T., Hüttmann, S., Mangold, K.-M., Schrader, J., Holtmann, D., 2011. Gas diffusion electrode as novel reaction system for an electro-enzymatic process with chloroperoxidase. Green Chem. 13 (10).
Lakner, F.J., Cain, K.P., Hager, L.P., 1997. Enantioselective Epoxidation of ω-Bromo-2-methyl-1-alkenes Catalyzed by Chloroperoxidase. Effect of Chain Length on Selectivity and Efficiency. J. Am. Chem. Soc. 119 (2), 443–444.
Lee, D.-S., Yamada, A., Sugimoto, H., Matsunaga, I., Ogura, H., Ichihara, K., Adachi, S.-i., Park, S.-Y., Shiro, Y., 2003. Substrate Recognition and Molecular Mechanism of Fatty Acid Hydroxylation by Cytochrome P450 from Bacillus subtilis : crystallographic, spectroscopic, and mutational studies. J. Biol. Chem. 278 (11), 9761–9767.
Liese, A., Hilterhaus, L., 2013. Evaluation of immobilized enzymes for industrial applications. Chem. Soc. Rev. 42 (15), 6236–6249.
Luetz, S., Steckhan, E., Liese, A., 2004. First asymmetric electroenzymatic oxidation catalyzed by a peroxidase. Electrochem. Commun. 6, 583–587.
Ma, Y., Li, Y., Ali, S., Li, P., Zhang, W., Rauch, M.C.R., Willot, S.J.P., Ribitsch, D., Choi, Y.H., Alcalde, M., Hollmann, F., Wang, Y., 2020. Natural Deep Eutectic Solvents as Performance Additives for Peroxygenase Catalysis. ChemCatChem 12, 989–994.
Martin-Diaz, J., Paret, C., García-Ruiz, E., Molina-Espeja, P., Alcalde, M., 2018. Shuffling the Neutral Drift of Unspecific Peroxygenase in Saccharomyces cerevisiae. Appl. Environ. Microbiol. 84 (15).
Mate, D.M., Palomino, M.A., Molina-Espeja, P., Martin-Diaz, J., Alcalde, M., 2017. Modification of the peroxygenative:peroxidative activity ratio in the unspecific peroxygenase from Agrocybe aegerita by structure-guided evolution. Protein Eng. Des. Sel. 30 (3), 191–198.
Molina-Espeja, P., Garcia-Ruiz, E., Gonzalez-Perez, D., Ullrich, R., Hofrichter, M., Alcalde, M., 2014. Directed Evolution of Unspecific Peroxygenase from Agrocybe aegerita. Appl. Environ. Microbiol. 80 (11), 3496–3507.
Molina-Espeja, P., Ma, S., Mate, D.M., Ludwig, R., Alcalde, M., 2015. Tandem-yeast expression system for engineering and producing unspecific peroxygenase. Enzym. Microb. Technol. 73-74, 29–33.
Molina-Espeja, P., Cañellas, M., Plou, F.J., Hofrichter, M., Lucas, F., Guallar, V., Alcalde, M., 2016. Synthesis of 1-Naphthol by a Natural Peroxygenase Engineered by Directed Evolution. ChemBioChem 17 (4), 341–349.
Molina-Espeja, P., Gomez de Santos, P., Alcalde, M., 2017. Directed Evolution of Unspecific Peroxygenase. In: Alcalde, M. (Ed.), Directed Enzyme Evolution: Advances and Applications. Springer International Publishing, Cham, pp. 127–143.

Molina-Espeja, P., Santos-Moriano, P., Garcia-Ruiz, E., Ballesteros, A., Plou, F.J., Alcalde, M., 2019. Structure-Guided Immobilization of an Evolved Unspecific Peroxygenase. Int. J. Mol. Sci. 20 (7).

Muñoz-Guerrero, F.A., Águila, S., Vazquez-Duhalt, R., Torres, C.C., Campos, C.H., Alderete, J.B., 2015. Biocatalytic Performance of Chloroperoxidase from Caldariomyces fumago Immobilized onto TiO2 Based Supports. Top. Catal. 59 (2-4), 387–393.

Munro, A.W., McLean, K.J., Grant, J.L., Makris, T.M., 2018. Structure and function of the cytochrome P450 peroxygenase enzymes. Biochem. Soc. Trans. 46 (1), 183–196.

Naapuri, J., Rolfes, J.D., Keil, J., Manzuna Sapu, C., Deska, J., 2017. Enzymatic halocyclization of allenic alcohols and carboxylates: a biocatalytic entry to functionalized O-heterocycles. Green Chem. 19 (2), 447–452.

Ni, Y., Fernandez-Fueyo, E., Gomez Baraibar, A., Ullrich, R., Hofrichter, M., Yanase, H., Alcalde, M., van Berkel, W.J., Hollmann, F., 2016. Peroxygenase-Catalyzed Oxyfunctionalization Reactions Promoted by the Complete Oxidation of Methanol. Angew. Chem. Int. Ed. Eng. 55 (2), 798–801.

Olmedo, A., Aranda, C., Del Rio, J.C., Kiebist, J., Scheibner, K., Martinez, A.T., Gutierrez, A., 2016. From Alkanes to Carboxylic Acids: Terminal Oxygenation by a Fungal Peroxygenase. Angew. Chem. Int. Ed. Eng. 55 (40), 12248–12251.

Olmedo, A., Rio, J.C.D., Kiebist, J., Ullrich, R., Hofrichter, M., Scheibner, K., Martinez, A.T., Gutierrez, A., 2017. Fatty Acid Chain Shortening by a Fungal Peroxygenase. Chem. Eur. J. 23 (67), 16985–16989.

Onoda, H., Shoji, O., Suzuki, K., Sugimoto, H., Shiro, Y., Watanabe, Y., 2018. α-Oxidative decarboxylation of fatty acids catalysed by cytochrome P450 peroxygenases yielding shorter-alkyl-chain fatty acids. Catal. Sci. Technol. 8 (2), 434–442.

Park, J.B., Clark, D.S., 2006. Deactivation mechanisms of chloroperoxidase during biotransformations. Biotechnol. Bioeng. 93 (6), 1190–1195.

Paul, C.E., Churakova, E., Maurits, E., Girhard, M., Urlacher, V.B., Hollmann, F., 2014. In situ formation of H2O2 for P450 peroxygenases. Bioorg. Med. Chem. 22 (20), 5692–5696.

Perez, D.I., Grau, M.M., Arends, I.W., Hollmann, F., 2009a. Visible light-driven and chloroperoxidase-catalyzed oxygenation reactions. Chem Commun (Camb) 44, 6848–6850.

Perez, D., van Rantwijk, F., Sheldon, R.A., 2009b. Cross-Linked Enzyme Aggregates of Chloroperoxidase: Synthesis, Optimization and Characterization. Adv. Synthes. Catal. 351 (13), 2133–2139.

Pešić, M., López, C., Álvaro, G., López-Santín, J., 2012. A novel immobilized chloroperoxidase biocatalyst with improved stability for the oxidation of amino alcohols to amino aldehydes. J. Mol. Catal. B Enzym. 84, 144–151.

Peter, S., Kinne, M., Wang, X., Ullrich, R., Kayser, G., Groves, J.T., Hofrichter, M., 2011. Selective hydroxylation of alkanes by an extracellular fungal peroxygenase. FEBS J. 278 (19), 3667–3675.

Peter, S., Kinne, M., Ullrich, R., Kayser, G., Hofrichter, M., 2013. Epoxidation of linear, branched and cyclic alkenes catalyzed by unspecific peroxygenase. Enzym. Microb. Technol. 52 (6-7), 370–376.

Peter, S., Karich, A., Ullrich, R., Gröbe, G., Scheibner, K., Hofrichter, M., 2014. Enzymatic one-pot conversion of cyclohexane into cyclohexanone: Comparison of four fungal peroxygenases. J. Mol. Catal. B Enzym. 103, 47–51.

Ping, G., Yuan, J.M., Vallieres, M., Dong, H., Sun, Z., Wei, Y., Li, F.Y., Lin, S.H., 2003. Effects of confinement on protein folding and protein stability. J. Chem. Phys. 118 (17), 8042–8048.

Ping, G., Yuan, J.M., Sun, Z., Wei, Y., 2004. Studies of effects of macromolecular crowding and confinement on protein folding and protein stability. J. Mol. Recognit. 17 (5), 433–440.

Poraj-Kobielska, M., Kinne, M., Ullrich, R., Scheibner, K., Kayser, G., Hammel, K.E., Hofrichter, M., 2011. Preparation of human drug metabolites using fungal peroxygenases. Biochem. Pharmacol. 82 (7), 789–796.

Poraj-Kobielska, M., Peter, S., Leonhardt, S., Ullrich, R., Scheibner, K., Hofrichter, M., 2015. Immobilization of unspecific peroxygenases (EC 1.11.2.1) in PVA/PEG gel and hollow fiber modules. Biochem. Eng. J. 98, 144–150.

Ramirez-Escudero, M., Molina-Espeja, P., Gomez de Santos, P., Hofrichter, M., Sanz-Aparicio, J., Alcalde, M., 2018. Structural Insights into the Substrate Promiscuity of a Laboratory-Evolved Peroxygenase. ACS Chem. Biol. 13 (12), 3259–3268.

Rauch, M.C.R., Tieves, F., Paul, C.E., Arends, I.W.C.E., Alcalde, M., Hollmann, F., 2019. Peroxygenase-Catalysed Epoxidation of Styrene Derivatives in Neat Reaction Media. ChemCatChem 11 (18), 4519–4523.

Ravindra, R., Zhao, S., Gies, H., Winter, R., 2004. Protein encapsulation in mesoporous silicate: the effects of confinement on protein stability, hydration, and volumetric properties. J. Am. Chem. Soc. 126 (39), 12224–12225.

Sheldon, R.A., Woodley, J.M., 2018. Role of Biocatalysis in Sustainable Chemistry. Chem. Rev. 118 (2), 801–838.

Tang, M.-C., Fu, C.-Y., Tang, G.-L., 2012. Characterization of SfmD as a Heme Peroxidase That Catalyzes the Regioselective Hydroxylation of 3-Methyltyrosine to 3-Hydroxy-5-methyltyrosine in Saframycin A Biosynthesis. J. Biol. Chem. 287 (7), 5112–5121.

Thiel, D., Doknic, D., Deska, J., 2014. Enzymatic aerobic ring rearrangement of optically active furylcarbinols. Nat. Commun. 5, 5278.

Tieves, F., Tonin, F., Fernández-Fueyo, E., Robbins, J.M., Bommarius, B., Bommarius, A.S., Alcalde, M., Hollmann, F., 2019. Energising the E-factor: The E+-factor. Tetrahedron 75 (10), 1311–1314.

Truppo, M.D., 2017. Biocatalysis in the Pharmaceutical Industry: The Need for Speed. ACS Med. Chem. Lett. 8 (5), 476–480.

Ullrich, R., Hofrichter, M., 2005. The haloperoxidase of the agaric fungus Agrocybe aegerita hydroxylates toluene and naphthalene. FEBS Lett. 579 (27), 6247–6250.

Ullrich, R., Nüske, J., Scheibner, K., Spantzel, J., Hofrichter, M., 2004. Novel Haloperoxidase from the Agaric Basidiomycete Agrocybe aegerita Oxidizes Aryl Alcohols and Aldehydes. Appl. Environ. Microbiol. 70 (8), 4575–4581.

Ullrich, R., Poraj-Kobielska, M., Scholze, S., Halbout, C., Sandvoss, M., Pecyna, M.J., Scheibner, K., Hofrichter, M., 2018. Side chain removal from corticosteroids by unspecific peroxygenase. J. Inorg. Biochem. 183, 84–93.

Urlacher, V.B., Girhard, M., 2019. Cytochrome P450 Monooxygenases in Biotechnology and Synthetic Biology. Trends Biotechnol. 37 (8), 882–897.

Vargas, R.R., Bechara, E.J.H., Marzorati, L., Wladislaw, B., 1999. Asymmetric sulfoxidation of a beta-carbonyl sulfide series by chloroperoxidase. Tetrahedron: Asymmetry(10) 3219–3227.

Wang, Y., Lan, D., Durrani, R., Hollmann, F., 2017. Peroxygenases en route to becoming dream catalysts. What are the opportunities and challenges? Curr. Opin. Chem. Biol. 37, 1–9.

Willot, S.J., Fernandez-Fueyo, E., Tieves, F., Pesic, M., Alcalde, M., Arends, I., Park, C.B., Hollmann, F., 2019. Expanding the Spectrum of Light-Driven Peroxygenase Reactions. ACS Catal. 9 (2), 890–894.

Woodley, J.M., 2019. Accelerating the implementation of biocatalysis in industry. Appl. Microbiol. Biotechnol. 103 (12), 4733–4739.

Woodley, J.M., 2020. New frontiers in biocatalysis for sustainable synthesis. Current Opinion in Green and Sustainable Chemistry 21, 22–26.

Xu, H., Ning, L., Yang, W., Fang, B., Wang, C., Wang, Y., Xu, J., Collin, S., Laeuffer, F., Fourage, L., Li, S., 2017. In vitro oxidative decarboxylation of free fatty acids to terminal alkenes by two new P450 peroxygenases. Biotechnol Biofuels 10, 208.

Younes, S.H.H., Tieves, F., Lan, D., Wang, Y., Suss, P., Brundiek, H., Wever, R., Hollmann, F., 2020. Chemoenzymatic Halocyclization of gamma,delta-Unsaturated Carboxylic Acids and Alcohols. ChemSusChem 13, 97–101.

Zachos, I., Gassmeyer, S.K., Bauer, D., Sieber, V., Hollmann, F., Kourist, R., 2015. Photobiocatalytic decarboxylation for olefin synthesis. Chem. Commun. (Camb.) 51 (10), 1918–1921.

Zaks, A., Dodds, D.R., 1995. Chloroperoxidase-catalyzed asymmetric oxidations: substrate specificity and mechanistic study. J. Am. Chem. Soc. 117 (42), 10419–10424.

Zhang, L.H., Bai, C.H., Wang, Y.S., Jiang, Y.C., Hu, M.C., Li, S.N., Zhai, Q.G., 2009. Improvement of chloroperoxidase stability by covalent immobilization on chitosan membranes. Biotechnol. Lett. 31 (8), 1269–1272.

Zhang, W., Burek, B.O., Fernandez-Fueyo, E., Alcalde, M., Bloh, J.Z., Hollmann, F., 2017. Selective Activation of C-H Bonds in a Cascade Process Combining Photochemistry and Biocatalysis. Angew. Chem. Int. Ed. Eng. 56 (48), 15451–15455.

Zhang, W., Fernandez-Fueyo, E., Ni, Y., van Schie, M., Gacs, J., Renirie, R., Wever, R., Mutti, F.G., Rother, D., Alcalde, M., Hollmann, F., 2018. Selective aerobic oxidation reactions using a combination of photocatalytic water oxidation and enzymatic oxyfunctionalisations. Nat. Catal. 1 (1), 55–62.

9.2. Technical Report

Automated Feeding and Fermentation Phase Transitions for the Production of Unspecific Peroxygenase by *Pichia pastoris*

Markus Hobisch, Selin Kara, bioRxiv, 2021, preprint, DOI: 10.1101/2021.07.29.454275

Automated Feeding and Fermentation Phase Transitions for the Production of Unspecific Peroxygenase by *Pichia pastoris*

Markus Hobisch and Prof. Selin Kara

Biocatalysis & Bioprocessing Group, Department of Biological and Chemical Engineering, Aarhus University, Gustav Wieds Vej 10, 8000 Aarhus, Denmark

Abstract

Fungal peroxygenases are promising biocatalysts for hydroxylation steps in various industry-relevant synthesis pathways. In this application note we describe a bioprocess for the production of unspecific peroxygenase (UPO) in Pichia pastoris. The process was divided in four phases, with different carbon requirements. Precise timing of culture feeding was crucial for optimal cell growth and protein expression. We demonstrate how the automation of culture feeding reduced manual work as well as the risk of process failure due to operator error.

Keywords: *Pichia pastoris*, fermentation, automation, unspecific peroxygenase, enzyme expression

Introduction

The unspecific peroxygenase (UPO) is a promising tool in synthesis chemistry for enzymatic syntheses based on hydrogen peroxide. Primarily, UPO catalyzes the hydroxylation of aliphatic, cyclic, and aromatic C-H bonds with high enantioselectivity [1,2]. UPO was first discovered in 2004 [3] and its potential for biocatalytic applications was soon apparent, as more and more possible substrates were reported. While there are other enzymes that perform similar functions, they all require elaborate cofactor systems such as P450 monooxygenases, and UPOs only require hydrogen peroxide as a cosubstrate. Besides C-H hydroxylation, the enzyme also catalyzes epoxidation of C-C double bonds and some sulfoxidation reactions. The most widely employed UPO originated from the fungus *Agrocybe aegerita* (*Aae*UPO), was engineered for increased activity and high expression in *Pichia pastoris* and named PaDa-I [4]. The gene is integrated in the yeast's genome under the control of the AOX1 promoter, which is induced by methanol. Therefore, to grow biomass, glycerol is used as a carbon source, while for protein expression, methanol is required. The process is divided into four phases: Glycerol batch, glycerol feed, methanol batch, and methanol feed phase. Especially during the methanol phase, the process has to be run under carbon limiting conditions to avoid the accumulation of methanol to cytotoxic levels. While it is possible to do this manually, in a fermentation run taking up to seven days, this is laborious and prone to errors that can ruin several days of work. The same is true for the two transitions between batch and feed phases. These components of the process can also be carried out manually, but precise timing and extensive experience are required to avoid stressing the cells without a carbon source or committing to 24/7 monitoring. Therefore developing an automated process was a critical priority.

Material and Methods

Pichia pastoris strain

The strain *P. pastoris* X-33_pPICZ-B-PaDa-I was kindly provided by Professor Miguel Alcalde, ICP-CSIC, Madrid. The strain carries the UPO gene under control of the AOX1 promotor, which is induced by methanol.

Culture medium

Pichia pastoris pre- and seed cultures were grown in Buffered Glycerol Complex Medium (BMGY) medium. 10 g yeast extract and 20 g peptone are filled up to 800 mL with dH_2O. After autoclaving 100 mL 1 M Potassium phosphate buffer (pH 6, sterile autoclaved), 100 mL 10% glycerol solution (sterile autoclaved), 2 mL 0.02% Biotin solution (sterile filtrated) are added.

The main fermentation was carried out in basal salt medium, supplemented with PTM1 trace salt solution (**Table 1, 2**).

Table 1, 2: Components of basal salt media and PTM1 trace salts solution

Basal salt media (550 mL)			**PTM1 trace salts solution**	
Phosphoric acid (85%)	24.70 g		Manganese sulfate-H_2O	3.00 g
Calcium sulfate 2xH_2O	0.51 g		Cupric sulfate 5xH_2O	6.00 g
Potassium sulfate	10.00 g		Sodium iodide	0.08 g
Magnesium sulfate-7xH_2O	8.20 g		Sodium molybdate-2xH_2O	0.20 g
Potassium hydroxide	2.27 g		Boric acid	0.02 g
Glycerol	22.00 g		Cobalt chloride	0.50 g
dH_2O	482.00 g		Zinc chloride	20.00 g
			Ferrous sulfate-7xH_2O	65.00 g
			Biotin	0.20 g
			Sulfuric acid	5.00 mL
			dH_2O to a final volume of 1 L	

Inoculum preparation

P. pastoris was grown on YPD plates containing 100 µg/ml Zeocin for 3 days at 30 °C. A 30 mL preculture (BMGY, 100 µg/ml Zeocin) was inoculated with a colony and grown overnight at 30 °C and 120 rpm in a shaker. A 200 mL seed culture is inoculated with the preculture to an OD_{600} of 0.05 and grown over night as well.

Bioprocess system and process parameters

Bioprocesses were carried out in a DASGIP® Parallel Bioreactor System with Bioblock equipped with DASGIP vessels (DS1000TPSS, **Figure 1**).Stirring was provided by two Rushton impellers. The bioreactor containing 550 mL basal salt medium was autoclaved and subsequently supplemented with PTM1 trace salt solution (2.4 mL/L). The pH was adjusted to 5.0 with 25 % ammonium hydroxide solution. After DO calibration, process conditions were set to 900 rpm, 30 °C, and 30 L/h air flow. The bioreactor was then inoculated with 50 mL of the seed culture, resulting in a start OD_{600} between 1.0 and 2.5. Antifoam (Antifoam C, Sigma-Aldrich) was added automatically controlled by a level sensor.

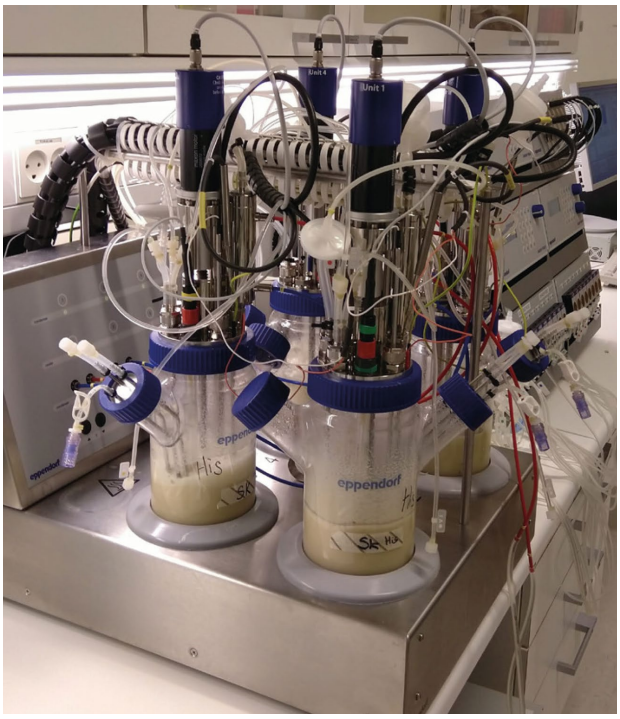

Figure 1: *The bioreactor system used in this study*

Bioprocess run

During the whole process the optical density at 600 nm (OD_{600}) and cell wet weight (CWW) are monitored. The *Pichia* bioprocess is based on previous publications on UPO expression [4,5] and is divided into four phases:

1. Glycerol batch phase: During the glycerol batch phase biomass is generated. During this phase, the dissolved oxygen (DO) will gradually decrease as more cells grow and consume glycerol. When all glycerol and other carbon sources are depleted the DO will spike, triggering the second phase.

2. Glycerol feeding phase: During this phase, the culture is fed using pump A of the bioprocess system. The feed solution consists of 25 % glycerol and 2.4 mL/L PTM1 trace salt solution. During this phase, the feed is adjusted automatically to keep the DO at ca. 30 %. This serves to adjust the cells to carbon limited growth conditions and allows formation of more biomass. When a sufficient cell concentration (around 180 g/L) is achieved glycerol feeding is stopped and the third phase, the methanol batch phase, is initiated.

3. Methanol batch phase: At the beginning of the methanol batch phase, the temperature is adjusted to 25 °C and methanol (0.5 % of the reactor volume) is slowly added so as to prevent the DO from dropping below 10 %. When all the methanol is metabolized, the DO will spike again and the methanol feed will begin.

4. Methanol feed phase: During this phase, the culture is fed musing pump D of the bioprocess system. The feed solution consists of pure methanol and 2.4 mL/L PTM1 trace salt solution. As soon as methanol is added, the enzyme activity in the supernatant is measured with an ABTS assay (see below) until the enzyme activity plateaus, at which time the fermentation is stopped.

Downstream processing

After cell removal by centrifugation, the supernatant containing the secreted enzyme is concentrated by a factor of 10 using Amicon Stirred Cells with a 10 kDa cut-off membrane. After buffer exchange to

potassium phosphate buffer (50 mM, pH 7) the enzyme is frozen by dripping it into liquid nitrogen with the peristaltic pumps from the DASGIP MP8 pump module and stored at -20 or -80 °C.

Automated feeding based on DO spike

The DO value of the culture medium is influenced by the amount of air supplied to the bioreactor through the bioprocess system's gassing device and the oxygen consumption of the growing cells. During the bioprocess run, the DO concentration is measured in real-time using a DO sensor. In the course of the bioprocess run it will decrease, reflecting the oxygen consumption of the growing cells. If the carbon sources are depleted, the cells' metabolic activity and therefore their oxygen consumption suddenly decreases, leading to a spike in the DO concentration. The DO spike therefore indicates substrate depletion and can be used to trigger automated culture feeding. To automate feeding based on the DO spike, a script was implemented in the DASware control 5 software. In the script, the DO spike was defined as the DO sensor rising from a lower trigger point of 25 % to an upper trigger point of 80 %. Upon reaching the upper trigger point, the feed pump was automatically initiated as described in detail in the Results section.

Analytics

Samples were taken manually to determine OD_{600}, cell wet weight, and enzyme activity offline. Determination of cell wet weight 500 µL of cell suspension were centrifuged (7 min, 13,000 rpm) in weighed tubes, and the supernatant was decanted. After another round of centrifugation (1 min, 13,000 rpm) the residual liquid was removed with a 100 µL pipette and cell wet weight determined.

Determination of Enzyme Activity

The enzyme assay was performed in 100 mM sodium phosphate/citrate buffer pH 4.4, with 0.3 mM 2,2'-azinobis(3-ethylbenzothiazoline-6-sulphonic acid) (ABTS) and 2 mM H_2O_2 in semimicro cuvettes (25 °C, at 405 nm, ε=36.8 mM^{-1} cm^{-1}).

Results

After inoculation, the DO started to decrease as expected as more and more biomass was formed, consuming the glycerol (**Figure 2**). It dropped to around 8 %, passing the lower trigger point of 25 %. After around 0.75 days all the glycerol was metabolized and the DO spiked as no more oxygen was being consumed. Upon reaching the upper trigger point of 80 %, the glycerol feed was automatically started with the maximum feed rate defined as 10 mL/h. At first this caused the DO to drop to 10 %, but it soon recovered to 30 % as the feed rate was automatically adjusted to around 8 mL/h. After 40 hours, a sufficient cell wet weight of 188 g/L was reached (**Figure 3**) and the glycerol feed was ended by setting the offline parameter A, which gives the glycerol feed duration from 400 h to 1 h.

After addition of the methanol for the second batch phase, the DO decreased again to around 15 % (below the lower trigger), but soon spiked as all methanol was consumed, surpassing the upper trigger of 80 % and therefore activating the automated methanol feeding (**Figure 2**). The feed started out with the maximum defined feed rate of 5 mL/h and then settled just below 2 mL/h keeping DO between 20 % and 50 %. Enzyme activity increased to 202 U/mL on the sixth day and slightly decreased to 186 U/mL on the seventh day which was the sign to harvest (**Figure 3**).

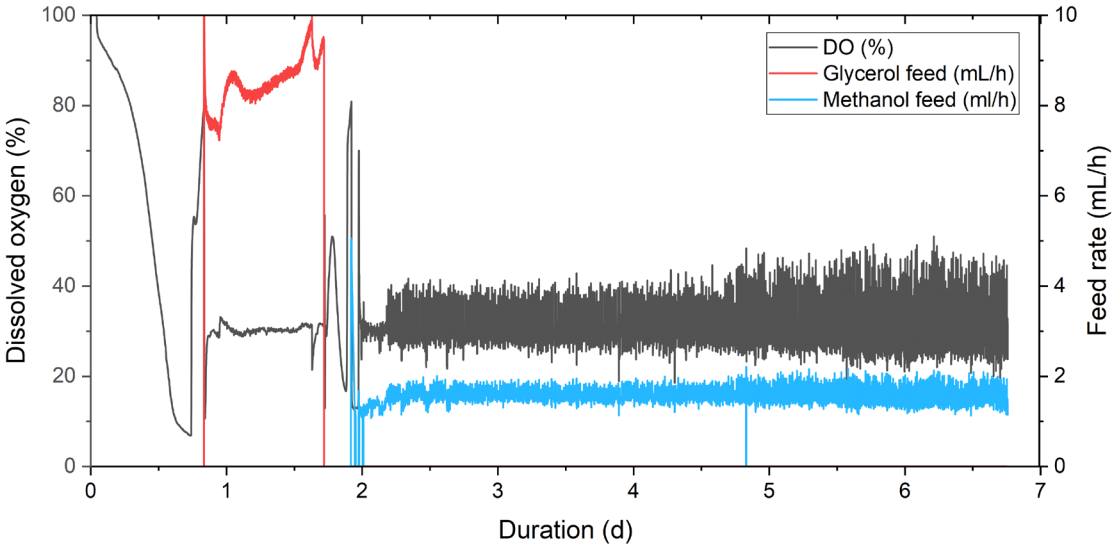

Figure 2: *Online parameters of the fermentation comprising dissolved oxygen (DO), glycerol feed and methanol feed.*

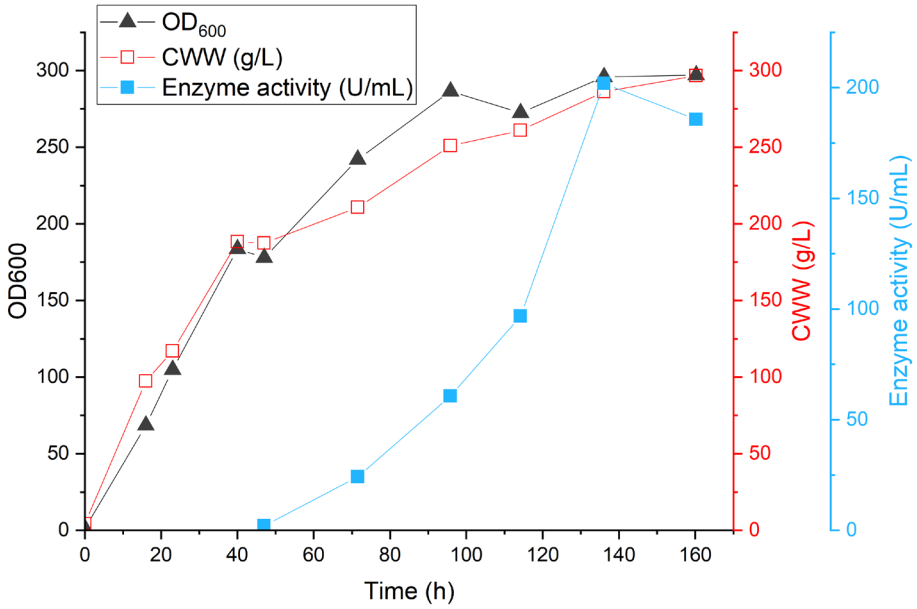

Figure 3: *Offline parameters of the fermentation: OD_{600}, cell wet weight (CWW) and enzyme activity.*

Conclusion

We automated glycerol and methanol feeding in a Pichia pastoris bioprocess for UPO production. To do so, a software script was implemented, which triggered the activity of the feed pumps based on spiking of the DO concentration. It was evident that automated feeding and phase transitions are optimal tools in a fermentation process, especially when dealing with a eukaryotic expression host such as *Pichia pastoris*. The complex process requirements comprising transitions from batch to fed-batch operation and careful methanol feeding over several days are the perfect example for the benefits of automation in a modern bioprocess platform. While a seven day *Pichia pastoris*

fermentation is still a demanding and labor intensive process, our proposed modifications represent significant time and labor saving improvements.

Acknowledgements

This project has received funding from the European Union's Horizon 2020 research and innovation program under the Marie Skłodowska-Curie grant agreement No 764920.

References

[1] Hobisch, M., et al., Recent developments in the use of peroxygenases - Exploring their high potential in selective oxyfunctionalisations. Biotechnology Advances, 2020: p. 107615.

[2] Wang, Y., et al., Peroxygenases en route to becoming dream catalysts. What are the opportunities and challenges? Curr Opin Chem Biol, 2017. 37: p. 1-9.

[3] Ullrich, R., et al., Novel haloperoxidase from the agaric basidiomycete Agrocybe aegerita oxidizes aryl alcohols and aldehydes. Appl Environ Microbiol, 2004. 70(8): p. 4575-81.

[4] Molina-Espeja, P., et al., Tandem-yeast expression system for engineering and producing unspecific peroxygenase. Enzyme Microb Technol, 2015. 73-74: p. 29-33.

[5] Tieves, F., et al., Energising the E-factor: The E+-factor. Tetrahedron, 2019. 75(10): p. 1311-1314.